Interstellar Germanium Dust Molecules: a Computational Study on Their Structure, Spectroscopy, and Detectability; or, One Small Step Down the Periodic Table, One Giant Leap in Interstellar Chemistry

by

Adam Mackenzie Flowers

A thesis submitted in partial fulfillment of the requirements for the degree of

Master of Science

Department of Chemistry
University of Alberta

Abstract

Alongside observational and experimental work, theoretical and computational research is just as vital to understanding the chemical composition of space. Although more molecules continue to be discovered in space, the molecular structures in which many of the elements in the periodic table exist in the interstellar medium (ISM) remain a mystery. With growing capabilities to discern more of the chemical composition of the ISM, an accurate database of reference material is required. The presence of carbon is ubiquitous in the ISM, and silicon is known to be present in interstellar dust grains, however germanium-containing molecules remain elusive. To begin understanding the presence and role of germanium in the ISM, this thesis presents a study of the vibrational and rotational spectroscopic properties of various germanium-containing molecules to aid in their potential identification in the ISM with modern observational tools such as the James Webb Space Telescope. Silicon-carbide dust grains are known to be prevalent in interstellar dust, and, therefore, by taking these as reference, germanium carbide and germanium silicide structures are proposed for detection in the ISM. An extensive, high-level theoretical study on tetra-atomic germanium carbide/silicide clusters, including calculations of accurate harmonic and anharmonic vibrational frequencies, rotational constants, and dipole moments done at the CCSD(T)-F12a(b)/cc-pVT(Q)Z-F12 levels of theory is presented in this work. Structures studied herein include rhomboidal (r-), diamond (d-), and trapezoidal (t-) tetra-atomic molecules of the form Ge_xC_{4-x} and Ge_xSi_{4-x}, where x=0-4. The most promising structure for detection is r-Ge_2C_2 via the ν_4 mode with a frequency of 802.7 cm^{-1} (12.5 μm) and an intensity of 307.2 km mol^{-1}. Other molecules potentially de-

tectable, i.e., through vibrational modes or rotational transitions, include r-Ge_3C, r-$GeSi_3$, d-GeC_3, r-GeC_3, and t-Ge_2C_2.

Alongside proposing germanium-containing molecules for detection, a thorough determination of the transition states between the different isomers of the cyclic tetra-atomic silicon-carbide, germanium carbide, and germanium silicide clusters is presented. Through use of density functional theory (B3LYP-D3BJ, M06-2X, ωB97X-D4, and B2GP-PLYP) in conjunction with the aug-cc-pVTZ basis set, transition state structures and their barrier heights are determined for the interconversions between the various isomers for the family of tetra-atomic SiC, GeC, and GeSi compounds. Determining which structures might be detectable not only depends on their intrinsic spectroscopic features, but whether or not they are likely to exist as isomers in interstellar environments. By examining the energy barrier heights for transitions between isomers, we determined that many of these structures are unlikely to exhibit interconversion in the ISM, outside of hotter circumstellar environments. Although Boltzmann population ratios at approximate circumstellar temperatures suggest the presence of higher energy minima, it is likely that once interconversion happens, as molecules travel away from a star and cool, they will get kinetically trapped in the potential energy well they inhabit, making how the ratios freeze out dependent on the time and pathways the molecules take to cool down. As such, many of these higher energy minima may still be good candidates for detection including r-SiC_3, r-GeC_3, r-$GeSi_3$, t-Si_2C_2, r-Ge_2C_2, and d-Si_3C.

Preface

A version of Chapter 2 has been published as "Anharmonic vibrational spectroscopy of germanium-containing clusters, Ge_xC_{4-x} and Ge_xSi_{4-x} (x = 0-4), for interstellar detection," in *The Journal of Physical Chemistry A*, **2024**, *128*(27), 5351–5361 by A. Mackenzie Flowers, Alex Brown, and Mariusz Klobukowski. A version of this work is also available on the *ChemRxiv* (doi:10.26434/chemrxiv-2024-6xq70). I performed all calculations, gathered and analysed all data, and wrote the manuscript for this work. Alex Brown and Mariusz Klobukowski edited the manuscript and provided guidance throughout the project.

The work presented in Chapter 3 has been accepted to the journal *Physical Chemistry Chemical Physics*, as "An investigation into transition states of cyclic tetra-atomic silicon and germanium interstellar dust compounds," by A. Mackenzie Flowers, Alex Brown, and Mariusz Klobukowski. A version of this work is also accessible on the *ChemRxiv* (doi:10.26434/chemrxiv-2024-ncvzn-v2). I performed all calculations and analysis of the data. Mariusz Klobukowski provided scripts to ease extraction of all required data from the outputs. Again, I wrote the manuscript, and Alex Brown and Mariusz Klobukowski edited the manuscript and provided guidance throughout the work.

Not presented in this thesis is collaborative project titled "Accurate Potential Energy Surfaces Using Atom-Centered Potentials and Minimal High-Level Data" published in *The Journal of Physical Chemistry A*, **2023**, *127*(38), 8015–8024 by Mahsa Nazemi Ashani, Qinan Huang, A. Mackenzie Flowers, Alex Brown, Antoine Aerts, Alberto Otero-de-la-Roza, and Gino A. DiLabio. The work was led by Gino A. DiLabio

at the University of British Columbia - Okanagan, and Alberto Otero-de-la-Roza at the University of Oviedo. I contributed geometry optimization and vibrational frequency computations as well as analysis of them to this work.

"If a conclusion is not poetically balanced, it cannot be scientifically true."

-Isaac Asimov

Acknowledgements

I would like to thank both Dr. Alex Brown and Dr. Mariusz Klobukowski for giving me the opportunity to be a graduate student under their supervision.[1] I will miss our weekly meetings which always went long past the one hour time slot due to off-topic conversations (but they always circled back to relevant science talk in the end). I hope to take all I have learned under your joint supervision and carry it with me as I continue my path as a researcher. Needless to say, I am very grateful for how much they have taught me and for helping me become the scientist that I am today.

This thesis could not have been possible without the support from my parents who are always behind me, no matter what I choose to pursue. Nor without all of my friends, both in Edmonton and back in Michigan, who provided much needed distractions outside of work.

I would also like to thank all who helped make the Chemistry Department here feel like home. The friends with whom you struggle through it all together are irreplaceable. I would like to thank those friends: Amanda, Dean, Harold, Shyam, Alex, and Juliette, the latter of whom I am grateful for always being around for entertaining conversations at the end of long days.

This list would not be complete without thanking Sydney, who I cannot express my love and appreciation for enough. Thank you for always being there to talk me off

[1] When I finished my undergraduate degree, I was unsure of what my next step would be, all I knew is that I no longer wanted to pursue mathematics (as much as I love it), and that I was determined to be an astrochemist. After a summer of stress and self-doubt, I reached out to them and asked for a chance to do computational chemistry work for them as a means to pursue astrochemistry. Following a last-minute suggestion to try to get me into the Master's program in the fall, I scrambled to get all I needed together for an application, and made it to orientation only two weeks later.

of the ledge when the claws of imposter syndrome would reach up and wrap around my ankles. All of your support from phone calls to long-distance movie nights, and short trips spent to see one another mean more than can be put into words; I could not have done this without you.

Table of Contents

List of Tables

List of Figures

List of Symbols

Φ	Trial wave function
Ψ	Wave function
Σ	Sum
χ	Basis function
ϵ	Orbital energies
$\hat{F}^{KS}$	Kohn-Sham operator
$\hat{H}$	Hamiltonian
$\hat{H}^{(0)}$	Unperturbed Hamiltonian
$\hat{H}_e$	Electronic Hamiltonian
$\hat{J}$	Coulomb operator
$\hat{K}$	Exchange operator
$\hat{T}$	Cluster operator
$\hat{V}$	Perturbation operator
$\hat{f}$	Fock operator
$\hat{h}$	One-electron operator
$\hbar$	Reduced Planck's constant
μ	Dipole moment
∇	Differential operator
ν	Frequency
ϕ	Orbital
ψ	Spin orbital
ρ	Electron density

e	Euler's number
k_B	Boltzmann constant
m_e	Electron mass
Å	Ångström

Abbreviations

AGB Asymptotic giant branch (stars).

ALMA Atacama Large Millimeter Array.

aug-cc-pVnZ Dunning's n-tuple correlation consistent basis set, augmented with diffuse functions.

B2GP-PLYP Gershom's double-hybrid density functional with Becke's parameters and Lee, Yang, Parr correlation with 65% Hartree-Fock exchange.

B3LYP Hybrid density functional with Becke's three parameters and 1988 exchange B88 with Lee, Yang, Parr correlation.

B3LYP-D3BJ Hybrid density functional with Becke's three parameters and 1988 exchange B88 with Lee, Yang, Parr correlation, paired with Grimme's D3 dispersion model and Becke-Johnson damping.

CAS Complete active space.

CASPT2 Complete active space second order perturbation theory.

CASSCF Complete active space-self consisten field method.

cc-pVnZ Dunning's n-tuple correlation consistent basis set.

CCSD(T) Coupled-cluster singles, doubles, and perturbative triples.

CCSD(T)-F12 Coupled-cluster singles, doubles, and perturbative triples with explicit electron correlation.

CSE Circumstellar envelope.

DFT Density functional theory.

EMR Electromagnetic radiation.

F12a/TZ Coupled-cluster singles, doubles, and perturbative triples with explicit electron correlation ("a" variation) and cc-pVTZ-F12 basis set.

F12b/QZ Coupled-cluster singles, doubles, and perturbative triples with explicit electron ("b" variation) and cc-pVQZ-F12 basis set.

GGA Generalized gradient approximation.

HF Hartree-Fock.

iCOM Interstellar complex organic molecule.

IR Infrared.

IRC Intrinsic reaction coordinate.

ISM Interstellar medium.

JWST James Webb Space Telescope.

KS Kohn-Sham.

M06-2X Truhlar's Minnesota 2006 hybrid meta-generalized gradient approximation functional with 54% Hartree-Fock exchange.

MAPD Mean absolute percent deviation.

MP2 Second-order Møller-Plesset perturbation theory.

PAH Polycyclic aromatic hydrocarbon.

PES Potential energy surface.

RIJCOSX Resolution of identity for Coulomb integrals with chain of spheres numerical integration.

VPT2 Second order vibrational perturbation theory.

WFT Wavefunction theory.

ZPVE Zero-point vibrational energy.

Chapter 1

Introduction

1.1 Background and Motivation

Since the Copernican revolution during the mid-16th century, the veil over the mysteries of the Universe we exist in has been pulled back more and more with each advancement in astronomical technologies. Over the years, astronomy as a field has broadened out its scope to not only just include astronomers, but astrophysicists, astrobiologists, and astrochemists as well. The advancement of technologies continues all the way to the current day where we can be considered to be in the midst of a "golden age" for astronomical discoveries.

The current state of astronomical surveying owes a lot to great advancements made in the field of observational apparatus, specifically to telescopes such as the Atacama Large Millimetre Array (ALMA) and the James Webb Space Telescope (JWST), and all of the scientists who interpret and analyse the obtained data. These telescopes, and many others, offer scientists the ability to peer out into the Universe through all lenses of the electromagnetic radiation spectrum (EMR). Stellar objects emit radiation across the entire spectrum and looking at celestial bodies through different parts of the spectrum can reveal many different features about them. This dependence on wavelength can be shown, for example, by looking at the molecular cloud Barnard 68 (Figure 1), which is an opaque region in the galaxy when seen through visible light/near-IR, but thousands of stars shine through if observed with

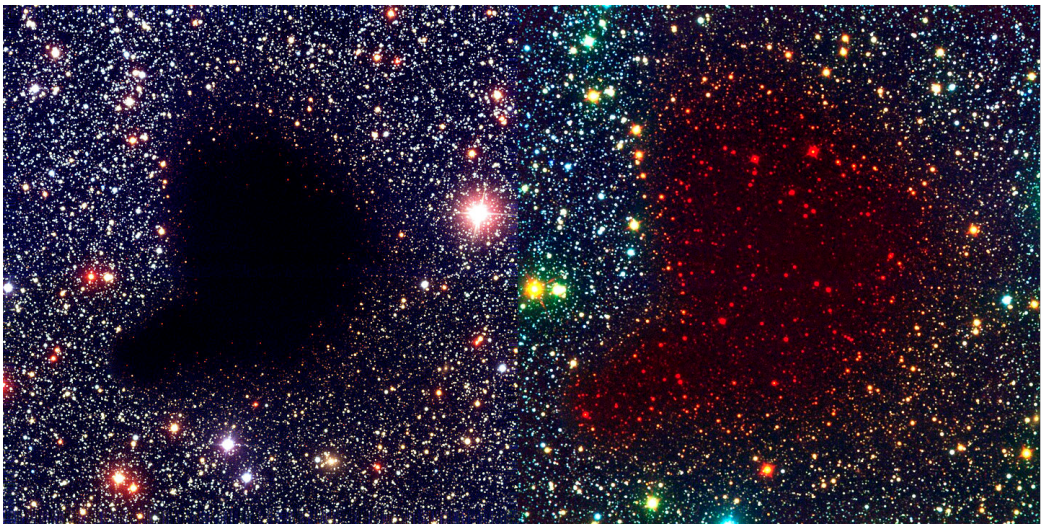

Figure 1.1: Molecular cloud Barnard 68 as seen through visible light (left) and infrared light (right). Figure adapted from ESO images.

an infrared telescope.

The visual difference in the molecular cloud when observed through different wavelengths is due to blocking (or extinction) of light behind it by the dust grains that make up the cloud [1]. There are many of these molecular clouds found in the Universe, found in regions where the gas and dust has grown more dense. The gas and dust that make up these clouds are full of various molecules that can absorb light at different wavelengths, making them sort of fog within the Universe [2, 3].

For astrochemists what might be of more concern is the chemical makeup of the Universe, including stars, planets, molecular clouds, and the vast apparent emptiness between celestial bodies, otherwise known as the interstellar medium (or ISM). This problem is perfect for chemists, as underneath it all, interpreting data collected from telescopes is just molecular spectroscopy. As atoms and molecules in stars or the ISM undergo transitions, their absorption or emission spectra are what is detected through telescopes. These spectral signatures are unique to each atom or molecule and are what allow the chemical characterization of the ISM [4, 5]. For molecules in particular, the most helpful regions of the EMR spectrum are the radio and infrared regions, which the two aforementioned telescopes observe in, respectively. These

two regions correspond to rotational and vibrational transitions within molecules, respectively. Those interested more in the theory and specifically within the context of astronomy are pointed towards relevant books on the subject [6, 7].

Over the past few decades, the cosmic inventory of molecules has rocketed to almost 300 known molecules having been detected [8]. This is mostly due to the many radio telescopes that are surveying different regions in space, but with the JWST covering wavelengths of 0.6 - 28.3 μm ($\sim$353 - $\sim$16667 cm^{-1}), the infrared region is now more accessible to astronomers.

Unfortunately, taking observations with the purpose of detecting molecules is not as simple as facing a telescope towards a certain region, gathering a signal, and assigning the lines in the spectrum. When a signal is gathered, the spectrum of the observed body might return looking like a dense forest of peaks. To then assign specific molecules to that forest, one needs to know what sort of trees they are looking for, or rather, what the spectrum of the molecule they are trying to assign looks like. As such, having accurate individual spectra to refer to is an important part of assigning peaks in a spectrum [5, 6]. Generating these data can be done either through laboratory experiments to observe spectra of individual molecules, or by accurate computational chemistry methods. Space itself is home to many strange molecules [9–13], some of which are not possible to synthesize or examine in the laboratory on Earth; computational chemistry offers another route to analyze some of these exotic molecules. As computational methods have become more and more accurate over the years, the importance of computational chemistry as a tool for astrochemistry has only proven itself more relevant. A thorough review on the relationship between quantum chemistry and astrochemistry was written by Fortenberry in 2017 [14].

Astrochemistry itself not only includes observational research and computational chemistry research, but also experimental work, such as gas-phase kinetics or spectroscopy experiments, and other theoretical work such as astrophysical models of reaction networks. Without further belabouring the point, the study of astrochem-

istry is a very interdisciplinary field. There are many, many subjects of study in space, hence the need for many different types of scientists.

While studies of exo-planets, stars, comets, black holes, and the myriad other celestial bodies that exist in space are fascinating, what is of more concern to this work is the aforementioned chemical makeup of the ISM. One area of particular interest in current-day astrochemistry is the research on interstellar complex organic molecules (iCOMs), and more specifically polycyclic aromatic hydrocarbons (PAHs) [15–20]. These PAHs make up a large fraction of all carbon in the Universe and are thought to be early molecular milestones along the origins of life pathway. PAHs are a stepping stone towards larger iCOMs such as amino acids and nucleotides; as such they are fundamental building blocks of what could later develop into life. Although not the focus of this work, they are important to point out as a current focus of all sub-disciplines of astrochemistry. Efforts to study and detect these have included observations of the Taurus molecular cloud (TMC-1) [21], low-temperature kinetic experiments [22], and computational studies either looking at properties of potentially detectable PAHs or determining the methods to accurately model PAHs [23, 24].

Another current area of study well represented by the union of observation, experiment, and theory is the study of interstellar dust grains and the molecules that comprise them [25–27]. Dust grains in the ISM eventually gravitate towards each other and aggregate into larger and larger clusters in the process of accretion. Therefore, as these dust particles turn into planetesimals and eventually planets, they bring whatever they are made up of with them. Determining what dust particles are made up of offers insight into how certain elements are dispersed throughout the Universe.

These dust grains are thought to be formed in the circumstellar environments (CSE) of stars [28]; this is discussed more in Chapter 3. More specifically, researchers have been interested in the asymptotic giant branch (AGB) star CW Leonis or IRC +10216 [9, 29–32]. Some AGB stars can build up a higher concentration of carbon in

their shells, rendering them so-called carbon stars. As solar winds carry out carbon-containing compounds from these stars, they become pieces of interstellar dust, hence making them good targets of study. Specifically, IRC +10216 has offered insight into the formation and makeup of dust grains due to its relatively higher abundance of carbon and silicon. Many dust particles are currently known to be made up of different forms of silicates and silicon-carbides.

In the Universe, all post-lithium [33] (and some beryllium) elements are formed in stars [34]. This is either through stellar nucleosynthesis (fusion within the cores and shells of stars) or neutron capture and subsequent beta-decays. The latter source, neutron capture, occurs in two ways: the slow neutron capture *s-process* [35], and rapid neutron capture *r-process* [34]. The first involves the capture of a neutron and β-decay before capture of another neutron, while the second involves the capture of multiple neutrons in rapid succession before β-decay occurs.

The neutron capture processes are the origin of all elements post-nickel. AGB stars are good sources of lower Z-value s- and r-process elements due to the outer shell of relatively proton-rich elements (in terms of stellar nucleosynthesis) [36]. Therefore, they might be an interesting source of elemental variety within the dust grains they send out into space.

Returning to interstellar dust grains being made up of silicon-carbides, it begs the question of what else they could possible be comprised. Following the periodic table, going from carbon to silicon, the next one to look at is germanium. Germanium has been seen in various parts of the ISM [37–39], and is known to form through the s- and r-processes [38, 40, 41]. Sharing the same valence electron configuration as carbon and silicon, it is a natural next step for investigation.

Although germanium may exhibit similar properties to carbon and silicon, it should be noted the abundance of germanium is much lower relative to these two elements. Where carbon and silicon are respectively around four and five magnitudes lower in abundance than hydrogen, germanium is around nine orders of magnitude lower in

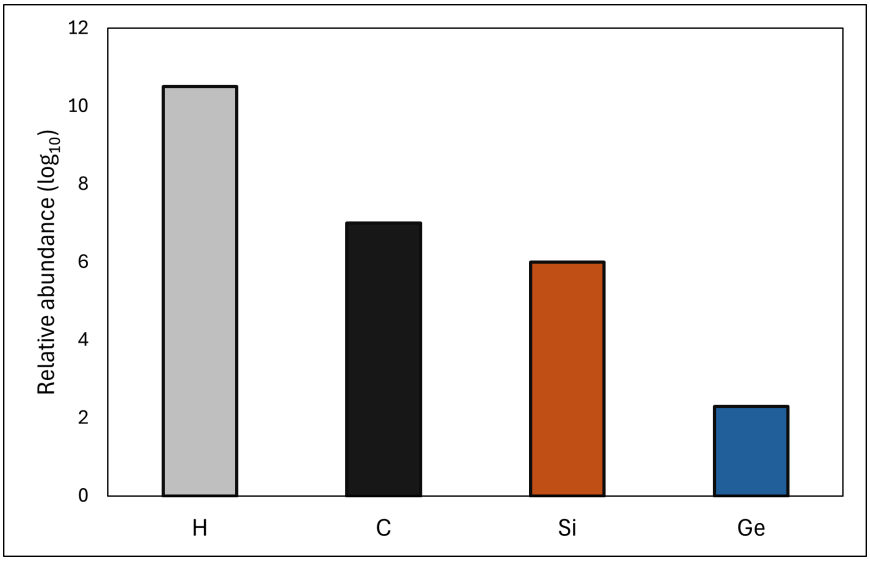

Figure 1.2: Abundance of elements (studied in this work) in the Universe relative to hydrogen (light grey). Carbon in black, silicon in orange, germanium in blue.

abundance [42]. This is illustrated in Figure 1.2. Due to its much lower abundance, germanium would be much more difficult to detect, making sensitive instruments and accurate theoretical methods a necessity.

Initiating this investigation into interstellar germanium, this work studies the properties of germanium carbide and germanium silicide molecules with the intent of providing data to aid in their detection in the ISM. By knowing what molecular forms germanium takes in the ISM, one can help elucidate how germanium makes it to the various reaches of the Universe. This investigation is done through the use of different computational tools to provide theoretical data for these (potential) interstellar dust molecules, representing a cornerstone of the field of astrochemistry.

Before delving into the research presented in this work, the background and theory for the methods used in this work are (lightly) detailed in the following section. For a comprehensive look at all computational methods both included and excluded from the following section, the reader is pointed towards various computational chemistry textbooks [43–48].

1.2 Theoretical Background

1.2.1 The Schrödinger Equation and Hartree-Fock Method

To begin looking at molecules through the lens of quantum mechanics, we first consider the time-independent Schrödinger equation [49]:

$$\hat{H}\Psi = E\Psi, \tag{1.1}$$

an eigenvalue equation where $\hat{H}$ is the Hamiltonian operator, Ψ is the wavefunction, and E is the energy. To solve this equation for the energies and the wavefunction from which other properties can be determined, we must make approximations. Approximations are need as this equation becomes very complicated very quickly for any scenario other than a one-electron system, for which it can be solved exactly [43]. As to not digress for too long in this thesis, this will only serve as a brief overview of the background behind the methods used in this work. Again, all of the methods discussed herein are beautifully derived and explained in detail in many textbooks on quantum chemistry [43–48].

First we will be more explicit with our portrayal of equation 1.1 (without taking spins into account):

$$\hat{H}(\{\vec{r}_i\},\{\vec{R}_I\})\Psi(\{\vec{r}_i\},\{\vec{R}_i\}) = E\Psi(\{\vec{r}_i\},\{\vec{R}_A\}), \tag{1.2}$$

where the $\{\vec{r}_i\}$ are coordinates of the electrons and the $\{\vec{R}_A\}$ are the coordinates of the nuclei. Now we can take a look at the non-relativistic form of the Hamiltonian operator in atomic units:

$$\begin{aligned}\hat{H} &= -\frac{1}{2}\sum_{i=1}^{N}\nabla_i^2 - \sum_{A=1}^{P}\frac{1}{2M_A}\nabla_A^2 - \sum_{i=1}^{N}\sum_{A=1}^{P}\frac{Z_A}{|\mathbf{r}_i - \mathbf{R}_A|} \\ &\quad + \sum_{i=1}^{N-1}\sum_{j>i}^{N}\frac{1}{|\mathbf{r}_i - \mathbf{r}_j|} + \sum_{A=1}^{P-1}\sum_{B>A}^{P}\frac{Z_A Z_B}{|\mathbf{R}_A - \mathbf{R}_B|}.\end{aligned} \tag{1.3}$$

This operator includes the kinetic energies of N electrons and P nuclei with terms one and two, respectively. Following this are the different interactions in the system,

being electron-nuclei, electron-electron, and nuclei-nuclei, respectively, where Z_A is the atomic number of nucleus A.

As one can already tell, this equation can become quite complicated with an increasing number of electrons (and nuclei), hence the need for approximations. One of the earliest approximations to make is the so-called Born-Oppenheimer approximation [50]. This approximation arises from the masses of electrons being much smaller than those of the nuclei (a factor of ∼1836 lighter already for the hydrogen atom), making the nuclei essentially appear stationary to the electrons. The Hamiltonian can then be simplified by dropping the term for the kinetic energy of the nuclei, giving the *electronic* Hamiltonian:

$$\hat{H}_e = -\frac{1}{2}\sum_{i=1}^{N}\nabla_i^2 - \sum_{i=1}^{N}\sum_{A=1}^{P}\frac{Z_A}{r_{Ai}} + \sum_{i=1}^{N-1}\sum_{j>i}^{N}\frac{1}{r_{ij}} + \sum_{A=1}^{P-1}\sum_{B>A}^{P}\frac{Z_A Z_B}{R_{AB}}. \tag{1.4}$$

If we wish then to solve the Schrödinger equation for a system in the ground state, we can manipulate the equation to get:

$$E_0 = \frac{\langle\Psi|\hat{H}|\Psi\rangle}{\langle\Psi|\Psi\rangle}. \tag{1.5}$$

This gives us the expectation value of the Hamiltonian operator, which is the ground state energy E_0.

Now, if we take a trial wavefunction, Φ, for which we wish to solve this equation, through the so-called Variational Principle, the energy of this system, E, will always be greater than or equal to the exact ground state energy E_0:

$$E = \frac{\langle\Phi|\hat{H}|\Phi\rangle}{\langle\Phi|\Phi\rangle} \geq E_0. \tag{1.6}$$

At this point, we need now the formulation for the trial wavefunction, which brings us to our first, and simplest method, the (closed-shell, restricted) Hartree-Fock method (HF) [51–57]. The RHF method approximates the wavefunction, Ψ, for an N electron system as a Slater determinant:

$$\Phi^{HF}(1,2,...,N) = |\psi_1(\mathbf{r}_1\sigma_1)\psi_2(\mathbf{r}_2\sigma_2)...\psi_N(\mathbf{r}_N\sigma_N)|, \tag{1.7}$$

where ψ is a spin-orbital, $\mathbf{r}_i$ is the Cartesian coordinates of electron i, and σ_i denotes the spin of electron i. The spin-orbtials are made as products of spatial orbitals ϕ and spin functions, spin up (α) or spin down (β):

$$\Psi_i(\vec{r}, \sigma) = \phi(\vec{r})\alpha(\sigma) \tag{1.8}$$

$$\Psi_j(\vec{r}, \sigma) = \phi(\vec{r})\beta(\sigma). \tag{1.9}$$

The Slater determinant takes into account the necessity for antisymmetry of the wavefunction due to the Pauli exclusion principle, as if two electrons shared the same coordinates and spin, the determinant would vanish.

This minimization of the energy E, Eq. 1.6, with the HF wavefunction, Eq. 1.7, brings us finally to the Hartree-Fock equations:

$$\hat{f}(\mathbf{r})\phi_a(\mathbf{r}) = \varepsilon_a\phi_a(\mathbf{r}). \tag{1.10}$$

for the best orbitals ϕ_a (i.e. those which minimize the energy). In Eq. 1.10 $\hat{f}$ is the Fock operator, of the form

$$\hat{f}(\mathbf{r}) = \hat{h}(\mathbf{r}) + \sum_{j=1}^{N/2}[2\hat{J}_j(\mathbf{r}) - \hat{K}_j(\mathbf{r})], \tag{1.11}$$

and $\hat{h}$, $\hat{J}$, $\hat{K}$ are the one-electron, Coulomb, and Exchange operators, respectively. Where this method falls short is in its ability to consider electron correlation. In the HF theory, the explicit interactions between the electron i and the other $N-1$ electrons, term 3 in Eq. 1.4, are approximated as a mean field of $N-1$ electrons. As such, the dynamic correlation is not properly described in the HF theory. The correlation energy is defined as the difference between the exact ground state energy and the Hartree-Fock energy:

$$E_{\text{corr}} = E_0 - E_{\text{HF}}. \tag{1.12}$$

Methods alleviating this shortcoming will be discussed further below.

1.2.2 Post-Hartree Fock Methods

Møller-Plesset Perturbation Theory

In an attempt to recover the correlation energy when studying systems quantum mechanically, the first method to introduce is the second-order Møller-Plesset Perturbation Theory (MP2) [58]. In perturbation theory, a perturbation ($\hat{V}$) is used in the Hamiltonian:

$$\hat{H} = \hat{H}^{(0)} + \hat{V}, \tag{1.13}$$

where $\hat{H}^{(0)}$ is the unperturbed Hamiltonian.

The most used version is the MP2 method, which goes up to a second-order correction (although it can be truncated at any order n correction, yielding MPn) to account for correlation energy:

$$E_{\text{MP2}} = E_{\text{HF}} + \sum_{k \neq 0} \frac{|\hat{V}_{k0}|^2}{E_0^{(0)} - E_k^{(0)}}. \tag{1.14}$$

A more rigorous breakdown of Hartree-Fock theory, perturbation theory, and Møller-Plesset theory in both single- and multireference contexts can be read in Helgaker et al. [45] and Cramer [46].

Coupled Cluster

Another technique for estimating the correlation energy of electrons is the popular coupled-cluster theory (CC) [59]. In CC, the wavefunction is defined as

$$\Psi = e^{\mathbf{T}} \Psi_{\text{HF}}. \tag{1.15}$$

The cluster operator $\mathbf{T}$ takes the form

$$\mathbf{T} = \mathbf{T}_1 + \mathbf{T}_2 + ... + \mathbf{T}_N, \tag{1.16}$$

where N is the total number of electrons considered. Each $\mathbf{T}_i$ operator generates all possible determinants created by considering i excitations of electrons from the

ground state. The $\mathbf{T}_2$ operator, for example, is

$$\mathbf{T}_2 = \sum_{i<j}^{\text{occ.}} \sum_{a<b}^{\text{vir.}} t_{ij}^{ab} \Psi_{ij}^{ab}, \tag{1.17}$$

where i, j are the occupied orbitals, and a, b are the virtual orbitals to which excitations are made, with each t_{ij}^{ab} as the coefficient associated with the excitation.

The most popular implementation of CC, and what is currently considered the "gold standard" method for single-reference calculations in computational chemistry, is the CCSD(T) method. This method considers single and double excitations, and adds perturbatively triple excitations. This method does have its drawback, being largely applicable to smaller systems, as computational time depends strongly on number of electrons, N, and basis functions, K (see Sec. 1.2.4).

As mentioned, the CC method is derived for a single-reference wavefunction, however it does allow assessment of the whether or not the system being studied has *multi*reference character through the so-called T_1 diagnostic formulated by Lee and Taylor [60]. This diagnostic is defined as

$$\mathrm{T}_1 = \sqrt{(\sum_{i}^{\text{occ.}} \sum_{a}^{\text{vir.}} (t_i^a)^2)/N}, \tag{1.18}$$

and typically a value larger than 0.02 points towards possible multireference character.

More details on this method can be read in the original works [59], or the review by Crawford and Schaefer [61].

1.2.3 Density Functional Theory

Adjacent to wavefunction theory (WFT), there exists an alternative formulation for solving the exact ground state energy of a system, proposed by Hohenberg and Kohn in 1964 [62]. Rather than using the wavefunction, which depends on three spatial coordinates and one spin coordinate for every electron, they proposed using a single observable property, the electron density of the system. In this method, known as density functional theory (DFT), the energy of the system is defined as a functional

(function of a function) of the electron density that depends on only three spatial coordinates:

$$E_0 = F[\rho(\mathbf{r})] = F[\rho(x, y, z)]. \tag{1.19}$$

Hohenberg and Kohn proposed that there exists a universal functional that describes a system exactly [62], however, its formulation still remains unknown. Shortly thereafter, Kohn and Sham proposed the Kohn-Sham (KS) equation [63]:

$$\hat{F}^{\mathrm{KS}}(\mathbf{r}_n)\phi_i^{\mathrm{KS}}(\mathbf{r}_n) = \varepsilon_i^{\mathrm{KS}}\phi_i^{\mathrm{KS}}(\mathbf{r}_n), \tag{1.20}$$

where $\hat{F}^{\mathrm{KS}}$ is the Kohn-Sham operator, ϕ_i^{KS} are the Kohn-Sham orbitals, and $\varepsilon_i^{\mathrm{KS}}$ the Kohn-Sham orbital energies. Similarly to the Fock operator, the KS operator contains a Coulomb operator, but it also contains an exchange-correlation operator which takes into account both the electron-electron exchange and correlation energetic effects. The total energy of a system can then be represented as

$$E_{\mathrm{total}}[\rho(\mathbf{r})] = \mathbf{T}[\rho(\mathbf{r})] + \mathbf{V}_{ne}[\rho(\mathbf{r})] + \mathbf{V}_{ee}[\rho(\mathbf{r})] + \mathbf{E}_{XC}[\rho(\mathbf{r})]. \tag{1.21}$$

A more thorough look at the formulae of DFT can be read in Cramer [46].

As the exact functional is unknown, there are many functionals for DFT which exist to describe chemical systems. Different styles of functionals exist too, ranging from the Local-Density Approximation (LDA), to double-hybrid functionals [64] which include the addition of both HF and MP2 electron correlation. These methods and the references to original works are discussed further in Chapter 3.

1.2.4 Basis Sets

The orbitals used in both WFT and DFT are made as linear combinations of many basis functions:

$$\phi_a(\mathbf{r}) = \sum_{i=1}^{K} a_i \chi_i(\mathbf{r}), \tag{1.22}$$

where χ_i are the basis functions and each a_i is an unknown coefficient for which we wish to solve. The basis functions themselves typically take the form of Gaussian-type

functions [65]. In order to better describe the system of study, we expand the size of our basis set to include more basis functions to represent each orbital.

Many different types of basis sets exist, each with their own uses. Basis sets can be augmented with extra diffuse functions, or include polarization functions. There are also many which aim to aid in the inclusion of relativistic effects. Lastly, there are basis sets which approximate inner core electrons as an average core potential, rather than include them all explicitly. For example, the work in Chapter 2 includes a so-called psuedopotential (effective core potential) for germanium atoms [66], which describes the inner ten electrons as a core potential.

1.3 Thesis Objectives

In this Thesis, using the methods outlined above, cyclic tetra-atomic germanium-containing molecules are investigated as novel targets for observation in the ISM. Silicon-carbide molecules are known to exist in the ISM as molecules making up interstellar dust, and specifically a cyclic tetra-atomic diamond-shaped silicon-carbide molecule has been detected [9]. This work offers accurate spectroscopic data for germanium analogues of these tetra-atomic silicon-carbide compounds. In Chapter 2, high-level computational methods are employed to generate anharmonic vibrational frequencies and vibrationally-averaged rotational constants of a suite of germanium carbide and germanium silicide molecules. These data are determined with the intention of providing a reference when searching for these compounds in the ISM. Chapter 3 then focuses on the possibility of interconversion between isomers of the same chemical formula in the ISM, examining the transition states and the barrier heights associated with them. This work in Chapter 3 not only examines the germanium-containing compounds explored in the Chapter 2, but also includes a study of the transition states between silicon-carbide molecules as well.

Chapter 2

Anharmonic vibrational spectroscopy of germanium-containing clusters, Ge_xC_{4-x} and Ge_xSi_{4-x} (x = 0-4), for interstellar detection

2.1 Introduction

With the launch of the James Webb Space Telescope (JWST) in 2021, the ability to peer into the Universe and pull out information from it has vastly improved. The instrumentation on JWST provides data in the mid-IR range (0.6 - 28.3 μm [$\sim$353 - $\sim$16667 cm^{-1}]) at a higher sensitivity, drastically increasing the possibility of identifying new compounds through infrared spectroscopy. For some of the more exotic and elusive molecules that might exist in the interstellar medium (ISM), high-level computational studies are an important step in potential identification of molecules in space. Accurate theoretical data provide reference points for collected astronomical observations. To that end, specifically with JWST's operations in the mid-IR range, accurate ro-vibrational data are needed to provide reference for the spectra that are measured.

An area of interest to astrochemists and astronomers is the study of star-forming regions and protoplanetary disk formation [67, 68], including the formation of dust

grains in the ISM. Determining the composition of these dust grains and observing their accretion into proto-planetary disks could help elucidate what kind of stars and planetesimals might be forming in different regions of space.

Silicon carbide clusters have been suggested to be involved in the formation of SiC dust grains in the ISM, which have been seen in proto-planetary dust clouds [29–31, 69, 70]. These clusters are thought to be formed from the result of carbon and silicon formation through nucleosynthesis in asymptotic giant branch (AGB) stars [36, 70]. However, their fellow group member germanium is also known to form through nucleosynthesis in AGB stars through the slow neutron capture s-process [38, 40].

Throughout the ISM, germanium is much less abundant than carbon and silicon and might prove more elusive to detect. As a result, interstellar germanium chemistry is less documented. Germanium has been detected both near and far: in the atmosphere of Jupiter, planetary nebulae, and in some of the most distant galaxies [37–39]. Understanding the pathways germanium takes to be dispersed throughout the Universe is an interesting topic that could give more insight into dust grain formation and rocky planet formation from resulting dust clouds. With the recent discovery of an iron-rich sub-earth exoplanet, GJ 367b, orbiting a nearby dwarf star, there is no end to the interesting exoplanets that could be found [71]. With the potential to discover more metal-rich planets, it's important to shed light on the chemistry of heavier elements throughout the ISM.

To begin understanding the chemistry of interstellar germanium, there is a need for determining structures and corresponding spectroscopic signatures for model molecules. Currently, a small group of silicon carbide molecules including the diatomic SiC, triatomic species SiC_2 and Si_2C, as well as the cyclic tetra-atomic SiC_3 has been identified in the ISM. [9, 29–31, 72] With the potential for various permutations of tetra-atomic germanium silicide and carbide analogues of SiC tetra-atomics, we can consider these tetra-atomics as a starting point of interest.

Multiple experimental and computational studies have been previously carried out

on silicon carbide tetra-atomic clusters [9, 32, 73–83], but only a few have investigated germanium carbide and silicide clusters [84, 85]. The smaller germanium carbide and germanium silicide (triatomic) molecules as well as linear molecules have been previously studied both experimentally and computationally at various levels of theory [84–90]. However, in the area of germanium tetra-atomics, an extensive study of the various permutations of tetra-atomic germanium carbide and silicide clusters has not yet been done, computationally or experimentally. Also, more accurate computational methods have become accessible since previous publications and the determination of results at a higher-level of theory is worthwhile for use in astrochemical pursuits.

As mentioned, in the context of interstellar dust grains, tetra-atomic silicon carbide clusters have recently been extensively studied by Sehring et al. using the CCSD(T)-F12b method with basis sets cc-pVTZ-F12 and cc-pCVTZ-F12 [73]. The second method employs the cc-pCVTZ-F12 basis set to incorporate core electron correlation and scalar relativity effects [91, 92]. Herein, we study tetra-atomic germanium carbide and silicide clusters at a similar level of theory. All structures studied consist of a quadrilateral motif with a transannular bond that include molecules of the form Ge_xZ_{4-x} (x=0-4), where Z is either carbon or silicon.

Both pure carbon and silicon tetra-atomic clusters have been previously studied at the coupled-cluster level of theory including CCSD(T)/cc-pCV5Z [93] and CCSD(T)-F12b/cc-p(C)VTZ-F12 respectively [73], and the pure carbon cluster has also been studied experimentally [94, 95]. Therefore quite accurate spectral data are already present for them. However, for completeness we have included them in our current study.

Moving to the first of the sets of germanium analogues, GeC_3 and $GeSi_3$, both have been looked at previously computationally, however only GeC_3 has had (harmonic) vibrational data generated [84]. For the cyclic GeZ_3 structures, there exist two isomers: diamond GeZ_3 and rhomboidal GeZ_3, which will be from here on be referred to as d-GeZ_3 and r-GeZ_3, respectively. The d-GeZ_3 is identified by the transannular

Z-Z bond and the r-GeZ_3 by a Ge-Z transannular bond. All four of these structures exhibit C_{2v} symmetry. In the case of both r- and d-GeC_3, the available theoretical data was obtained using density functional theory (DFT) with the B3LYP functional [96, 97], CCSD [98], and second-order Møller-Plesset perturbation theory (MP2), all in conjunction with the aug-cc-pVTZ basis set [84].

With the Ge_2Z_2 structures, there are three isomers to consider: d- and r- as well as a trapezoidal shaped (t-) isomer. For these structures, the d- isomers are identified by a transannular Ge-Ge bond, the t- isomers by a transannular Ge-Z bond, and the r- isomers by a transannular Z-Z bond. Both r- isomers and the d-Ge_2Si_2 isomer exhibit D_{2h} symmetry. The two t-Ge_2Z_2 structures exhibit C_s symmetry. Finding an optimized structure for the remaining d-Ge_2C_2 isomer proved challenging and this will be discussed further below. However, we predict it to exist in either a planar or a boat-like configuration, both with C_{2v} symmetry. Similarly to the r- and d- structures of GeC_3, previous theoretical data for the r- and t-Ge_2Z_2 structures are available [84].

Lastly, there are four Ge_3Z structures of interest, with d- and r- isomers as in the GeZ_3 structures. The r- isomers are again distinguished by a Ge-Z transannular bond and the d- isomers by a Ge-Ge transannular bond. The d-Ge_3C has C_s symmetry, having a slight dihedral angle taking it out of plane and out of C_{2v} symmetry, which is seen in the three other structures in this group (r-Ge_3C, d-Ge_3Si, r-Ge_3Si). Of these four structures, only d-Ge_3C has been studied previously at the B3LYP/6-311G(3df) level of theory [86].

It is worth noting that while both carbon and silicon have one naturally occurring isotope dominating in abundance (>90%), germanium has multiple isotopes with relatively high abundances, specifically ^{74}Ge, ^{72}Ge, and ^{70}Ge, with abundances of 36.5%, 27.4%, and 20.5%, respectively [99]. Other naturally occuring isotopes with smallar abundances are ^{73}Ge and ^{76}Ge, with abundances of 7.76% and 7.75%, respectively [99]. The effect of these isotopes on detectable spectra will be discussed further below. For the purpose of this study, we have used the most abundant isotope masses for

each atom (^{12}C, ^{28}Si, and ^{74}Ge).

As many of these structures have not yet been examined computationally, and those that have been studied have not had high-level methods applied to them, there exists an opening to apply modern wavefunction-based approaches to the study of these tetra-atomic germanium-contatining structures and their corresponding rovibrational spectra. Herein, we present theoretical spectroscopic data for structures described above using high-level computational methods. Accurate (harmonic and anharmonic) vibrational frequencies and (vibrationally-averaged) rotational constants could help in identifying these structures in planetary atmospheres, planetary nebulae, near distant AGB stars, and other ISM environments through use of JWST.

2.2 Computational Methods

All computations were carried out as follows. Geometries, harmonic, and anharmonic vibrational frequencies were determined using the explicitly-correlated coupled-cluster theory at the singles, doubles, and perturbative triples level CCSD(T)-F12 [100–102]; depending on the basis set size, either the F12a or F12b formalism was used [101]. The cc-pVXZ-F12 basis sets were used for carbon and silicon atoms, while a pseudopotential with associated basis set (cc-pVXZ-PP-F12) was used for germanium atoms, where X=T or Q [66, 103]. It has been previously shown that the F12a method provides a better estimate of correlation energies for smaller basis sets (double-/triple-zeta), while the F12b method is reportedly better when using larger basis sets (quadruple-zeta); both methods converge to the complete basis set (CBS) limit from above and below, respectively [101, 104]. The names of the two methods will be herein shortened as F12a/TZ and F12b/QZ.

The MOLPRO 2023.2 software was used for all calculations in this work [105–107]. For each molecule, geometry optimization was first carried out at the F12a/TZ or F12b/QZ level of theory followed by harmonic frequency calculations [108–111]. Default convergence criteria were used for all optimization calculations. Dipole mo-

ments were retrieved at all optimized geometries, using the PROPERTY directive at the CCSD(T)-F12a level of theory. Subsequently, anharmonic frequencies were calculated through second-order vibrational perturbation theory (VPT2) as implemented in MOLPRO [112–114]. An analytical representation of the potential energy surface is generated in the form of a quartic force field, which is then used to retrieve force constants. Using VPT2, anharmonic vibrational frequencies and vibrationally-averaged rotational constants were obtained. As the F12a/TZ and F12b/QZ methods are both able to converge to the complete basis set limit [101, 102], F12b/QZ was only applied to a select few systems for comparison with F12a/TZ and determination of the cost/accuracy benefit.

2.3 Results and Discussion

Using the methods outlined above, computations were performed on the suite of germanium carbide and germanium silicide molecules of the form Ge_xZ_{4-x}, where x = 0-4. Across all species, the frequencies of the calculated anharmonic vibrational modes mostly fall within the 0.6 - 28.3 μm ($\sim$353 - $\sim$16667 cm^{-1}) mid-IR range of JWST.

As mentioned previously, many of these molecules have not yet been studied experimentally or theoretically. However, there exist previous studies on a few structures investigated herein, which have been used for comparison with the present work [73, 84]. Equilibrium structures of all systems studied are presented in figures with bond distances and angles shown, while Cartesian coordinates and energies for the optimized structures are found in Appendix A.

Table 2.1 shows relative electronic energies, corrected for harmonic and anharmonic zero-point vibrational energies (ZPVE), of optimized structures (in kJ mol^{-1}), with respect to the lowest lying isomer in each group, as well as symmetry of each structure and dipole moments. The zero-point energies as well as the energies of each structure with the ZPVE added and their relative energies are shown in Table A1.

Table 2.1: Ge_xZ_{4-x} family relative energies (in kJ mol^{-1}) of optimized geometries with inclusion of harmonic and anharmonic zero-point vibrational energy (ZPVE). Relative energies are taken with respect to the lowest energy isomer in each group. Dipole moments (μ, in Debye) at each optimized geometry are included. All results at F12a/TZ level of theory.

Structure	Symmetry	ΔE_0^{ZPVE}		μ
		(Harmonic)	(Anharmonic)	
d-GeC_3	C_{2v}	0.000	0.000	5.40
r-GeC_3	C_{2v}	10.540	10.603	2.95
t-Ge_2C_2	C_s	0.000	0.000	3.52
r-Ge_2C_2	D_{2h}	20.414	20.381	0.00
d-Ge_2C_2[a]	C_{2v}	397.491		2.03
r-Ge_3C	C_{2v}	0.000	0.000	0.11
d-Ge_3C	C_s	189.830	189.778	0.98
d-$GeSi_3$	C_{2v}	0.000	0.000	0.79
r-$GeSi_3$	C_{2v}	16.982	16.957	0.01
r-Ge_2Si_2	D_{2h}	0.000	0.000	0.00
t-Ge_2Si_2	C_s	12.871	12.862	0.77
d-Ge_2Si_2	D_{2h}	32.643	32.637	0.00
r-Ge_3Si	C_{2v}	0.000	0.000	0.04
d-Ge_3Si	C_{2v}	15.666	15.660	0.76

[a]CCSD(T)-F12a/cc-pVDZ-F12

To test the effects of correlating the d-orbitals of germanium, geometry optimizations and harmonic frequency calculations were carried out including d-orbitals in the valence space for the r-Ge_2C_2 and t-Ge_2C_2 isomers. These results are provided in Tables A7 and A8. Correlating the d-orbitals can be seen to lead to small changes in vibrational frequencies (<10 cm^{-1} or <2%), rotational constants (<160 MHz or <2.5%), dipole moment (0.07 D or 2%), and relative energies including ZPVE (∼1 kJ mol^{-1}). Thus, results reported herein are for computations without correlating the d-orbitals. Therefore, the present vibrational frequencies are only accurate to ca. ± 5-10 cm^{-1}, however, they are reported here to one decimal place to ease comparison with any future computational work.

2.3.1 r-Z_4

The equilibrium structures of the mono-elemental tetra-atomic clusters, C_4, Si_4, and Ge_4 are shown in Figure 1. Vibrational frequencies for r-Si_4 and r-Ge_4 are shown in Table 2.2, while their rotational constants can be found in Table A2. As the tetra-atomic carbon cluster has been studied extensively, only Si_4 and Ge_4 results are shown here; those for carbon can be found in Tables A3 and A4. Anharmonic vibrational frequencies for r-C_4 were calculated at both the F12a/TZ and F12b/QZ levels of theory. To compare different methods, the mean absolute percent deviation (MAPD), defined as the absolute difference between results obtained with the two methods divided by the more accurate method divided by the number of cases multipled by 100%, is reported where relevant, i.e.

$$\text{MAPD} = \left(\frac{1}{N} \sum_{i=1}^{N} \left| \frac{A_i - A_{\text{ref}}}{A_{\text{ref}}} \right| \right) \times 100\%.$$

For r-C_4 the F12a/TZ method is seen to have a MAPD of 0.12% from the F12b/QZ results, but with the computation taking around nine times less wall clock time to complete. This comparison supports the previous observation [101, 102] that the two methods converge to similar results. For r-Si_4, computed results are similar to those

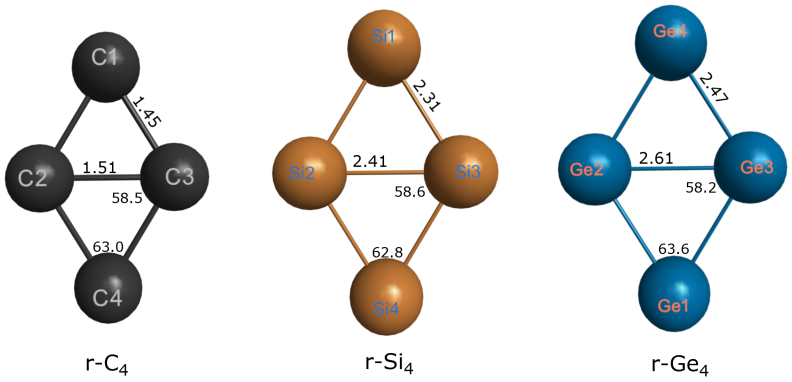

Figure 2.1: Optimized geometries of Z_4 structures at the CCSD(T)-F12a/cc-pVTZ-F12 level of theory. Bond lengths shown in Å, angles in degrees.

computed at the best current level of theory in the literature from Sehring et al [73]. Computed anharmonic vibrational frequencies and rotational constants show MAPDs (for F12a/TZ with respect to F12-TZ-cCR) of 0.60% and 1.31% respectively, indicating the F12a/TZ method has exceptionally high accuracy in comparison with the F12-TZ-cCR method used in the work of Sehring et al [73]. This comparison illustrates the small but non-negligible effects of core-valence correlation and relativistic effects that are accounted for in the F12-TZ-cCR approach [73].

For the tetra-atomic pure germanium structure, the vibrational mode most promising for observation would be ν_6 with an intensity of 58.8 km mol^{-1}, however its frequency of 280.0 cm^{-1} falls outside the range of JWST's mid-IR observing capabilities. With no permanent dipole moment, this molecule is unlikely to be detected with current instruments whether through IR spectroscopy or rotational spectroscopy.

2.3.2 GeZ_3

Optimized geometries for each GeZ_3 structure are shown in Figure 2. Between the two GeC_3 structures, d-GeC_3 was found to lie 1.140 kJ mol^{-1} lower (0.776 kJ mol^{-1} when corrected for ZPVE) than r-GeC_3. Although these two isomers have a very

Table 2.2: Harmonic and anharmonic fundamental vibrational frequencies (in cm^{-1}) of r-Si_4 and r-Ge_4. MAPD is shown for F12a/TZ with respect to F12-TZ-cCR for anharmonic frequencies. Anharmonic intensities (in km mol^{-1}) for F12a/TZ calculations are from this work.

Mode	Symmetry	Harmonic		Anharmonic		Intensity
r-Si_4	D_{2h}	F12a/TZ	F12-TZ-cCR[a]	F12a/TZ	F12-TZ-cCR[a]	
6	B_{1u}	510.4	512.5	503.3	505.9	147.1
5	A_g	476.9	479.2	471.7	476.1	0.0
4	B_{2g}	439.4	442.4	433.3	436.6	0.0
3	A_g	350.4	353.0	347.5	350.0	0.0
2	B_{3u}	253.0	254.0	250.5	251.9	8.3
1	B_{2u}	75.4	75.1	76.3	76.2	2.2
MAPD				0.60		
r-Ge_4	D_{2h}					
6	B_{1u}	282.8		280.0		58.8
5	A_g	265.4		266.6		0.0
4	B_{2g}	239.5		237.1		0.0
3	A_g	188.1		187.0		0.0
2	B_{3u}	133.1		132.0		0.1
1	B_{2u}	49.1		49.4		0.2

[a]Sehring et al. 2022

small energy difference between them, recent work has shown that there is an energy barrier between the two of 166.2 kJ mol^{-1} at the B2GP-PLYP/aug-cc-pVTZ level of theory [115]. With a slightly larger energy difference, d-$GeSi_3$ was found to be the lower energy isomer compared to r-$GeSi_3$, with an energy difference of only 17.256 kJ mol^{-1}. Previously, d-SiC_3 was detected in space towards IRC+10216 through its rotational spectrum by the ALMA telescope array [9]. When considering similarities between d-SiC_3 and d-GeC_3, they both have large dipole moments of 4.2 and 5.4 D, respectively [73]. Although d-GeC_3 does not have the most intense of vibrational modes between the GeC_3 isomers, its large dipole moment indicates the possibility of detection by rotational spectroscopy.

Vibrational frequencies and rotational constants for the GeZ_3 structures are presented in Tables 2.3-2.5. All four structures have one vibrational mode with relatively strong intensity, with the r- isomers having the strongest at 112.0 and 107.0 km mol^{-1} for GeC_3 and $GeSi_3$, respectively. These two vibrational modes correspond to the 2-3-4 asymmetric stretch where atoms 2, 3, and 4 are either carbon or silicon as seen in Figure 2. Many vibrational modes fall within the observable range of JWST, however the smaller frequency modes (<353 cm^{-1}, about half of them for the $GeSi_3$ isomers), fall outside of that range.

Computed anharmonic vibrational frequencies for d-GeC_3 at the F12a/TZ level have a MAPD of 0.12% relative to the F12b/QZ frequencies. However, the computation time increased by almost a factor of six for the F12b/QZ calculation compared to the F12a/TZ calculation. Therefore, when considering the method of choice for these systems, the increase in computational cost associated with F12b/QZ is likely not worth the small gain in accuracy.

2.3.3 Ge_2Z_2

Six Ge_2Z_2 structures were considered. Equilibrium structures for the three Ge_2C_2 and three Ge_2Si_2 isomers are shown in Figure 3. Vibrational frequencies and rotational

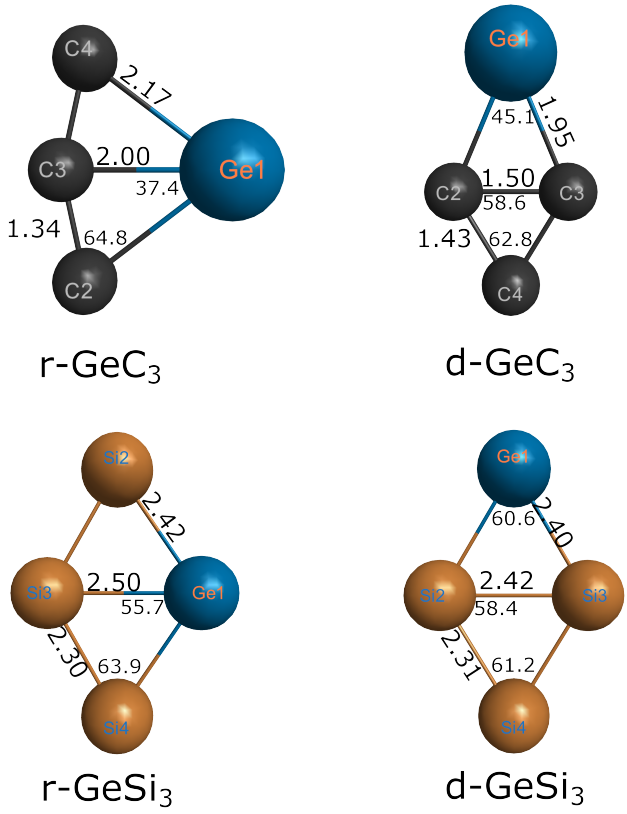

Figure 2.2: Optimized geometries of GeZ_3 structures at the CCSD(T)-F12a/cc-pVTZ-F12 level of theory. Bond lengths shown in Å, angles in degrees.

Table 2.3: Harmonic and anharmonic fundamental vibrational frequencies (in cm^{-1}) of GeC_3 isomers. Both F12a/TZ and F12b/QZ have been used for d-GeC_3. MAPD is shown for F12a/TZ with respect to F12b/QZ for anharmonic frequencies. Anharmonic intensities in km mol^{-1}.

Mode	Symmetry	Harmonic		Anharmonic		Intensity
d-GeC_3		a/TZ	b/QZ	a/TZ	b/QZ	
6	A_1	1389.7	1390.6	1421.8	1422.8	88.9
5	B_1	1020.6	1021.3	993.0	993.6	1.4
4	A_1	912.2	912.4	891.9	892.2	50.6
3	A_1	518.5	519.0	512.7	513.3	72.8
2	B_1	355.4	356.3	348.1	349.0	36.9
1	B_2	219.9	220.0	219.9	220.3	3.5
MAPD				0.12		
r-GeC_3						
6	B_2	1574.4		1538.3		112.0
5	A_1	1118.0		1096.3		2.2
4	A_1	720.4		709.8		28.1
3	A_1	415.1		408.8		26.9
2	B_2	338.1		332.4		2.4
1	B_1	178.3		191.8		24.6

[a]F12a/TZ intensities

Table 2.4: Harmonic and anharmonic fundamental vibrational frequencies (in cm^{-1}) of $GeSi_3$ isomers using F12a/TZ. Anharmonic intensities in km mol^{-1}.

Mode	Symmetry	Harmonic	Anharmonic	Intensity
d-$GeSi_3$				
6	A_1	496.4	490.0	92.1
5	A_1	426.2	421.9	29.2
4	B_1	416.7	411.1	0.1
3	A_1	273.5	271.7	7.9
2	B_1	217.8	216.4	5.5
1	B_2	69.0	69.7	1.1
r-$GeSi_3$				
6	B_2	503.3	495.8	107.0
5	A_1	430.2	430.0	1.5
4	B_2	326.5	322.6	13.9
3	A_1	308.1	305.8	1.9
2	A_1	209.2	207.5	1.1
1	B_1	72.9	73.1	2.0

Table 2.5: Equilibrium (e) and vibrationally-averaged (0) rotational constants of GeC_3 and $GeSi_3$ isomers in MHz at the F12a/TZ level of theory and F12b/QZ for d-GeC_3. In each case, ν_6 was the most intense mode, thus vibrationally-averaged constants for this mode are included (6).

Constant	d-GeC_3	F12b/QZ	Constant	r-GeC_3	Constant	d-$GeSi_3$	Constant	r-$GeSi_3$
A_e	37654.4	37685.7	A_e	12195.1	A_e	6175.1	A_e	3530.6
B_e	3891.2	3893.8	B_e	6286.6	B_e	1387.7	B_e	2264.8
C_e	3526.7	3529.1	C_e	4148.2	C_e	1133.1	C_e	1379.7
A_0	37333.8	37364.3	A_0	12929.4	A_0	6150.5	A_0	3520.1
B_0	3876.4	3879.0	B_0	6252.5	B_0	1385.3	B_0	2260.3
C_0	3509.5	3511.9	C_0	4128.7	C_0	1130.5	C_0	1376.1
A_6	36031.0	36065.6	A_6	12287.4	A_6	6096.4	A_6	3500.4
B_6	3885.1	3887.6	B_6	6223.3	B_6	1388.6	B_6	2264.3
C_6	3521.0	3523.4	C_6	4142.8	C_6	1134.0	C_6	1379.0
MAPD	0.08							

constants for each structure are presented in Tables 2.6 and 2.7. For this group of structures we have again chosen to use both F12a/TZ and F12b/QZ to compare results for r-Ge_2C_2. Frequencies and rotational constants for the two methods show MAPDs of 0.18% and 0.07%, respectively, for F12a/TZ with respect to F12b/QZ, again supporting the conclusion that the increase in computational cost (a factor of eight in this case) has a negligible effect on accuracy gained. Among all structures studied in this work, r-Ge_2C_2 showed a vibrational frequency with an intensity well above all other vibrational modes. An intensity of 307.2 km mol^{-1} is predicted for ν_3 which is the Ge(1)-C(1) and Ge(2)-C(2) symmetric stretch at 801.7 cm^{-1}. With such a large intensity, observation of this mode is a likely candidate for detection by JWST. The t-isomer does not have any vibrational modes with high intensities, and is thus less likely to be detected by JWST.

As mentioned, the d-Ge_2C_2 structure posed a challenge to optimize. An equilibrium

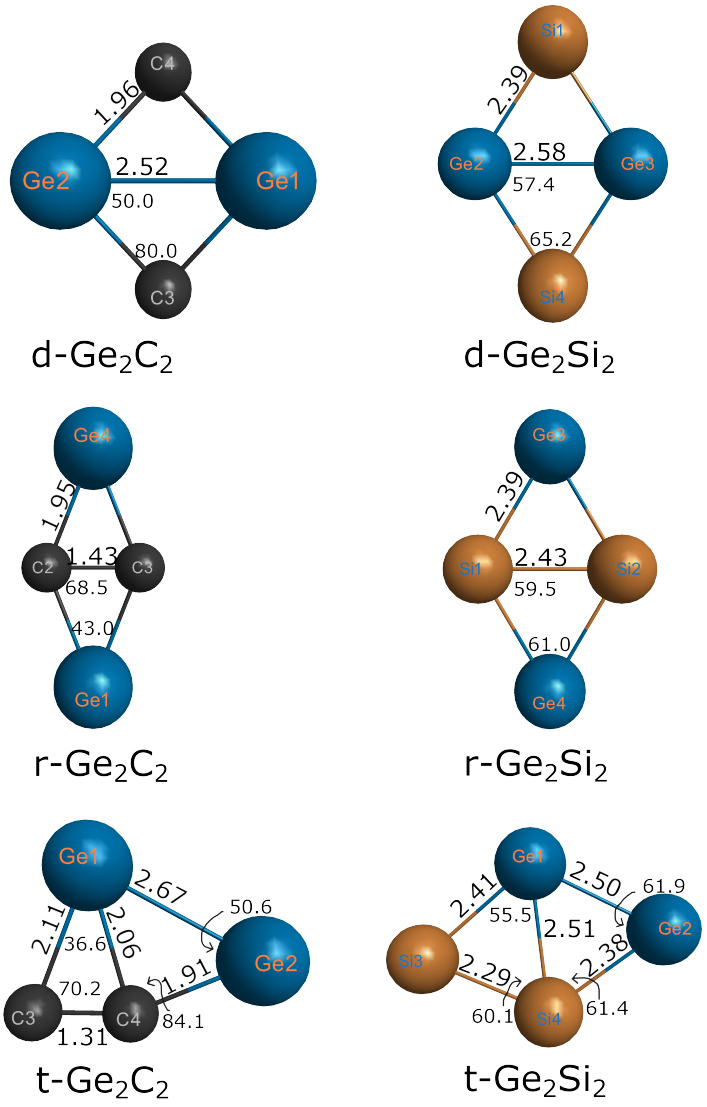

Figure 2.3: Optimized geometries of Ge_2Z_2 structures at the CCSD(T)-F12a/cc-pVTZ-F12 level of theory. Bond lengths shown in Å, angles in degrees. The d-Ge_2C_2 structure is in C_{2v} symmetry, with the carbon atoms going out of plane.

structure was found using the smaller double-zeta basis set (cc-pVDZ-F12) [103], with a boat-like geometry. However, this structure was found to have a T_1 diagnostic [60] of 0.098, suggesting multi-reference character, and thus this level of theory might not allow for an accurate description of this structure. A table of T_1 diagnostics for all clusters considered in this work is shown in Table A5. For the majority of structures, T_1 was below the 0.02 threshold indicating single-reference character. The d-Ge_3C has a T_1 value of 0.039, which indicates that this structure likely shows some multi-reference character. To confirm the multi-reference character of the d-Ge_2C_2 structure, we carried out a CASSCF(16,16)/aug-cc-pVTZ [116–122] calculation at the CCSD(T)-F12a/cc-pVDZ-F12 optimized geometry to determine the configuration coefficients. The leading coefficient for the d-Ge_2C_2 structure is 0.8573, indicating large contributions from other configurations. To confirm single-reference character of the species, CASSCF single point calculations were carried out on each optimized structure and results are shown in Table A6. Notably, the leading coefficients in the expansion of the wavefunction for all other structures (not d-Ge_2C_2) were about 0.9. For the two Ge_3C structures which had T_1 values larger than 0.02, their CASSCF leading coefficients are still similar to those of the structures with smaller T_1 values. It may be worth re-examining these two Ge_3C structures more thoroughly with multi-reference methods to see how the resulting structures and spectroscopic properties are affected.

Of the three Ge_2C_2 isomers, the t- structure has the lowest energy. The total energy of the r- structure is larger by 20 kJ mol^{-1}, and the d- isomer by 402 kJ mol^{-1}. The CASSCF single point calculations predict the same trends in energies, but predict a gap twice as large between the t- and d- structures at 800 kJ mol^{-1}. The CASSCF total and relative energies are shown in Table A6.

None of the vibrational modes for the t- isomer are relatively intense, however this molecule has a dipole moment of 3.52 D. The d- isomer has dipole moment of 2.52 D at the F12a/DZ level of theory, however, due to its multi-reference character it is

uncertain whether this structure and dipole value are reliable. Lastly, the r- isomer of Ge_2C_2 has no net dipole moment, making only the t- isomer a likely candidate for detection by rotational spectroscopy.

Predicted vibrational frequencies for the Ge_2Si_2 isomers fall on the lower end of the detection range for JWST. Results for these three structures are shown in Tables A9 and A10. Each structure has only one vibrational mode that could be detected, with the r- isomer having the largest intensity for the ν_5 mode, the symmetric stretch of Ge(1)-Si(1) and Ge(1)-Si(2) at 402.0 cm^{-1}, with an intensity of 119.8 km mol^{-1}. The isomer d-Ge_2Si_2 also has a relatively intense mode at 391.2 cm^{-1} with an intensity of 86.9 km mol^{-1}, however, it has larger energy by 32.637 kJ mol^{-1} than the isomer with the lowest energy, r-Ge_2Si_2.

Having D_{2h} symmetry, neither the r- nor d- isomer of Ge_2Si_2 exhibit dipole moments, and therefore could not be detected through rotational spectroscopy. Unlike the carbon analogue of the t- isomer, t-Ge_2Si_2 has a very small permanent dipole moment of 0.76 D, making it a less likely candidate for detection via rotational spectroscopy.

2.3.4 Ge_3Z

The optimized Ge_3Z structures are shown in Figure 4. None of these four molecules show strong permanent dipole moments with the d-Ge_3C and d-Ge_3Si isomers having the largest at 0.98 D and 0.76 D, respectively. These molecules are thus more likely to be identified through their vibrational spectra. Results for the Ge_3C structures are shown in Tables 2.8 and 2.9, while vibrational frequencies for the Ge_3Si structures are collected in Table A11. Both r- isomers exhibit ν_6 vibrational modes at 941.8 cm^{-1} and 407.3 cm^{-1}, and with relatively large intensities of 103.2 km mol^{-1} and 81.1 km mol^{-1} for r-Ge_3C and r-Ge_3Si, respectively. Another predicted intense mode is the ν_5 mode of r-Ge_3C at 513.6 cm^{-1} with an intensity of 87.9 km mol^{-1}. The r- carbon structure lies 189.778 kJ mol^{-1} below the d- isomer (Table 2.1), making it more likely

Table 2.6: Harmonic and anharmonic fundamental vibrational frequencies (in cm^{-1}) of Ge_2C_2 isomers at the F12a/TZ (and F12b/QZ, or F12a/DZ) level of theory. Anharmonic intensities in km mol^{-1}.

Mode	Symmetry	Harmonic		Anharmonic		Intensity
r-Ge_2C_2		F12a/TZ	F12b/QZ	F12a/TZ	F12b/QZ	
6	A_g	1102.2	1103.2	1070.7	1071.8	0.0
5	B_{2g}	868.4	869.2	850.0	851.2	0.0
4	B_{1u}	816.1	816.9	801.7	802.7	307.2
3	A_g	281.9	282.3	271.9	272.0	0.0
2	B_{3u}	276.7	277.1	273.0	274.0	64.5
1	B_{2u}	147.3	147.2	147.1	147.6	11.9
MAPD				0.18		
t-Ge_2C_2		F12a/TZ				
6	A'	1581.2		1555.8		29.0
5	A'	575.8		570.2		45.8
4	A'	515.5		509.5		35.6
3	A'	392.5		391.0		11.0
2	A'	182.7		181.4		0.8
1	A''	179.1		178.7		3.8
d-Ge_2C_2		F12a/DZ				
6	A_1	599.7				0.0
5	B_1	550.7				0.0
4	B_2	444.4				0.0
3	A_2	415.0				0.0
2	A_1	280.9				0.0
1	A_1	233.1				0.0

Table 2.7: Equilibrium (e) and vibrationally-averaged (0) rotational constants of Ge_2C_2 isomers in MHz at the F12a/TZ level of theory and F12b/QZ level for r-Ge_2C_2. For r-Ge_2C_2, vibrationally-averaged rotational constants for its most intense mode, ν_4, are also included.

Constant	r-Ge_2C_2	F12b/QZ
A_e	41435.1	41476.6
B_e	1039.7	1040.3
C_e	1014.3	1014.8
A_0	41100.2	41140.1
B_0	1036.9	1037.5
C_0	1011.3	1011.8
A_4	41110.0	41149.5
B_4	1035.6	1036.2
C_4	1010.0	1010.6
MAPD		0.07
	t-Ge_2C_2	F12a/TZ
A_e		7721.4
B_e		1824.1
C_e		1475.5
A_0		7684.6
B_0		1822.3
C_0		1472.0
	d-Ge_2C_2	F12a/DZ
A_e		9435.3
B_e		2129.4
C_e		1770.7

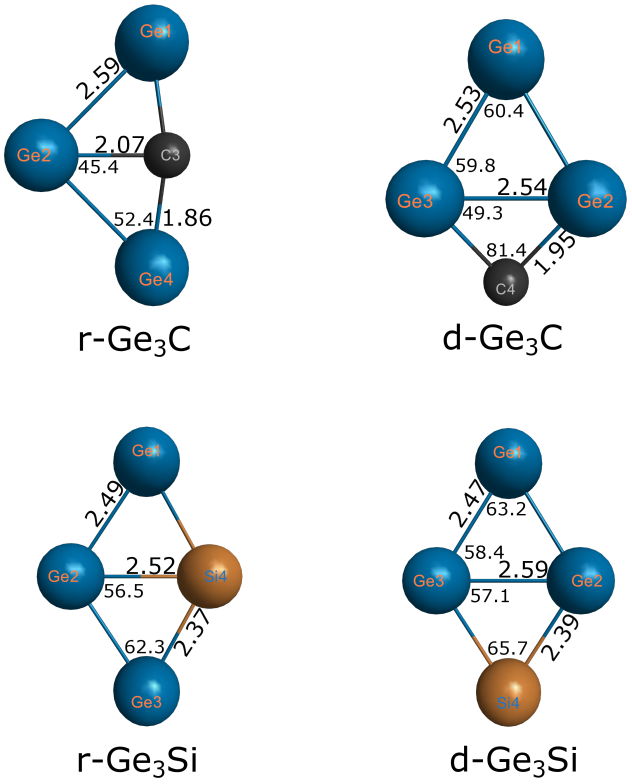

Figure 2.4: Optimized geometries of Ge_3Z structures at the CCSD(T)-F12a/cc-pVTZ-F12 level of theory. Bond lengths shown in Å, angles in degrees.

to be detected through its stronger IR spectra. The r- silicon isomer lies only 15.670 kJ mol^{-1} below the d- isomer, suggesting it may be possible to see interconversion between the two with such a small energy difference, assuming a small barrier between them. However, due to the r- isomer having a more intense vibrational mode in its spectrum, it is likely that the r- isomer would be detected over the d- isomer.

2.3.5 Isotopic Substitution

Unlike carbon and silicon, germanium does not have a dominant, naturally occurring isotope. Instead, the majority of abundance is split between three isotopes: ^{74}Ge, ^{72}Ge, and ^{70}Ge, with abundances of 36.5%, 27.4%, and 20.5%, respectively [99]. The two other naturally occurring isotopes, ^{73}Ge and ^{76}Ge, have abundances of 7.76%

Table 2.8: Harmonic and anharmonic fundamental vibrational frequencies in cm^{-1} of Ge_3C isomers using F12a/TZ. Anharmonic intensities in km mol^{-1}.

Mode	Symmetry	Harmonic	Anharmonic	Intensity
d-Ge_3C				
6	A'	626.0	619.2	6.8
5	A''	513.0	499.7	0.7
4	A'	271.6	271.1	0.4
3	A'	228.6	225.0	26.3
2	A''	151.0	150.0	0.1
1	A'	63.6	31.8	18.3
r-Ge_3C				
6	B_2	956.4	941.8	103.2
5	A_1	518.4	513.6	87.9
4	A_1	291.8	300.7	7.7
3	B_2	200.8	198.7	10.4
2	A_1	178.9	176.7	2.3
1	B_1	140.5	141.5	2.9

Table 2.9: Equilibrium (e) and vibrationally-averaged (0) rotational constants of Ge_3C and Ge_3Si isomers in MHz at the F12a/TZ level of theory. Vibrationally-averaged constants for the most intense vibration for each isomer are also included.

Constant	d-Ge_3C	Constant	r-Ge_3C	Constant	d-Ge_3Si	r-Ge_3Si	
A_e	2108.1	A_e	2949.3	A_e	2031.9	A_e	3216.0
B_e	1746.3	B_e	1002.5	B_e	1259.3	B_e	789.8
C_e	959.8	C_e	748.2	C_e	777.5	C_e	634.0
A_0	2113.4	A_0	2937.6	A_0	2027.8	A_0	3207.8
B_0	1736.0	B_0	1001.5	B_0	1257.2	B_0	788.7
C_0	955.1	C_0	746.4	C_0	775.8	C_0	632.9
A_3	2107.6	A_6	2916.9	A_6	2019.8	A_6	3186.0
B_3	1737.4	B_6	1005.7	B_6	1258.5	B_6	790.2
C_3	954.5	C_6	748.4	C_6	777.0	C_6	634.3

and 7.75%, respectively [99]. As there is no singular dominant isotope of germanium, it is important to consider how isotopic substitution will affect the results of each structure studied herein.

Electronic energies will not change, and optimized structures will stay the same within 1x10^{-5} Å (due to numerical convergence thresholds), but frequencies, rotational constants, and zero-point energies will change. To show how they might change, results were also collected using the average isotopic mass of germanium as calculated by MOLPRO (72.59 amu). Anharmonic frequencies and intensities for r-GeC_3, r-Ge_2C_2, and r-Ge_3C are collected in Table 2.10 and compared with the results obtained used the mass of ^{74}Ge (73.92 amu). Frequencies using the average isotopic mass of germanium show a MAPD of 0.05%, 0.20%, and 0.54% for r-GeC_3, r-Ge_2C_2, and r-Ge_3C, respectively. Clearly, there is some deviation as the masses change, and that deviation will be larger as the masses are further changed from ^{74}Ge, but the deviation will likely be quite small for each isotopic substitution. This will result in broader peaks in the IR spectra, but they will likely still be distinguishable for each

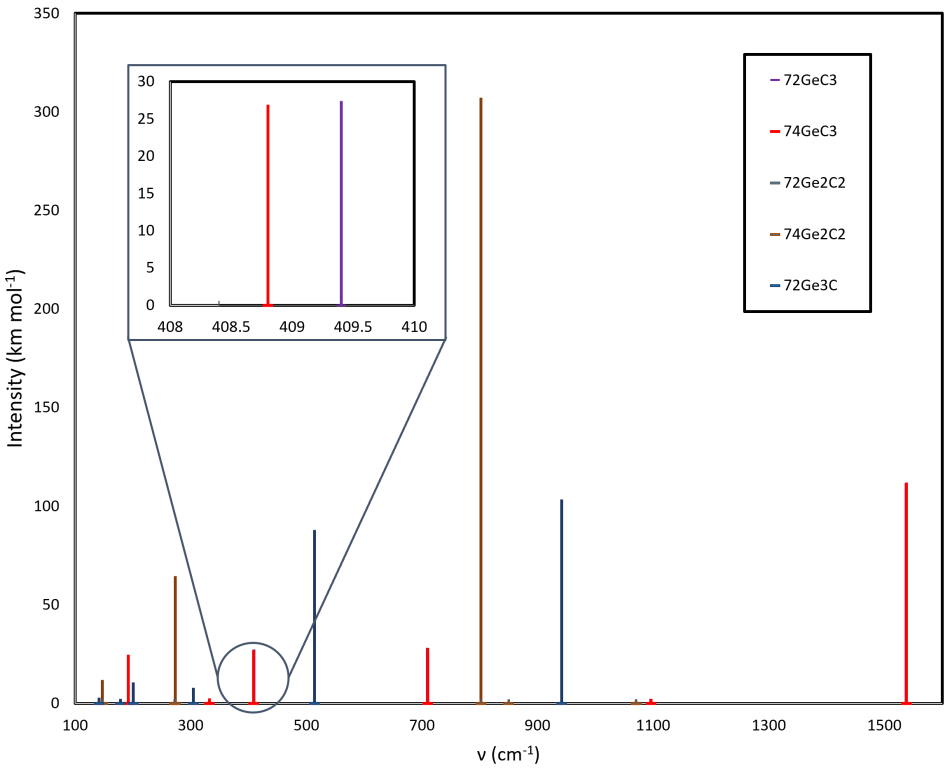

Figure 2.5: Theoretical IR spectra of r-GeC_3, r-Ge_2C_2, and r-Ge_3C computed using the mass of ^{74}Ge (73.92 amu) and the average isotopic mass (72.59 amu).

species even with the inclusion of varying isotopes of germanium. The difference in frequencies and intensities between the two germanium masses (72.59 and 73.92 amu) is represented graphically in Figure 5.

One should also consider the likelihood of finding each species with each isotope present to know which combinations are the most likely to be observed. The probabilities of all unique combinations (320, excluding chemically equivalent duplicates) of the five germanium isotopes for each species considered in this work are collected in Tables A12-A15. For each species, those composed of entirely ^{74}Ge isotopes have the highest probability of being present, while substitutions with ^{72}Ge follow as next most likely.

Table 2.10: Anharmonic vibrational frequencies (in cm^{-1}), intensities (in km mol^{-1}), and their relatives values when atomic mass of germanium is changed. Masses used are that of ^{74}Ge (73.92 amu), and the average atomic isotopic mass of germanium as calculated by MOLPRO (72.59 amu). MAPDs are shown for the values calculated with the average isotopic mass with respect to those calculated with the mass of ^{74}Ge.

Mode	Symmetry	m(Ge)=72.59		m(Ge)=73.92	
r-GeC_3		Anharm.	Int.	Anharm.	Int.
6	B_2	1537.5	111.9	1538.3	112.0
5	A_1	1096.0	2.2	1096.3	2.2
4	A_1	709.7	28.3	709.8	28.1
3	A_1	409.4	27.4	408.8	26.9
2	B_2	332.5	2.4	332.4	2.4
1	B_1	191.7	24.6	191.8	24.6
MAPD		0.05	0.44		
r-Ge_2C_2		Anharm.	Int.	Anharm.	Int.
6	A_g	1070.5	0.0	1070.7	0.0
5	B_{2g}	850.3	0.0	850.0	0.0
4	B_{1u}	802.5	307.7	801.7	307.2
3	A_g	273.1	0.0	271.9	0.0
2	B_{3u}	274.3	64.6	273.0	64.5
1	B_{2u}	147.3	12.0	147.1	11.9
MAPD		0.20	0.17		
r-Ge_3C		Anharm.	Int.	Anharm.	Int.
6	B_2	942.1	103.5	941.8	103.2
5	A_1	514.1	87.9	513.6	87.9
4	A_1	304.7	7.9	300.7	7.7
3	B_2	200.4	10.6	198.7	10.4
2	A_1	178.2	2.3	176.7	2.3
1	B_1	141.6	2.9	141.5	2.9
MAPD		0.54	0.80		

2.4 Conclusions

This work presents anharmonic vibrational frequencies and rotational constants evaluated at a high-level of theory for a suite of tetra-atomic germanium carbide and silicide molecules. For many of these molecules, we report the only available computed frequencies and rotational constants, and for those that have already been studied, this work offers results from more accurate, recent methods. The spectroscopic data provide a reference for potential observation of the various species in the interstellar medium, specifically with instruments such as JWST through their IR spectra. Multiple structures have vibrational modes that are suitable for observation, the most promising of which is the ν_4 mode of r-Ge_2C_2 with a frequency of 802.7 cm^{-1} (12.5 μm) and an intensity of 307.2 km mol^{-1}. Other modes of potential interest include the ν_5 mode of r-Ge_2Si_2 at 402.0 cm^{-1} (24.9 μm) and 119.8 km mol^{-1}, the ν_6 mode of r-Ge_3C at 941.8 cm^{-1} (10.6 μm) and 103.2 km mol^{-1}, and the ν_6 modes of r-GeC_3 and r-$GeSi_3$ at 1538.3 cm^{-1} (6.5 μm) and 112.0 km mol^{-1} and 495.8 cm^{-1} (20.2 μm) and 107.0 km mol^{-1}, respectively. Some molecules also could be detected through their rotational spectra due to their larger permanent dipole moments. These include d- and r-GeC_3 as well as t-Ge_2C_2 with net dipole moments of 5.40 D, 2.95 D and 3.52 D, respectively.

Many of the studied isomers have small energy differences; however, recent work has shown that most transition states between isomers are separated by large energy barriers [115]. In principle, the present results for vibrational frequencies and intensities as well as rotational constants and dipole moments are of sufficient accuracy to aid in the detection of theses species in the ISM. However, if candidate lines are identified, unambiguous assignment of a specific species could require further computations including correlation of the d-electrons and, perhaps, explicit treatment of relativistic effects beyond the pseudopotential on germanium. Moreover, the d-Ge_2C_2 structure, as well as some of the other species that show slight multi-reference char-

acter, also open up an interesting path for further computational study with accurate multi-reference approaches.

Due to germanium having isotopes with comparable, large abundances, it is important to consider the effect of different isotopes on the observed spectra. As the impact of isotopic substitution on vibrational frequencies is quite small, the result will be a slight broadening of the peaks in the IR spectrum, but the species should still be distinguishable. Combinations of isotopes containing primarily ^{74}Ge are most likely to be observed as ^{74}Ge is the most abundant isotope of the five naturally occurring isotopes.

With the present spectroscopic data for these germanium-containing species, the presence of this heavier element in the interstellar medium can be studied more thoroughly. If identified, these species could offer insight into the pathways germanium takes to end up in stars, proto-planetary systems and eventually other celestial bodies.

Chapter 3

An investigation into transition states of cyclic tetra-atomic silicon and germanium interstellar dust compounds

3.1 Introduction

Over the past few decades, with leaps and bounds in our capabilities of studying the interstellar medium (ISM), much of the Universe's interesting chemistry has shown itself to us through the growing catalog of detected chemical species in space [8]. Many astrophysicists and astrochemists are interested in the formation routes of the detected molecules, at this time specfically polycyclic aromatic hydrocarbons, due to their potential important contributions to interstellar chemistry [17–20]. However, others are interested in the mechanisms which allow these reactions to occur, and, more specifically, the venue at which species can react with one another - interstellar dust grains.

Interstellar dust grains make up roughly one percent of the mass within our own galaxy, but that does not represent their importance. The properties of dust grains are vital to how we observe the galaxy spectroscopically, and what types of stars and planets can be found in different regions, as planets, for instance, are ultimately made up of the accretion of smaller particles and planetesimals. While many reactions can

occur in the gas phase, dust grains provide a surface for many other reactions to occur that could not happen in the gas phase [25–27]. Dust grains are currently understood to help in catalyzing the addition of hydrogen atoms to one another to form molecular hydrogen [123]. Researchers are interested in the types of reactions that occur on the surface of these dust grains, but others are also interested in primarily studying the origins of these dust grains and their chemical composition [124]. The interested reader is pointed towards a few review articles on the physics, chemistry, and importance of interstellar dust grains [25–27].

Dust grain formation primarily tends to happen in circumstellar envelopes (CSEs) of asymptotic giant branch (AGB) stars [28]. One stellar body that has been the focus of recent studies is the carbonaceous AGB star CW Leonis or IRC+10216 which has been the source of interesting silicon chemistry [9, 29–32]. The chemistry in IRC+10216 has led to the detection of unique silicon carbide molecules, such as diamond-shaped silicon tricarbide, which are precursors in the aggregation of SiC dust grains [9]. As carbon flows away from the central star through dredge-up processes from thermal pulses, creation of molecules found in dust grains can readily occur in the CSE, i.e., within five stellar radii where the temperature and density are sufficiently high ($\sim$1000 K and 10^{10} cm^{-3}, respectively). As the molecules cool and aggregate while they move away from the star (between 5 and 15 solar radii from the central star), small dust grains begin to form and make their way out to the ISM [28].

Another important aspect of AGB stars is that these can be good sources of atoms generated through the s-process due to dredge-up of core material [125]. Alongside being formed in the CSEs of AGB stars, supernovae are also believed to be contributors to interstellar dust [126]. One element that has been seen in various stellar sources and forms through r- (supernovae) and s-processes (later-stage stars) is germanium [38, 40, 41]. Germanium has the same valence electron configuration as carbon and silicon, and thus might show similar interesting chemical phenomena in space. Furthermore, it might also contribute to formation of dust grains and give more insight

into how it ends up in various corners of the Universe in the forms of meteorites or planetesimals.

From older data taken from the Hubble Space Telescope, the observed abundance of interstellar germanium can be seen to show a slight decrease from average solar values with increasing fraction of molecular hydrogen, which can be attributed to depletion through dust-grain related pathways [127]. However, those pathways are unexplored for atomic germanium, as well as molecular forms of germanium. With detection and identification capabilities continuing to increase as advances are made in space observation instruments, there is potential to see interesting chemistry in the ISM. As such, studying how and in what forms germanium makes its way through the Universe could offer valuable contributions to the overall network of ISM pathways. To that end, a recent theoretical study considered germanium-containing dust grain molecules [128], following an investigation of analogous silicon carbide containing tetra-atomics inspired by the detection of cyclic silicon carbide (d-SiC_3) in IRC+10216 [9, 73]. Silicon carbide clusters have been of interest for multiple decades, with one of the first computational studies of SiC_3 in the context of astrochemistry dating back to 1990 to provide data to help with its detection [129]. These more recent studies [73, 128] included a suite of cyclic tetra-atomic silicon carbides and germanium carbides/silicides of the form $Si(Ge)_x(C/Si)_{4-x}$. The nomenclature for these structures is derived from the shapes of the isomers, with those being diamond (d-), rhomboidal (r-), and trapezoidal (t-). Anharmonic vibrational frequencies and intensities as well as rotational constants and dipole moments were obtained at very accurate levels of theory [CCSD(T)-F12b-cCR/cc-pCVTZ-F12 and CCSD(T)-F12a/cc-pVTZ-F12], with some species being more likely to be detected through their spectroscopic properties than others [128].

Although theoretical work has been carried to provide data for potential detection, there has been no work studying routes of formation for these germanium-containing molecules. There has been joint experimental and theoretical work done investigat-

ing the gas-phase formation of the cyclic silicon tricarbide molecules (d- and r- SiC_3) [130], which could provide a starting point for study on the germanium analogues; however, this mechanistic study lies outside the scope of the present work. Many of the structures sharing the same chemical formulae showed relatively small energy differences between one another, such as the d- and r- isomers of GeC_3 being separated by only 10.6 kJ mol^{-1}, suggesting that there might be the possibility for these isomers to interconvert [128]. Inspired by these low energy differences between many of these structures, the present work explores the possibility of interconversion between isomers both in the case of silicon carbides and of germanium-containing analogues. The transition states studied herein include those that exist between the two XY_3 isomers, the two X_3Y isomers, the r-X_2Y_2 and t-X_2Y_2 isomers, and the d-X_2Y_2 and r-X_2Y_2 isomers. Based on computations, we do not believe there exists a direct pathway connecting the d-X_2Y_2 and t-X_2Y_2 isomers, but rather these two structures would have to pass through the intermediate r- isomer.

Seeing as there is a wide range of environments in the ISM in terms of temperature and densities which alter whether the chemical environment is thermodynamically or kinetically dominated, this begs the question of whether interconversion between these species is possible in space. Furthermore, once these structures are formed, is there a tendency to interconvert to reach the more energetically favorable isomer? In this work, the interconversions and their accompanying energy barriers between all isomers have been investigated for these families of cyclic, tetra-atomic silicon carbide, germanium carbide, and germanium silicide molecules. The determination of the magnitude of the energy barriers for these transition states will help to confirm whether or not interconversion between these structures is feasible in the various regions of the ISM.

3.2 Computational Methods

The majority of computations in this work were carried out with density functional theory (DFT) using ORCA 5.0.4 [131]. Initial geometry optimizations using default parameters were carried out for the known minimum energy structures [73, 128] of all species (Ge_xC_{4-x}, Ge_xSi_{4-x}, and Si_xC_{4-x}, $x \in \{1, 2, 3\}$) to verify that DFT could determine the correct energy ordering of species in accordance with the explicitly-correlated coupled-cluster theory at the singles, doubles, and perturbative triples level, with the cc-pVTZ-F12 basis set [CCSD(T)-F12a/cc-pVTZ-F12] [66, 100–103]. Reference coupled-cluster data for the germanium-containing structures were taken from previous work [128], but computations for the silicon carbide molecules were done for this work using the MOLPRO 2023.2 software package [105–107]. The best available data for the silicon carbide clusters can be found in the work of Sehring et al. [73], but for consistency of comparison, the computations were re-done using the CCSD(T)-F12a/cc-pVTZ-F12 method (which differs from results of Sehring et al. in relative energy by at most 3.5% for the case of d-Si_2C_2). The Nudged Elastic Band (NEB) [132] method as implemented in ORCA was used to find transition states between the species of identical chemical formulae, e.g., between r- and d-$GeSi_3$. This NEB procedure was followed by a geometry optimization and frequency calculation to determine that the found structures were indeed transition states, i.e., had a single imaginary frequency. An intrinsic reaction coordinate (IRC) [133–135] calculation was then carried out on each transition state to determine that it connected the correct structures.

The initial optimized geometries, vibrational frequencies, NEB structure, and IRC were determined using the B3LYP functional [96, 97], with inclusion of dispersion via Grimme's Becke-Johnson damped (D3BJ) model [136, 137], and in conjunction with the aug-cc-pVTZ basis set [119–121]. After transition states were found and confirmed, optimizations with tighter convergence criteria were carried out on all

systems (minima and transition states) by using the DEFGRID3 and TightOpt keywords, with functionals of various types to study how they might describe the systems differently. Functionals used for subsequent tighter optimization and frequency calculations include the hybrid B3LYP-D3BJ [96, 97, 137] once again, the hybrid meta-GGA M06-2X [138, 139], the range-separated hybrid ωB97X-D4 [140–143], and the double-hybrid B2GP-PLYP [64]. By default, all DFT calculations in ORCA were done within the RIJCOSX framework [144]. For the double-hybrid functional, the resolution of identity approximation for the MP2 was used as implemented in ORCA [145]. All calculations used the aug-cc-pVTZ basis set [119–121]. After re-optimization of each species, each transition state was inspected both visually and through its imaginary vibrational mode to ensure that each functional had obtained the same structure. Lastly, an IRC computation was carried out on each transition state to confirm that the re-optimized transition states still connected the correct structures. Note that all calculations were carried out using average atomic masses by default in ORCA.

3.3 Results and Discussion

As stated, initial DFT calculations were needed to confirm that DFT could correctly determine the relative energy ordering of all species studied in this work. This initial comparison was between the relative energies of all structures as calculated using the B3LYP-D3BJ functional and the aug-cc-pVTZ basis set (B3LYP-D3BJ/AVTZ) with those calculated using the CCSD(T)-F12a/cc-pVTZ-F12 method [128]. As shown in Table 3.1, B3LYP-D3BJ is able to follow the trends in energies relatively well, although it does have a wide range in accuracy for most isomers, deviating from CCSD(T)-F12a results by between 4.1% (for d-Si_2C_2) and 40.7% (for r-SiC_3). However, it should be noted that in the case of d- and r-GeC_3, B3LYP reorders the two isomers, from the r- isomer being lower by 10.9 kJ mol^{-1}, to the d- isomer being lower by 0.5 kJ mol^{-1}. As seen from the coupled cluster results, these two structures have

the smallest difference in their minimum energies so the reordering by B3LYP-D3BJ might reflect on this functional, and does not rule out DFT, with alternate functionals, as a means for studying these systems. To represent all rungs on Jacob's Ladder [146] for DFT (excluding the local density approximation), we opted to choose one funtional from the top four rungs: B3LYP (hybrid) with dispersion (-D3BJ), M06-2X (hybrid meta-GGA), ωB97X-D4 (range-separated hybrid), and B2GP-PLYP (double-hybrid).

Table 3.1: X_xY_{4-x} ($x \in \{1, 2, 3\}$) family relative electronic energies (in kJ mol^{-1}) of optimized geometries. Relative energies are taken with respect to the lowest energy isomer in each group. Results are computed at the B3LYP-D3BJ/AVTZ and the CCSD(T)-F12a/cc-pVTZ-F12 (F12a/TZ) levels of theory.

	B3LYP-D3BJ/AVTZ			F12a/TZ		
Structure	SiC	GeC	GeSi	SiC	GeC[a]	GeSi[a]
			XY_3			
d	0.0	0.0	0.0	0.0	0.0	0.0
r	15.4	-0.5	16.5	26.4	10.9	17.3
			X_2Y_2			
r	0.0	25.3	0.0	0.0	20.0	0.0
t	20.0	0.0	13.0	32.0	0.0	13.1
d	350.8	401.2	34.1	338.2	402.9	33.3
			X_3Y			
r	0.0	0.0	0.0	0.0	0.0	0.0
d	218.3	201.7	15.8	207.4	192.4	16.0

[a]Flowers et al. 2024 [128]

All results from optimization and frequency calculations with each functional, including relative electronic energies (with zero-point corrections), Gibbs free energies, and zero-point vibrational energies can be found in Appendix B, in Tables B1-B6. Cartesian coordinates of all structures can also be found in Appendix B. On the basis

of discussing results that are, on average, the most accurate relative to coupled-cluster calculations for these systems, the results discussed herein are those obtained with the B2GP-PLYP functional. For relative energies, B2GP-PLYP produced mean absolute percent errors of 6.7%, 8.2%, and 32.8% for SiC, GeC, and GeSi structures, respectively. Note that the larger percentage deviation for GeSi is due to their smaller relative energy values (all < 35 kJ mol^{-1}), see Table 3.1. Pictured in Table 3.2 are the relative electronic energies with zero-point energy corrections as determined using B2GP-PLYP/AVTZ. Relative to the other functionals (see Table B1), B2GP-PLYP reordered the transition states for the Ge_2Si_2 conformers, placing the d- to r- transition state lower relative to the minimum structure of the group, as opposed to the other three functionals which place the r- to t- transition state lower (by 7.5 - 14.2 kJ mol^{-1}). This reordering, however, does not change the conclusions drawn from the present work.

As can be seen from Table 3.2, the d- and r- isomers for the XY_3 structures and the r- and t- isomers for the X_2Y_2 structures (plus d- for Ge_2Si_2) show relatively small energy differences between minima (ranging from 11.0 to 25.8 kJ mol^{-1}); similarly, the d- and r- isomers for Ge_3Si also show a small energy separation (10.2 kJ mol^{-1}). For the remaining Si_3C, Ge_3C, d-Si_2C_2, and d-Ge_2C_2 structures, the energies differences are quite substantial, indicating a strong preference for the lower energy isomers, especially for the latter two structures. In the case of d-Si_2C_2, the structure was shown [73] to have strong pseudo-Jahn-Teller distortion effects in its potential energy surface [147], which contributes to its instability (this is also the cause for a singular negative frequency in the d-Si_2C_2 structures as seen in Table B16 for B2GP-PLYP results). For d-Ge_2C_2, the structure was shown to have high multi-reference character [128], indicating that this structure might not be accurately described by the single reference DFT methods used herein.

Table 3.2: X_xY_{4-x} ($x \in \{1, 2, 3\}$) family relative energies (in kJ mol^{-1}) of optimized geometries with inclusion of harmonic zero-point vibrational energy (ZPVE). Relative energies are taken with respect to the lowest energy isomer in each group. All results at the B2GP-PLYP/AVTZ level of theory.

Structure	SiC	GeC	GeSi
XY_3			
d	0.0	0.0	0.0
r	23.9	11.0	11.2
TS	187.9	166.2	138.8
X_2Y_2			
r	0.0	15.9	0.0
t	25.8	0.0	8.7
d	336.7	365.8	21.2
TS r-t	181.3	158.3	147.5
TS d-r	351.9	387.3	139.5
X_3Y			
r	0.0	0.0	0.0
d	210.1	193.3	10.2
TS	258.7	241.2	130.5

3.3.1 Transition state barrier heights

The barrier heights between each structure and corresponding transition states are visually represented in Figures 1-3, along with the relative energies between isomers and their transition state(s). Each will be discussed in turn below. Vibrational frequencies for all structures at each level of theory can be found in Tables B7-B18 in Appendix B.

Starting with the SiC_3, GeC_3, and $GeSi_3$ structures, it's apparent that in all cases, although the energy difference between the two isomers is low, the barrier to the transition from d- to r- is very high, being 187.9, 166.2, and 138.8 kJ mol^{-1}, respec-

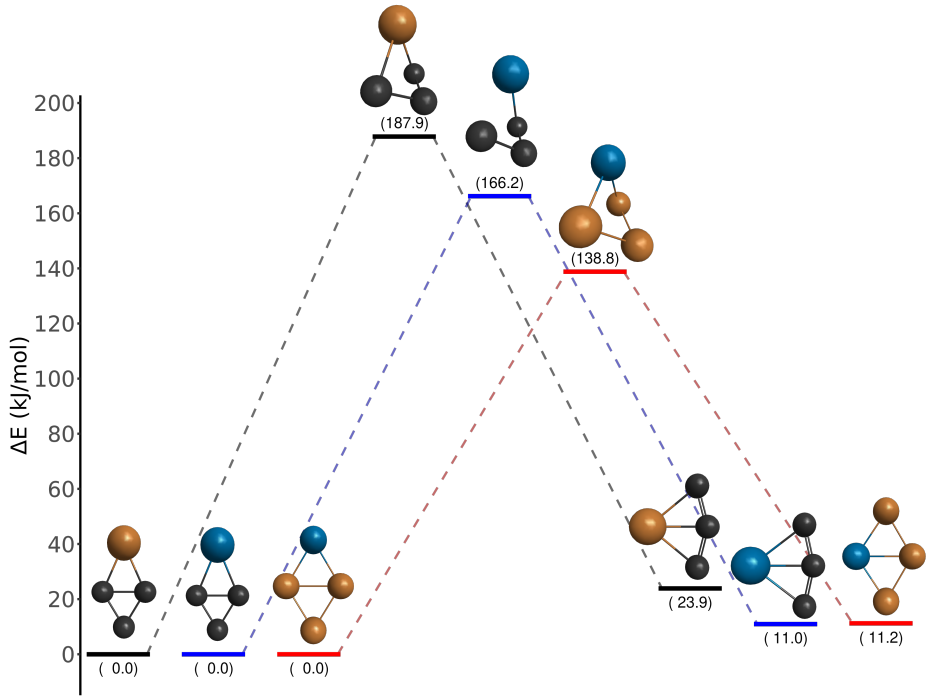

Figure 3.1: Potential energy diagram for the relative energies (with zero-point energy corrections) of optimized structures for the XY_3 isomers at the B2GP-PLYP/AVTZ level of theory. Carbon atoms shown in black, silicon atoms in orange, and germanium atoms in blue.

tively. Since the r- isomers for each structure are relatively similar in energy to the d- structures, the barriers from r- to d- are almost as high (164.1, 155.2, and 127.6 kJ mol^{-1}, respectively). Unless these structures are in a very energetic environment, it is unlikely that the r- structures would show any conversion towards the d- structures. That being said, if they do have the energy available to do so, it is likely that the isomers would reach thermodynamic equilibrium with one another, with the d- isomer being the majority of the population. In the case that these structures are in a very cold environment, which is likely in the case of interstellar dust, which structure is more prominent would depend on the exact formation mechanism of these molecules. If they are formed in the relatively hot CSE of a star, there would likely be a certain amount of interconversion to the more favorable structure that occurs until population ratios freeze out as they travel away from the star into colder interstel-

lar environments. Furthermore, even over a tremendous amount of time, due to the height of these barriers, it is unlikely that tunneling would allow any interconversion of these species.

In regards to the transition states themselves, following the trajectories of the IRC calculations starting from the d- isomers, the transition states are accessible through an out-of-plane bend of the two atoms on the vertices of the diamond structure that are not bonded. As these bend out of the plane, the angle between the heavier atom and the two adjacent carbon/silicon atoms bonded to it increases, allowing the third carbon/silicon to get close enough to form a bond with the heavier atom.

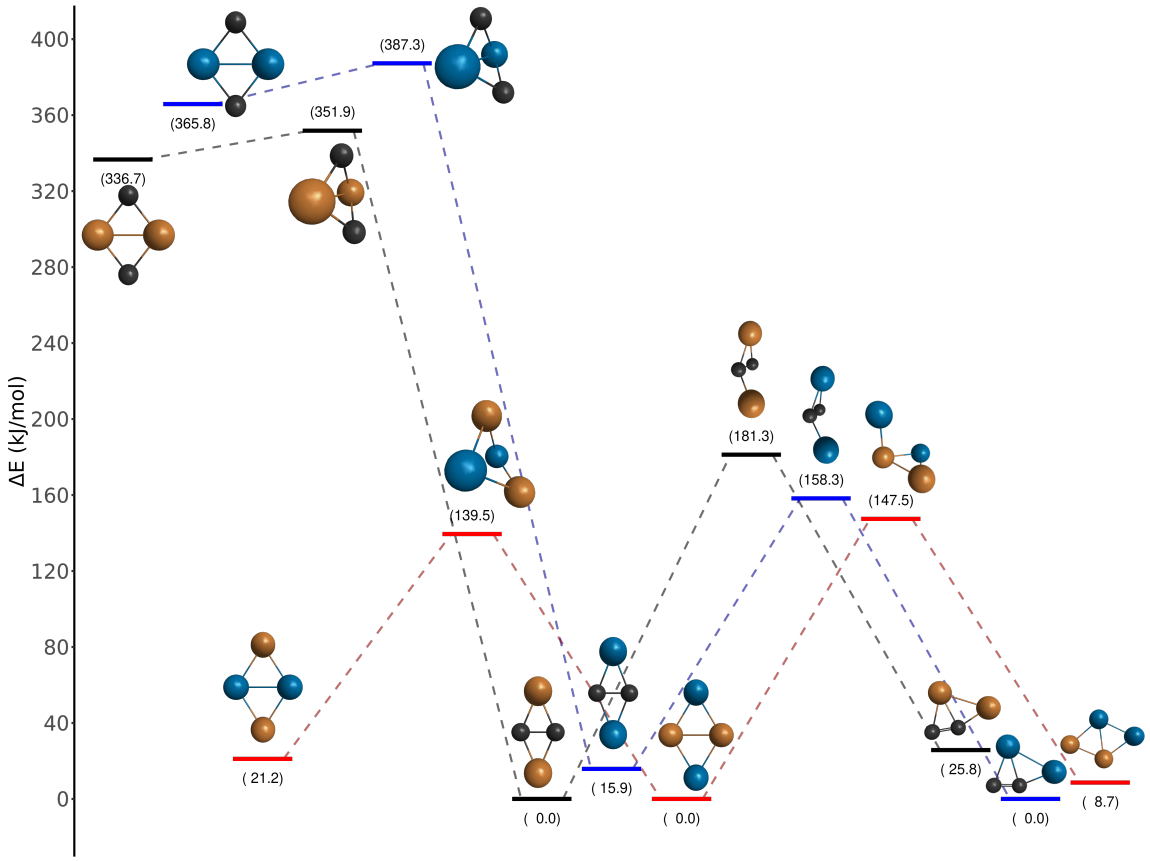

Figure 3.2: Potential energy diagram for the relative energies (with zero-point energy corrections) of optimized structures for the X_2Y_2 isomers at the B2GP-PLYP/AVTZ level of theory. Carbon atoms shown in black, silicon atoms in orange, and germanium atoms in blue.

The X_2Y_2 structures offer more variety in their transition states, however the

transition between r- and t- isomers shows the same high barriers as above in the case of all six structures (Si_2C_2, Ge_2C_2, Ge_2Si_2). These two transitions show barriers of 181.3, 142.4, and 147.5 kJ mol^{-1} for the r- to t- transitions (155.4, 158.3, and 138.7 for t- to r-), respectively. Once again for this case, with such deep wells, it is unlikely that there would be any interconversion between these species outside of a hot CSE.

The transition between d- and r- structures, however, is quite different in the cases of Si_2C_2 and Ge_2C_2. Due to the aforementioned relative instability of d-Si_2C_2 and d-Ge_2C_2, they have a strong preference for their respective r- compositions and are more readily interconverted to reach a lower energy minimum structure. This (relative) ease of interconversion can be seen by the barriers for the d- to r- transition being 15.2 and 21.4 kJ mol^{-1}, respectively, much smaller than all other barriers discussed thus far. This transition would be very likely to occur in energetic circumstances, and could possibly occur in (moderately) low temperature environments as well. Once the d- isomer converts to the r- isomer, it is also very unlikely that it will transition back. With barrier heights of 351.9 and 371.4 kJ mol^{-1} for this transition for Si_2C_2 and Ge_2C_2 respectively, unless the molecules had quite an excess of energy available, it is very likely that they would get stuck in the r- configuration.

The d-Ge_2Si_2 structure did not show the same unstable nature as its Si_2C_2 and Ge_2C_2 analogues, and this could be why it has deeper wells on either side of the transition state between the r- and d- structures. The difference in energies between the wells and transition state in the case of Ge_2Si_2 are 139.5 and 118.3 kJ mol^{-1}, putting it in the same group as the other transitions with high energy differences, making it less likely that this interconversion would occur.

The transition states connecting r- and t- structures show an interesting path from one structure to the other in all three cases. Starting from the r- structure, one of the heavier atoms at one of the vertices swings out of plane over one of the lighter atoms to take its place next to the other heavy atom. The r- to d- transition is also similar between Si_2C_2, Ge_2C_2, and Ge_2Si_2. All three move through a "breathing"

vibrational mode as they go through the transition state. Following the trajectory from the r- structure for all three cases, the structures initially bend out of plane slightly into a boat-like configuration before the lighter atoms push apart, and the heavier atoms pull inward, followed by returning to a more planar configuration. Of the three, d-Si_2C_2 and d-Ge_2Si_2 return to fully planar configurations, while d-Ge_2C_2 remains in a boat-like structure.

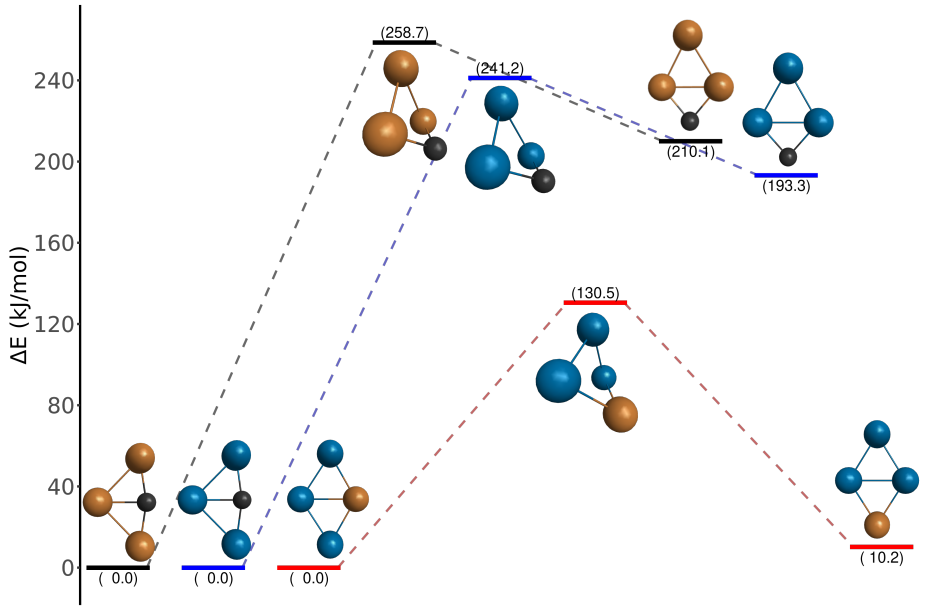

Figure 3.3: Potential energy diagram for the relative energies (with zero-point energy corrections) of optimized structures for the X_3Y isomers at the B2GP-PLYP/AVTZ level of theory. Carbon atoms shown in black, silicon atoms in orange, and germanium atoms in blue.

Lastly, for the r- to d-Si_3C and Ge_3C transitions, we have computed barriers of 48.6 and 47.9 kJ mol^{-1}, respectively. These barriers are not quite as high as most others previously discussed and might be more easily surmountable in energetic conditions. For the reverse, from d- to r-, barrier heights are 258.7 and 241.2 kJ mol^{-1}, respectively, indicating that it would be much easier for any structures in the d- configuration to surmount the barrier and get stuck in the r- configuration. Ge_3Si, on the other hand, has roughly equally deep wells on either side of the transition state. The minimum structures themselves are separated by only 10.2 kJ mol^{-1}, putting the

energy requirements to reach the transition state at 130.5 and 120.3 kJ mol^{-1} for the r-d and d-r transitions, respectively, making this transition unlikely in the cold ISM.

All three transitions are made along similar pathways for Si_3C, Ge_3C, and Ge_3Si. Beginning with the d- structure in this case, there is a slight out of plane bend about the middle two heavy atoms, followed by these two atoms pushing apart and pulling in the lighter atom to slot between them as the structure returns to a more planar configuration. Of the three, only Ge_3Si rests at a fully planar configuration at the minimum of the well, while the other two show slight out of plane dihedrals about the middle two heavy atoms.

It is worth noting that there is one other transition state that was found for both Ge_3C and Ge_3Si. This other structure represents the middle point between a symmetric well potential between two d- isomers of these two structures. It is visualized as the motion of the carbon/silicon atom out of plane from one side of the germanium triangle to the other. Since these structures are identical, in terms of relative atomic locations, this motion could be considered (if the three germanium atoms are identical) a rotation. However, this is not the case if different isotopes of germanium are present. As there is no dominant, naturally occurring isotope of germanium, there exists the possibility for these structures to be composed of various combinations of the five naturally occurring isotopes of germanium (Ge-74, 72, 70, 73, and 76 in decreasing abundance) [99]. If there were different isotopes that the moving carbon/silicon were to bind to in this transition, then the saddle point would be a genuine transition state. However, like many of the other found transition states, the barrier for interconversion is quite high at 130 and 180 kJ mol^{-1} for Ge_3C and Ge_3Si, respectively. Due to the high barriers, it is again unlikely that these interconversions would occur. Furthermore, as it is a transition between the same isomers, it would not affect the abundance of d- vs r- isomers that are detectable.

3.3.2 Population ratios and detectability

To further investigate the likelihood of each isomer appearing, we consider the Boltzmann population ratios for each isomer. Populations are determined through use of the Boltzmann factor equation,

$$\frac{p_i}{p_j} = \exp\left(\frac{\Delta E}{k_{\mathrm{B}} T}\right) \times 100\%$$

where p_i/p_j is the ratio of probabilities for which each population is occupied, ΔE is the energy difference between isomers, k_B is the Boltzmann constant, and T is the temperature in Kelvin.

Table 3.3 shows the Boltzmann population ratios for each isomer at 1000 K if we are considering the (approximate) temperature of a CSE. As can be seen, in many cases, there is no isomer that occupies 100% of the population. For the XY_3 structures, the d- isomers are seen to be the majority of the population, at 94.66%, 78.97%, and 79.36% for SiC_3, GeC_3, and $GeSi_3$, respectively. However, there are still r- isomers present in significant amounts, especially in the case of GeC_3 and $GeSi_3$ (at 21.03% and 20.64%, respectively). The same can be said about the r- and t- isomers for the X_2Y_2 structures, with the exception of Ge_2C_2 being in favor of the t- isomer rather than the r- isomer. Here we see populations of 95.70%, 12.87%, and 69.96%, for r- isomers, and 4.30%, 87.13%, and 24.57%, for t- isomers, for Si_2C_2, Ge_2C_2, and Ge_2Si_2, respectively. For the X_3Y isomers, the larger difference in energy for Si_3C and Ge_3C puts the r- isomers at 100% of the population, but for Ge_3Si these are 77.33% and 22.67% for r- and d-, respectively.

Although there are some isomers that exist with a majority of the population, that does not necessarily rule out any possibility of detecting the minority population isomer. As these molecules travel outward from the CSE and cool down, it is possible that they might get kinetically trapped in a well that would have been otherwise surmountable in more energetic conditions. Therefore, these populations serve as good indication as what the ratios might look like, but in the cold ISM, it would be

Table 3.3: X_xY_{4-x} ($x \in \{1, 2, 3\}$) family Boltzmann populations at 1000 K in percentages.

Structure	SiC	GeC	GeSi
XY_3			
d	94.66	78.97	79.36
r	5.34	21.03	20.64
X_2Y_2			
r	95.70	12.87	69.96
t	4.30	87.13	24.57
d	0.00	0.00	5.47
X_3Y			
r	100.00	100.00	77.33
d	0.00	0.00	22.67

dependent on the pathways of formation and time taken to freeze out. Once these molecules find themselves in colder regions of the ISM where temperatures are around 10 K, there is not enough energy for them to surmount the high energy barriers that have been determined.

With many of these transitions being unable to occur outside of hot CSEs, this gives us some interesting insight into what the abundances of the isomers might look like in the cold ISM. Unless there is an overwhelming majority of one isomer for each species reached in thermodynamic equilibrium before ratios freeze out, there might be an appreciable abundance of most isomers in colder environments where transitions are unable to occur. As such, it might be possible to detect various isomers (if their spectroscopic parameters allow them to be detectable with current methods) when probing regions for these structures.

For most of these structures, the barriers are high enough where this could be the case. Specifically, those would be the systems that have barriers which lie above

100 kJ mol^{-1}, which includes all XY_3 structures, all Ge_2Si_2 structures, r- and t-isomers for Si_2C_2 and Ge_2C_2, and the two Ge_3Si isomers. Regarding the d- isomers for Si_2C_2 and Ge_2C_2, it is unlikely that they would remain present due to their instability and low barrier for conversion to the r- isomer. With the four d- and r-isomers of Si_3C and Ge_3C, based on the Boltzmann population ratios at 1000 K, it would be sensible to think that the ratio of d- to r- would likely be in the favor of the r- isomers. This is also supported by the relatively smaller energy barrier needed for the d- to r- transition.

In the context of detectability, this information is important to have, because previous work has proposed that some of the possibly detectable species are not the most energetically favorable isomers within their family [73, 128]. Structures that are not the lowest-lying minima that have been proposed to have detectable vibrational modes include r-SiC_3, r-GeC_3, and r-Ge_2C_2. Additionally, there are some that could be detectable through rotational spectroscopy due to their large dipole moments. These include r-SiC_3, r-GeC_3, t-Si_2C_2, and d-Si_3C. Since it's possible that there is not an overwhelming majority of one certain isomer in most cases, it makes it more promising that these higher energy minima could be detectable.

3.4 Conclusions

In this work, we have conducted a comprehensive study of the transition states between various isomers of cyclic tetra-atomic silicon carbide, germanium carbide, and germanium silicide structures. They were determined through the use of density functional theory and the employment of several functionals (B3LYP-D3BJ, M06-2X, ωB97X-D4, and B2GP-PLYP); all of which provided qualitatively (if not near quantitatively) the same picture. To our knowledge, this study offers the first look at the transition states for these structures, as well as insight into the possibilities for these structures to interconvert between one another.

Due to the very high relative energies of transition states for many of these struc-

tures, it is very unlikely that any interconversion would happen unless in an energetic (high temperature) environment. As such, it could be possible for conversion to the more energetically favorable species to occur if these were to form in circumstellar envelopes before they make their way too far from the star and freeze out. Structures that have smaller barriers, specifically the transition from d-Si_2C_2 and d-Ge_2C_2 to their r- isomers where the barriers are roughly between 15-20 kJ mol^{-1}, might be more likely to interconvert, making it very unlikely that these two d- isomers would be detected anywhere. The d- to r- conversions for Si_3C and Ge_3C also have relatively lower barriers, around 48 kJ mol^{-1}, however this is still high enough for interconversion in colder interstellar environments to be unlikely.

The remaining structures, which all have very high barriers (>100 kJ mol^{-1}), offer some interesting insight into what the chemical landscape might look like in regards to these molecules, if they do exist and are detectable. Due to the very high energy differences between minima and transition states, reaching a thermodynamic equilibrium between the different isomers could only occur while these molecules are within close enough proximity of a star where the envelope is hot enough to surmount these barriers. Otherwise, if the ratios between isomers freeze out before the population of one of them reaches an overwhelming majority, it could be possible to detect multiple isomers of one species in the ISM. This possibility is exciting, as previous studies of the rotational and vibrational spectroscopic characteristics of these structures showed that some of the most intense vibrational modes arise from structures which are not the lowest in energy relative to their other isomer(s) [73, 128]. Along with those with large dipole moments, higher energy minima of potential interest include r-SiC_3, r-GeC_3, r-$GeSi_3$, t-Si_2C_2, r-Ge_2C_2, and d-Si_3C.

So far, the only detected species of those studied in this work is d-SiC_3 [9], however, as outlined in this work, it would be worthwhile to search for the higher energy minimum structures mentioned above, along with those lower energy minimum structures that are potentially detectable. Detection of the higher energy structures will also

open up interesting questions regarding molecule formation. In regards to interstellar molecules containing germanium, much more work needs to be done to understand its impact in interstellar chemistry, along with the pathways it takes to propagate throughout the ISM.

Chapter 4

Conclusions

4.1 Conclusions

Collected in this thesis is an investigation into cyclic tetra-atomic interstellar dust compounds composed of silicon-carbides, germanium carbides, and germanium-silicides, including a high-level study of spectroscopic properties of the latter two groups, and a thorough look at the transition states between various isomers that exist for all three groups.

In Chapter 2, in light of diamond shaped (d-)SiC_3 being detected in the interstellar medium (ISM) and a study of the remaining cyclic tetra-atomic permutations of silicon carbide [9, 73], germanium analogues were studied using the coupled-cluster singles, doubles, and pertubative triples with explicit electron correlation (CCSD(T)-F12) method. This study was done with the intention of providing accurate anharmonic vibrational frequencies, rotational constants, and dipole moments to aid in the detection of these germanium-containing molecules in the ISM. Of those studied, rhomboidal (r-)Ge_2C_2 has the most promising vibrational mode for observation at a frequency of 802.7 cm^{-1} and an intensity of 307.2 km mol^{-1}. Other species that might be suitable for detection via their vibrational spectra are r-GeC_3 with a mode at 1538.3 cm^{-1} and an intensity of 112.0 km mol^{-1}, r-$GeSi_3$ having a mode at 495.8 cm^{-1} and an intensity of 107.0 km mol^{-1}, and lastly, r-Ge_3C with a mode at 941.8 cm^{-1} with an intensity of 103.2 km mol^{-1}. Other molecules of interest due to their

large dipole moments are d- and r-GeC_3 and trapezoidal (t)-Ge_2C_2 with net dipole moments of 5.40 D, 2.95 D and 3.52 D, respectively, allowing them to be potentially detectable through their rotational spectra.

Following up on the small energy differences between some of the studied isomers, such as the 10.6 kJ mol^{-1} difference between d- and r-GeC_3, in Chapter 3 the transition states and barrier heights between the isomers of the silicon-carbide, germanium carbide, and germanium silicide structures were studied. This study was done with the purpose of shedding light on whether or not interconversion between species would be possible in the ISM, as this might affect the detectability of species. These structures and their transition states were studied through use of density functional theory with a small variety of functionals. In spite of the small energy differences of some of the isomers, many of the barriers were much too high to allow for any interconversion outside of relatively hot circumstellar environments ($\sim$1000 K). As such, as these molecules travel away from hotter areas into the cold ISM, the ratios between isomers will remain unchanged as they get kinetically trapped on either side of the energy barrier for transition. This possible trapping points towards the potential meaningful population of less energetically favourable isomers, which is interesting to consider for detectability. Computational studies show that some of the less favourable structures have the potential to be detected, such as the aforementioned r-GeC_3, r-$GeSi_3$, r-Ge_2C_2, and t-Ge_2C_2, as well as r-SiC_3, t-Si_2C_2, and d-Si_3C [73, 128].

With the James Webb Space Telescope covering much of the infrared region in which many of these vibrational modes lie, it is worthwhile to keep an eye out for the structures studied in this work. Also with many molecules that have been currently detected in the ISM via their rotational spectra, some of these molecules are also worth surveying for with radio telescopes, such as the Atacama Large Millimeter Array in Chile. Following the study of the transition states, this suggestion not only holds for the minimum energy structures, but also those that lie higher in energy on their respective potential energy surfaces.

4.2 Future Work

As technological advancements continue to be made in the field of space observation, there will continue to be more sensitive instruments being made which will allow researchers to discern more of the chemical inventory of the cosmos. One could continue to ask "Why not search for molecule X?", a valid question as it is always interesting to see what forms different elements take in space. However, in relation to this work, for the time being, future work could focus on efforts to detect other silicon-carbide structures, as well as germanium carbides and germanium silicides.

Alongside work to detect these structures, there is the matter of how they form in the ISM. There has been some experimental and theoretical work done investigating the formation routes of d- and r-SiC_3 [130], however the pathways of formation for the rest of the species presented in this thesis remain nebulous. To help elucidate how some of these structures might form, there would need to be precursors proposed and kinetic studies done on their formation mechanisms.

Apart from their direct implications for studying the ISM, some of the molecules studied in this work are quite interesting in their own right and would warrant more research into their behaviour. This further investigation is specifically for the case of the strange computational results of d-Si_2C_2 and d-Ge_2C_2, where challenges arose using the single-reference CC approach. Along with the other molecules that show slight multireference character, more theoretical work could be done looking into these two structures using accurate multireference methods.

Bibliography

[1] J. A. Cardelli, G. C. Clayton, J. S. Mathis, "The Relationship between Infrared, Optical, and Ultraviolet Extinction", *Astrophys. J.* **1989**, *345*, 245–256.

[2] E. A. Bergin, M. Tafalla, "Cold Dark Clouds: The Initial Conditions for Star Formation", *Annu. Rev. Astron. Astrophys.* **2007**, *45*, 339–396.

[3] M. Heyer, T. Dame, "Molecular Clouds in the Milky Way", *Annu. Rev. Astron. Astrophys.* **2015**, *53*, 583–629.

[4] F. Shu, *The physical universe*, University Science Books, **1982**.

[5] C. Kitchin, *Stars, nebulae and the interstellar medium*, CRC Press, **2005**.

[6] J. Tennyson, *Astronomical Spectroscopy*, World Scientific, **2010**.

[7] P. F. Bernath, *Spectra of atoms and molecules*, Oxford University Press, USA, **2020**.

[8] B. A. McGuire, "2021 Census of Interstellar, Circumstellar, Extragalactic, Protoplanetary Disk, and Exoplanetary Molecules", *Astrophys. J. Suppl. S.* **2022**, *259*, 30–80.

[9] A. J. Apponi, M. C. McCarthy, C. A. Gottlieb, P. Thaddeus, "Astronomical Detection of Rhomboidal SiC_3", *Astrophys. J.* **1999**, *516*, L103–L106.

[10] S. Brünken, H. Gupta, C. A. Gottlieb, M. C. McCarthy, P. Thaddeus, "Detection of the Carbon Chain Negative Ion C_8H^- in TMC-1", *Astrophys. J.* **2007**, *664*, L43–L46.

[11] J. Cernicharo, M. Guélin, M. Agúndez, M. C. McCarthy, P. Thaddeus, "Detection of C_5N^- and Vibrationally Excited C_6H in IRC +10216", *Astrophys. J.* **2008**, *688*, L83–L86.

[12] M. J. Barlow, B. M. Swinyard, P. J. Owen, J. Cernicharo, H. L. Gomez, R. J. Ivison, O. Krause, T. L. Lim, M. Matsuura, S. Miller, G. Olofsson, E. T. Polehampton, "Detection of a Noble Gas Molecular Ion, $^{36}ArH^+$, in the Crab Nebula", *Science* **2013**, *342*, 1343–1345.

[13] E. K. Campbell, M. Holz, D. Gerlich, J. P. Maier, "Laboratory confirmation of C_{60}^+ as the carrier of two diffuse interstellar bands", *Nature* **2015**, *523*, 322–323.

[14] R. C. Fortenberry, "Quantum astrochemical spectroscopy", *Int. J. Quantum Chem.* **2017**, *117*, 81–91.

[15] D. M. Hudgins, J. Charles W. Bauschlicher, L. J. Allamandola, "Variations in the Peak Position of the 6.2 μm Interstellar Emission Feature: A Tracer of N in the Interstellar Polycyclic Aromatic Hydrocarbon Population", *Astrophys. J.* **2005**, *632*, 316–332.

[16] G. Mulas, G. Malloci, C. Joblin, D. Toublanc, "Estimated IR and phosphorescence emission fluxes for specific polycyclic aromatic hydrocarbons in the Red Rectangle", *Astron. Astrophys.* **2006**, *446*, 537–549.

[17] P. Thaddeus, "The prebiotic molecules observed in the interstellar gas", *Philos. Trans. R. Soc. B* **2006**, *361*, 1681–1687.

[18] A. Tielens, "Interstellar Polycyclic Aromatic Hydrocarbon Molecules", *Annu. Rev. Astron. Astrophys.* **2008**, *46*, 289–337.

[19] A. M. Burkhardt, K. L. K. Lee, P. B. Changala, C. N. Shingledecker, I. R. Cooke, R. A. Loomis, H. Wei, S. B. Charnley, E. Herbst, M. C. McCarthy, B. A. McGuire, "Discovery of the Pure Polycyclic Aromatic Hydrocarbon Indene (c-C_9H_8) with GOTHAM Observations of TMC-1", *Astrophys. J. Lett.* **2021**, *913*, L18–L30.

[20] B. A. McGuire, R. A. Loomis, A. M. Burkhardt, K. L. K. Lee, C. N. Shingledecker, S. B. Charnley, I. R. Cooke, M. A. Cordiner, E. Herbst, S. Kalenskii, M. A. Siebert, E. R. Willis, C. Xue, A. J. Remijan, M. C. McCarthy, "Detection of two interstellar polycyclic aromatic hydrocarbons via spectral matched filtering", *Science* **2021**, *371*, 1265–1269.

[21] B. A. McGuire, A. M. Burkhardt, R. A. Loomis, C. N. Shingledecker, K. L. K. Lee, S. B. Charnley, M. A. Cordiner, E. Herbst, S. Kalenskii, E. Momjian, E. R. Willis, C. Xue, A. J. Remijan, M. C. McCarthy, "Early Science from GOTHAM: Project Overview, Methods, and the Detection of Interstellar Propargyl Cyanide ($HCCCH_2CN$) in TMC-1", *The Astrophys. J. Lett.* **2020**, *900*, L10–L21.

[22] I. R. Cooke, D. Gupta, J. P. Messinger, I. R. Sims, "Benzonitrile as a Proxy for Benzene in the Cold ISM: Low-temperature Rate Coefficients for CN + C_6H_6", *The Astrophys. J. Lett.* **2020**, *891*, L41–L47.

[23] B. Kerkeni, I. García-Bernete, D. Rigopoulou, D. P. Tew, P. F. Roche, D. C. Clary, "Probing computational methodologies in predicting mid-infrared spectra for large polycyclic aromatic hydrocarbons", *Mon. Not. R. Astron. Soc.* **2022**, *513*, 3663–3681.

[24] M. E. Strauss, T. J. Santaloci, R. C. Fortenberry, "Valence-, Dipole- and Quadrupole-Bound Electronically Excited States of Closed-Shell Anions Formed by Deprotonation of Cyano- and Ethynyl-Disubstituted Polycyclic Aromatic Hydrocarbons", *Chemistry* **2022**, *4*, 42–56.

[25] E. F. van Dishoeck, "Astrochemistry of dust, ice and gas: introduction and overview", *Faraday Discuss.* **2014**, *168*, 9–47.

[26] A. Potapov, M. McCoustra, "Physics and chemistry on the surface of cosmic dust grains: a laboratory view", *International Reviews in Physical Chemistry* **2021**, *40*, 299–364.

[27] A. Tielens, "Dust Formation in Astrophysical Environments: The Importance of Kinetics", *Front. Astron. Space Sci.* **2022**, *9*, 908217.

[28] L. M. Ziurys, "The chemistry in circumstellar envelopes of evolved stars: Following the origin of the elements to the origin of life", *Proc. Natl. Acad. Sci. U.S.A.* **2006**, *103*, 12274–12279.

[29] P. Thaddeus, S. E. Cummins, R. A. Linke, "Identification of the SiCC radical toward IRC +10216 : the first molecular ring in an astronomical source", *Astrophys. J. Lett.* **1984**, *283*, L45–L48.

[30] J. Cernicharo, C. A. Gottlieb, M. Guelin, P. Thaddeus, J. M. Vrtilek, "Astronomical and Laboratory Detection of the SiC Radical", *Astrophys. J. Lett.* **1989**, *341*, L25–L28.

[31] J. Cernicharo, M. C. McCarthy, C. A. Gottlieb, M. Agúndez, L. V. Prieto, J. H. Baraban, P. B. Changala, M. Guélin, C. Kahane, M. A. M. Drumel, N. A. Patel, N. J. Reilly, J. F. Stanton, G. Quintana-Lacaci, S. Thorwirth, K. H. Young, "Discovery of SiCSi in IRC+10216: A missing link between gas and dust carriers of Si–C bonds", *Astrophys. J. Lett.* **2015**, *806*, L3–L8.

[32] M. C. McCarthy, C. A. Gottlieb, J. Cernicharo, "Building blocks of dust: A coordinated laboratory and astronomical study of the archtype AGB carbon star IRC+10216", *J. Mol. Spectrosc.* **2019**, *356*, 7–20.

[33] R. V. Wagoner, W. A. Fowler, F. Hoyle, "On the Synthesis of Elements at Very High Temperatures", *Astrophys. J.* **1967**, *148*, 3–49.

[34] D. D. Clayton, *Principles of stellar evolution and nucleosynthesis*, University of Chicago Press, **1983**.

[35] D. Clayton, W. Fowler, T. Hull, B. Zimmerman, "Neutron capture chains in heavy element synthesis", *Annals of Physics* **1961**, *12*, 331–408.

[36] S. Wooley, T. Janka, "The physics of core-collapse supernovae", *Nat. Phys* **2005**, *1*, 147–154.

[37] V. Kunde, R Hanel, W Maguire, D Gautier, J. P. Baluteau, A Marten, A Chedin, N Husson, N Scott, "The tropospheric gas composition of Jupiter's north equatorial belt (NH_3, PH_3, CH_3D, GeH_4, H_2O) and the Jovian D/H isotopic ratio", *Astrophys. J.* **1982**, *263*, 443–467.

[38] N. C. Sterling, H. L. Dinerstein, C. W. Bowers, "Discovery of enhanced germanium abundances in planetary nebulae with the far ultraviolet spectroscopic explorer", *Astrophys. J.* **2002**, *578*, L55–L58.

[39] J. Cowan, "Astronomy: Elements of surprise", *Nature* **2003**, *423*, 29.

[40] E. M. Burbidge, G. R. Burbidge, W. A. Fowler, F. Hoyle, "Synthesis of the elements in stars", *Rev. Mod. Phys.* **1957**, *29*, 547–650.

[41] S. I. B. Cartledge, J. T. Lauroesch, D. M. Meyer, U. J. Sofia, "The Homogeneity of Interstellar Elemental Abundances in the Galactic Disk", *Astrophys. J.* **2006**, *641*, 327–346.

[42] K. Lodders, "Solar System Abundances and Condensation Temperatures of the Elements", *Astrophys. J.* **2003**, *591*, 1220–1247.

[43] D. A. McQuarrie, *Quantum Chemistry*, Oxford University Press, Oxford, **1983**.

[44] A. Szabo, N. S. Ostlund, *Modern Quantum Chemistry*, Dover Publications, **1996**.

[45] T. Helgaker, P. Jorgensen, J. Olsen, *Molecular Electronic-Structure Theory*, John Wiley and Sons, **2000**.

[46] C. J. Cramer, *Essentials of Computational Chemistry*, John Wiley and Sons, **2004**.

[47] L. Piela, *Ideas of Quantum Chemistry*, Elsevier, **2007**.

[48] E. G. Lewars, *Computational Chemistry*, Springer, **2011**.

[49] E. Schrödinger, "An Undulatory Theory of the Mechanics of Atoms and Molecules", *Phys. Rev.* **1926**, *28*, 1049–1070.

[50] M. Born, R. Oppenheimer, "Zur Quantentheorie der Molekeln", *Ann. Phys. (Berl.)* **1927**, *389*, 457–484.

[51] D. R. Hartree, "The Wave Mechanics of an Atom with a Non-Coulomb Central Field. Part I. Theory and Methods", *Math. Proc. Camb. Philos. Soc.* **1928**, *24*, 89–110.

[52] D. R. Hartree, "The Wave Mechanics of an Atom with a Non-Coulomb Central Field. Part II. Some Results and Discussion", *Math. Proc. Camb. Philos. Soc.* **1928**, *24*, 111–132.

[53] D. R. Hartree, "The Wave Mechanics of an Atom with a non-Coulomb Central Field. Part III. Term Values and Intensities in Series in Optical Spectra", *Math. Proc. Camb. Philos. Soc.* **1928**, *24*, 426–437.

[54] J. C. Slater, "The Self Consistent Field and the Structure of Atoms", *Phys. Rev.* **1928**, *32*, 339–348.

[55] J. A. Gaunt, "A Theory of Hartree's Atomic Fields", *Math. Proc. Camb. Philos. Soc.* **1928**, *24*, 328–342.

[56] V. Fock, "Näherungsmethode zur Lösung des quantenmechanischen Mehrkörperproblems", *Z. Phys.* **1930**, *61*, 126–148.

[57] D. R. Hartree, W. Hartree, "Self-consistent field, with exchange, for beryllium", *Proc. R. Soc. A* **1935**, *150*, 9–33.

[58] C. Møller, M. S. Plesset, "Note on an Approximation Treatment for Many-Electron Systems", *Phys. Rev.* **1934**, *46*, 618–622.

[59] J. Čížek, "On the Correlation Problem in Atomic and Molecular Systems. Calculation of Wavefunction Components in Ursell-Type Expansion Using Quantum-Field Theoretical Methods", *J. Chem. Phys.* **1966**, *45*, 4256–4266.

[60] T. J. Lee, P. R. Taylor, "A diagnostic for determining the quality of single-reference electron correlation methods", *Int. J. Quantum Chem.* **1989**, *36*, 199–207.

[61] T. D. Crawford, H. F. Schaefer III in *Reviews in Computational Chemistry*, John Wiley & Sons, Ltd, **2000**, pp. 33–136.

[62] P. Hohenberg, W. Kohn, "Inhomogeneous Electron Gas", *Phys. Rev.* **1964**, *136*, B864–B871.

[63] W. Kohn, L. J. Sham, "Self-Consistent Equations Including Exchange and Correlation Effects", *Phys. Rev.* **1965**, *140*, A1133–A1138.

[64] A. Karton, A. Tarnopolsky, J.-F. Lamère, G. C. Schatz, J. M. L. Martin, "Highly Accurate First-Principles Benchmark Data Sets for the Parametrization and Validation of Density Functional and Other Approximate Methods. Derivation of a Robust, Generally Applicable, Double-Hybrid Functional for Thermochemistry and Thermochemical Kinetics", *J. Phys. Chem. A.* **2008**, *112*, 12868–12886.

[65] S. F. Boys, A. C. Egerton, "Electronic wave functions - I. A general method of calculation for the stationary states of any molecular system", *Proc. R. Soc. A* **1950**, *200*, 542–554.

[66] J. G. Hill, K. A. Peterson, "Correlation consistent basis sets for explicitly correlated wavefunctions: Pseudopotential-based basis sets for the post-d main group elements Ga–Rn", *J. Chem. Phys.* **2014**, *141*, 094106.

[67] O. Osman, K. Bekki, L. Cortese, "The role of dust destruction and dust growth in the evolution of the interstellar medium", *Mon. Not. R. Astron. Soc* **2020**, *497*, 2002–2017.

[68] J. K. Jørgensen, A. Belloche, R. T. Garrod, "Astrochemistry During the Formation of Stars", *Annu. Rev. Astron. Astrophys.* **2020**, *58*, 727–778.

[69] T. Bernatowicz, G. Fraundorf, T. Ming, E. Anders, B. Wopenka, E. Zinner, P. Fraundorf, "Evidence for interstellar SiC in the Murray carbonaceous meteorite", *Nature* **1987**, *330*, 728–730.

[70] P. Mélinon, B. Masenelli, F. Tournus, A. Perez, "Playing with carbon and silicon at the nanoscale", *Nat. Mater.* **2007**, *6*, 479–490.

[71] K. W. F. Lam, S. Csizmadia, N. Astudillo-Defru, X. Bonfils, D. Gandolfi, S. Padovan, M. Esposito, C. Hellier, T. Hirano, J. Livingston, et al., "GJ 367b: A dense, ultrashort-period sub-Earth planet transiting a nearby red dwarf star", *Science*, *374*, 1271–1275.

[72] L. V. Prieto, J Cernicharo, G Quintana-Lacaci, M Agúndez, A Castro-Carrizo, J. P. Fonfría, N Marcelino, J Zúñiga, A Requena, A Bastida, F Lique, M Guélin, "Si-Bearing molecules toward IRC+10216: ALMA unveils the molecular envelope of CWLeo", *Astrophys. J. Lett.* **2015**, *805*, L13–L19.

[73] C. M. Sehring, C. Z. Palmer, B. R. Westbrook, R. C. Fortenberry, "The spectral features and detectability of small, cyclic silicon carbide clusters", *Front. Astron. Space Sci.* **2022**, *9*, 1074879.

[74] A. J. Apponi, M. C. McCarthy, C. A. Gottlieb, P. Thaddeus, "The rotational spectrum of rhomboidal SiC_3", *J. Chem. Phys.* **1999**, *111*, 3911–3918.

[75] M. C. McCarthy, A. J. Apponi, P. Thaddeus, "A second rhomboidal isomer of SiC_3", *J. Chem. Phys.* **1999**, *111*, 7175–7178.

[76] J. D. Presilla-Márquez, W. R. M. Graham, "Vibrational spectra of tetra-atomic silicon–carbon clusters. I. Rhomboidal Si_3C in Ar at 10 K", *J. Chem. Phys.* **1992**, *96*, 6509–6514.

[77] K. Lammertsma, O. F. Guner, "Structures and energies of disilicon dicarbide, C_2Si_2", *J. Am. Chem. Soc.* **1988**, *110*, 5239–5245.

[78] C. M. L. Rittby, "An ab initio study of the structure and infrared spectrum of Si_3C", *J. Chem. Phys.* **1992**, *96*, 6768–6772.

[79] N. X. Truong, M. Savoca, D. J. Harding, A. Fielicke, O. Dopfer, "Vibrational spectra and structures of Si_nC clusters (n = 3–8)", *Phys. Chem. Chem. Phys.* **2015**, *17*, 18961–18970.

[80] M. Savoca, J. Langer, D. J. Harding, O. Dopfer, A. Fielicke, "Incipient chemical bond formation of Xe to a cationic silicon cluster: Vibrational spectroscopy and structure of the Si_4Xe^+ complex", *Chem. Phys. Lett.* **2013**, *557*, 49–52.

[81] J. F. Stanton, J. Dudek, P. Theulé, H. Gupta, M. C. McCarthy, P. Thaddeus, "Laser spectroscopy of Si_3C", *J. Chem. Phys.* **2005**, *122*, 124314.

[82] J. D. Presilla-Márquez, S. C. Gay, C. M. L. Rittby, W. R. M. Graham, "Vibrational spectra of tetra-atomic silicon–carbon clusters. II. Si_2C_2 in Ar at 10 K", *J. Chem. Phys.* **1995**, *102*, 6354–6361.

[83] P. Yadav, R. Yadav, S. Agrawal, B. Agrawal, "Theoretical study of the physical properties of binary Si_mC_n (m+n $\leq$ 5) clusters: An ab initio study", *Physica E Low Dimens. Syst. Nanostruct.* **2006**, *33*, 249–262.

[84] P. Wielgus, S. Roszak, D. Majumdar, J. Leszczynski, "Thermodynamic properties of germanium/carbon microclusters", *J. Chem. Phys.* **2005**, *123*, 234309.

[85] P. Wielgus, S. Roszak, D. Majumdar, J. Saloni, J. Leszczynski, "Theoretical studies on the bonding and thermodynamic properties of GeSi clusters: The precursors of germanium/silicon nanomaterials", *J. Chem. Phys.* **2008**, *128*, 144305.

[86] S. Goswami, S. Saha, R. Yadav, "Structural, electronic and vibrational properties of Ge_xC_y (x+y=2–5) nanoclusters: A B3LYP-DFT study", *Physica E Low Dimens. Syst. Nanostruct.* **2015**, *74*, 175–192.

[87] O. Zingsheim, M.-A. Martin-Drumel, S. Thorwirth, S. Schlemmer, C. A. Gottlieb, J. Gauss, M. C. McCarthy, "Germanium Dicarbide: Evidence for a T-Shaped Ground State Structure", *J. Phys. Chem. Lett.* **2017**, *8*, 3776–3781.

[88] J. Koput, "Ab initio potential energy surface and vibration–rotation energy levels of germanium dicarbide, GeC_2", *J. Comput. Chem.* **2018**, *39*, 1327–1334.

[89] M.-A. Martin-Drumel, J. H. Baraban, P. B. Changala, J. F. Stanton, M. C. McCarthy, "The Hunt for Elusive Molecules: Insights from Joint Theoretical and Experimental Investigations", *Chem. Eur. J.* **2019**, *25*, 7243–7258.

[90] K. L. K. Lee, S. Thorwirth, M.-A. Martin-Drumel, M. C. McCarthy, "Generation and structural characterization of Ge carbides GeC_n (n = 4, 5, 6) by laser ablation, broadband rotational spectroscopy, and quantum chemistry", *Phys. Chem. Chem. Phys.* **2019**, *21*, 18911–18919.

[91] J. G. Hill, K. A. Peterson, "Correlation consistent basis sets for explicitly correlated wavefunctions: valence and core–valence basis sets for Li, Be, Na, and Mg", *Phys. Chem. Chem. Phys.* **2010**, *12*, 10460–10468.

[92] A. G. Watrous, B. R. Westbrook, R. C. Fortenberry, "F12-TZ-cCR: A Methodology for Faster and Still Highly Accurate Quartic Force Fields", *J. Phys. Chem. A* **2021**, *125*, 10532–10540.

[93] X. Wang, X. Huang, J. M. Bowman, T. J. Lee, "Anharmonic rovibrational calculations of singlet cyclic C_4 using a new ab initio potential and a quartic force field", *J. Chem. Phys.* **2013**, *139*, 224302.

[94] M. Algranati, H. Feldman, D. Kella, E. Malkin, E. Miklazky, R. Naaman, Z. Vager, J. Zajfman, "The structure of C_4 as studied by the Coulomb explosion method", *J. Chem. Phys.* **1989**, *90*, 4617–4618.

[95] S. J. Blanksby, D. Schröder, S. Dua, J. H. Bowie, H. Schwarz, "Conversion of Linear to Rhombic C_4 in the Gas Phase: A Joint Experimental and Theoretical Study", *J. Am. Chem. Soc.* **2000**, *122*, 7105–7113.

[96] A. D. Becke, "Density-functional thermochemistry. III. The role of exact exchange", *J. Chem. Phys.* **1993**, *98*, 5648–5652.

[97] C. Lee, W. Yang, R. G. Parr, "Development of the Colle-Salvetti correlation-energy formula into a functional of the electron density", *Phys. Rev. B* **1988**, *37*, 785–789.

[98] C. Hampel, K. A. Peterson, H.-J. Werner, "A comparison of the efficiency and accuracy of the quadratic configuration interaction (QCISD), coupled cluster (CCSD), and Brueckner coupled cluster (BCCD) methods", *Chem. Phys. Lett.* **1992**, *190*, 1–12.

[99] F. Kondev, M. Wang, W. Huang, S. Naimi, G. Audi, "The NUBASE2020 evaluation of nuclear physics properties", *Chin. Phys. C* **2021**, *45*, 030001.

[100] K. Raghavachari, G. W. Trucks, J. A. Pople, M. Head-Gordon, "A fifth-order perturbation comparison of electron correlation theories", *Chem. Phys. Lett.* **1989**, *157*, 479–483.

[101] T. B. Adler, G. Knizia, H.-J. Werner, "A simple and efficient CCSD(T)-F12 approximation", *J. Chem. Phys.* **2007**, *127*, 221106.

[102] G. Knizia, T. B. Adler, H.-J. Werner, "Simplified CCSD(T)-F12 methods: Theory and benchmarks", *J. Chem. Phys.* **2009**, *130*, 054104.

[103] K. A. Peterson, T. B. Adler, H.-J. Werner, "Systematically convergent basis sets for explicitly correlated wavefunctions: The atoms H, He, B–Ne, and Al–Ar", *J. Chem. Phys.* **2008**, *128*, 084102.

[104] D. Feller, K. A. Peterson, J. G. Hill, "Calibration study of the CCSD(T)-F12a/b methods for C_2 and small hydrocarbons", *J. Chem. Phys.* **2010**, *133*, 184102.

[105] H.-J. Werner, P. J. Knowles, G. Knizia, F. R. Manby, M. Schütz, "Molpro: a general-purpose quantum chemistry program package", *Wiley Interdiscip. Rev. Comput. Mol. Sci.* **2012**, *2*, 242–253.

[106] H.-J. Werner, P. J. Knowles, F. R. Manby, J. A. Black, K. Doll, A. Heßelmann, D. Kats, A. Köhn, T. Korona, D. A. Kreplin, Q. Ma, I. Miller, Thomas F., A. Mitrushchenkov, K. A. Peterson, I. Polyak, G. Rauhut, M. Sibaev, "The Molpro quantum chemistry package", *J. Chem. Phys.* **2020**, *152*, 144107.

[107] H.-J. Werner, P. J. Knowles, et al., MOLPRO, 2023.2 , a package of ab initio programs, see https://www.molpro.net.

[108] F. Eckert, P. Pulay, H.-J. Werner, "*Ab Initio* Geometry Optimization for Large Molecules", *J. Comput. Chem.* **1997**, *18*, 1473–1483.

[109] G. Rauhut, A. El Azhary, F. Eckert, U. Schumann, H.-J. Werner, "Impact of Local Approximations on MP2 Vibrational Frequencies", *Spectrochim. Acta A* **1999**, *55*, 647–658.

[110] T. Hrenar, G. Rauhut, H.-J. Werner, "Impact of Local and Density Fitting Approximations on Harmonic Vibrational Frequencies", *J. Phys. Chem. A* **2006**, *110*, 2060–2064.

[111] B. Ziegler, G. Rauhut, "Efficient generation of sum-of-products representations of high-dimensional potential energy surfaces based on multimode expansions", *J. Chem. Phys.* **2016**, *144*, 114114.

[112] G. Rauhut, "Efficient calculation of potential energy surfaces for the generation of vibrational wave functions", *J. Chem. Phys.* **2004**, *121*, 9313–9322.

[113] R. Ramakrishnan, G. Rauhut, "Semi-quartic force fields retrieved from multimode expansions: Accuracy, scaling behavior, and approximations", *J. Chem. Phys.* **2015**, *142*, 154118.

[114] B. Ziegler, G. Rauhut, "Rigorous use of symmetry within the construction of multidimensional potential energy surfaces", *J. Chem. Phys.* **2018**, *149*, 164110.

[115] A. M. Flowers, A. Brown, M. Klobukowski, "An Investigation into Transition States of Cyclic Tetra-Atomic Silicon and Germanium Interstellar Dust Compounds: Si_xC_{4-x}, Ge_xC_{4-x}, and Ge_xSi_{4-x} ($x \in \{1, 2, 3\}$)", *ChemRxiv.* **2024**, This content is a preprint and has not been peer-reviewed. doi:10.26434/chemrxiv-2024-6xq70.

[116] B. O. Roos, P. R. Taylor, P. E. Sigbahn, "A complete active space SCF method (CASSCF) using a density matrix formulated super-CI approach", *Chem. Phys.* **1980**, *48*, 157–173.

[117] H. Werner, P. J. Knowles, "A second order multiconfiguration SCF procedure with optimum convergence", *J. Chem. Phys.* **1985**, *82*, 5053–5063.

[118] B. O. Roos, "The Complete Active Space Self-Consistent Field Method and its Applications in Electronic Structure Calculations", *Adv. Chem. Phys.* **1987**, *69*, 399–445.

[119] R. A. Kendall, T. H. Dunning, R. J. Harrison, "Electron affinities of the first-row atoms revisited. Systematic basis sets and wave functions", *J. Chem. Phys.* **1992**, *96*, 6796–6806.

[120] D. E. Woon, T. H. Dunning, "Gaussian basis sets for use in correlated molecular calculations. III. The atoms aluminum through argon", *J. Chem. Phys.* **1993**, *98*, 1358–1371.

[121] A. K. Wilson, D. E. Woon, K. A. Peterson, T. H. Dunning, "Gaussian basis sets for use in correlated molecular calculations. IX. The atoms gallium through krypton", *J. Chem. Phys.* **1999**, *110*, 7667–7676.

[122] D. A. Kreplin, P. J. Knowles, H.-J. Werner, "Second-order MCSCF optimization revisited. I. Improved algorithms for fast and robust second-order CASSCF convergence", *J. Chem. Phys.* **2019**, *150*, 194106.

[123] V. Wakelam, E. Bron, S. Cazaux, F. Dulieu, C. Gry, P. Guillard, E. Habart, L. Hornekær, S. Morisset, G. Nyman, V. Pirronello, S. D. Price, V. Valdivia, G. Vidali, N. Watanabe, "H_2 formation on interstellar dust grains: The viewpoints of theory, experiments, models and observations", *Mol. Astrophys.* **2017**, *9*, 1–36.

[124] V. J. Herrero, M. Jiménez-Redondo, R. J. Peláez, B. Maté, I. Tanarro, "Structure and evolution of interstellar carbonaceous dust. Insights from the laboratory", *Front. Astron. Space Sci.* **2022**, *9*, 1083288.

[125] S. Kwok in *The Origin and Evolution of Planetary Nebulae*, Cambridge University Press, **2000**, 199–207.

[126] P. Hoppe, J. Leitner, J. Kodolńyi, S. Borrmann, A. P. Jones, "Dust from supernovae and their progenitors in the solar nebula", *Nat. Astron.* **2022**, *6*, 1027–1034.

[127] J. A. Cardelli, "The Abundance of Heavy Elements in Interstellar Gas", *Science* **1994**, *265*, 209–213.

[128] A. M. Flowers, A. Brown, M. Klobukowski, "Anharmonic vibrational spectroscopy of germanium-containing clusters, Ge_xC_{4-x} and Ge_xSi_{4-x} (x = 0-4), for interstellar detection", *J. Phys. Chem. A.* **2024**, *128*, 5351–5361.

[129] I. L. Alberts, R. S. Grev, H. F. Schaefer, "Geometrical structures and vibrational frequencies of the energetically low-lying isomers of SiC3", *J. Chem. Phys* **1990**, *93*, 5046–5052.

[130] T. Yang, L. Bertels, B. B. Dangi, X. Li, M. Head-Gordon, R. I. Kaiser, "Gas phase formation of c-SiC_3 molecules in the circumstellar envelope of carbon stars", *Proc. Natl. Acad. Sci. U.S.A.* **2019**, *116*, 14471–14478.

[131] F. Neese, "Software update: The ORCA program system—Version 5.0", *Wiley Interdiscip. Rev.: Comput. Mol. Sci.* **2022**, *12*, e1606.

[132] V. Ásgeirsson, B. O. Birgisson, R. Bjornsson, U. Becker, F. Neese, C. Riplinger, H. Jónsson, "Nudged Elastic Band Method for Molecular Reactions Using Energy-Weighted Springs Combined with Eigenvector Following", *J. Chem. Theory Comput.* **2021**, *17*, 4929–4945.

[133] K. Fukui, "Formulation of the reaction coordinate", *J. Phys. Chem.* **1970**, *74*, 4161–4163.

[134] K. Fukui, "The path of chemical reactions - the IRC approach", *Acc. Chem. Res.* **1981**, *14*, 363–368.

[135] L. Deng, T. Ziegler, "The determination of intrinsic reaction coordinates by density functional theory", *Int. J. Quantum Chem.* **1994**, *52*, 731–765.

[136] S. Grimme, J. Antony, S. Ehrlich, H. Krieg, "A consistent and accurate ab initio parametrization of density functional dispersion correction (DFT-D) for the 94 elements H-Pu", *J. Chem. Phys.* **2010**, *132*, 154104.

[137] S. Grimme, S. Ehrlich, L. Goerigk, "Effect of the damping function in dispersion corrected density functional theory", *J. Comput. Chem.* **2011**, *32*, 1456–1465.

[138] Y. Zhao, D. G. Truhlar, "The M06 suite of density functionals for main group thermochemistry, thermochemical kinetics, noncovalent interactions, excited states, and transition elements: two new functionals and systematic testing of four M06-class functionals and 12 other functionals", *Theor. Chem. Acc.* **2008**, *120*, 215–241.

[139] Y. Zhao, D. G. Truhlar, "Density Functionals with Broad Applicability in Chemistry", *Acc. Chem. Res.* **2008**, *41*, 157–167.

[140] J.-D. Chai, M. Head-Gordon, "Systematic optimization of long-range corrected hybrid density functionals", *J. Chem. Phys.* **2008**, *128*, 084106.

[141] J.-D. Chai, M. Head-Gordon, "Long-range corrected hybrid density functionals with damped atom–atom dispersion corrections", *Phys. Chem. Chem. Phys.* **2008**, *10*, 6615–6620.

[142] E. Caldeweyher, C. Bannwarth, S. Grimme, "Extension of the D3 dispersion coefficient model", *J. Chem. Phys.* **2017**, *147*, 034112.

[143] E. Caldeweyher, S. Ehlert, A. Hansen, H. Neugebauer, S. Spicher, C. Bannwarth, S. Grimme, "A generally applicable atomic-charge dependent London dispersion correction", *J. Chem. Phys.* **2019**, *150*, 154122.

[144] B. Helmich-Paris, B. de Souza, F. Neese, R. Izsák, "An improved chain of spheres for exchange algorithm", *J. Chem. Phys.* **2021**, *155*, 104109.

[145] F. Weigend, A. Köhn, C. Hättig, "Efficient use of the correlation consistent basis sets in resolution of the identity MP2 calculations", *J. Chem. Phys.* **2002**, *116*, 3175–3183.

[146] J. P. Perdew, K. Schmidt, "Jacob's ladder of density functional approximations for the exchange-correlation energy", *AIP Conf. Proc.* **2001**, *577*, 1–20.

[147] I. B. Bersuker, "Jahn–Teller and Pseudo-Jahn–Teller Effects: From Particular Features to General Tools in Exploring Molecular and Solid State Properties", *Chem. Rev.* **2021**, *121*, 1463–1512.

Appendix A: Chapter 2 Supporting Information

In this Appendix accompanying Chapter 2, the relative zero-point vibrational energies of all species are included. Also shown are the vibrational frequencies and/or rotational constants for r-C_4, r-Si_4, Ge_2Si_2 isomers, and Ge_3Si isomers are also collected in the SI. The effects of correlating d-orbitals for r-Ge_2C_2 and t-Ge_2C_2 on vibrational frequencies, rotational constants, dipole moment, and relative energies are also found within. Probabilities of all possible combinations of germanium isotopes for each group of structures are included. Lastly, T_1 diagnostics, configuration coefficients from CASSCF computations, and Cartesian coordinates of all species studied are found herein.

A.1 Supporting Data

Table A.1: Ge_xZ_{4-x} family zero-point energies in cm^{-1} and the relative energies of optimized geometries with inclusions of ZPVE. Relative energies are taken with respect to the lowest energy isomer in each family. Values obtained at the CCSD(T)-F12a/cc-pVTZ-F12 level of theory

Structure	Symmetry	ZPVE (cm^{-1})		ΔE_0^{ZPVE} (kJ mol^{-1})	
		Harmonic	Anharmonic	Harmonic	Anharmonic
d-GeC_3	C_{2v}	2208.64	2195.09	0.000	0.000
r-GeC_3	C_{2v}	2173.25	2164.95	10.540	10.603
t-Ge_2C_2	C_s	1712.92	1706.31	0.000	0.000
r-Ge_2C_2	D_{2h}	1745.95	1736.58	20.413	20.381
d-Ge_2C_2	C_{2v}	1261.86[a]	*b*	397.491	*b*
r-Ge_3C	C_{2v}	1142.51	1140.80	0.000	0.000
d-Ge_3C	C_s	925.44	918.73	189.830	189.778
d-$GeSi_3$	C_{2v}	949.07	947.69	0.000	0.000
r-$GeSi_3$	C_{2v}	926.16	922.53	16.982	16.957
r-Ge_2Si_2	D_{2h}	840.73	839.26	0.000	0.000
t-Ge_2Si_2	C_s	820.90	818.69	12.871	12.862
d-Ge_2Si_2	D_{2h}	790.63	788.66	32.643	32.637
r-Ge_3Si	C_{2v}	712.73	711.15	0.000	0.000
d-Ge_3Si	C_{2v}	685.72	684.72	15.666	15.660
Ge_4	D_{2h}	579.88	577.77	0.000	0.000
Si_4	D_{2h}	1052.98	1050.10	0.000	0.000
C_4	D_{2h}	2733.73	2715.29	0.000	0.000

[a]CCSD(T)-F12a/cc-pVDZ-F12

[b]Anharmonic frequencies could not be determined(see main text for details).

Table A.2: Harmonic and anharmonic vibrational frequencies for r-C_4 in cm^{-1}. Intensities in km mol^{-1}. MAD of F12a/TZ shown with respect to F12b/QZ and F12-TZ-cCR under the respective columns methods.

Mode	Symmetry	F12a/TZ	F12b/QZ	F12-TZ-cCR[a]	Intensity[b]
Harmonic					
6	B_{1u}	1386.7	1387.8	1395.8	
5	A_g	1264.3	1264.9	1272.5	
4	B_{2g}	1031.8	1032.4	1038.1	
3	A_g	944.1	945.0	949.6	
2	B_{3u}	536.7	538.3	541.1	
1	B_{2u}	303.9	304.5	306.4	
Anharmonic					
6	B_{1u}	1306.5	1307.6	1315.1	144.1
5	A_g	1248.7	1249.4	1252.8	0.0
4	B_{2g}	996.9	997.5	1002.9	0.0
3	A_g	925.7	926.7	931.1	0.0
2	B_{3u}	521.1	522.5	525.2	96.7
1	B_{2u}	303.0	303.5	305.9	27.1
MAD			0.12	0.65	

[a]Sehring et al. 2022[73]

[b]F12a/TZ intensities

Table A.3: Equilibrium (e) and vibrationally-averaged (0) rotational constants of r-C_4 (in MHz) at the F12a/TZ and F12b/QZ levels of theory. MAD of F12a/TZ shown with respect to F12b/QZ and F12-TZ-cCR methods.

Constant	F12a/TZ	F12b/QZ	F12-TZ-cCR[a]
A_e	36844.1	36878.7	37154.2
B_e	13786.9	13797.6	13875.6
C_e	10032.7	10040.9	10102.7
A_0	36591.3	36623.8	36897.8
B_0	13720.9	13731.5	13809.2
C_0	9963.9	9972.0	10033.3
MAD		0.26	0.83

[a]Sehring et al. 2022[73]

Table A.4: Equilibrium (e) and vibrationally-averaged (0) rotational constants of r-Si_4 and r-Ge_4 (in MHz) at the F12a/TZ level of theory. MAD is shown for the F12a/TZ method with respect to the F12-TZ-cCR method.

r-Si_4	F12a/TZ	F12-TZ-cCR[a]	r-Ge_4	F12a/TZ
A_e	6207.9	6294.7	A_e	2013.5
B_e	2304.8	2334.5	B_e	776.3
C_e	1680.8	1702.8	C_e	560.3
A_0	6182.9	6269.0	A_0	2009.6
B_0	2300.1	2329.6	B_0	775.2
C_0	1676.2	1698.3	C_0	559.3
MAD	1.31			

[a]Sehring et al. 2022[73]

Table A.5: T_1 diagnostics for Ge_xZ_y family.

Structure	T_1 diagnostic
d-GeC_3	0.0171
r-GeC_3	0.0199
d-Ge_2C_2	0.0978
r-Ge_2C_2	0.0156
t-Ge_2C_2	0.0193
d-Ge_3C	0.0393
r-Ge_3C	0.0175
d-GeC_3	0.0189
r-GeC_3	0.0199
d-Ge_2Si_2	0.0201
r-Ge_2Si_2	0.0185
t-Ge_2Si_2	0.0196
d-Ge_3Si	0.0198
r-Ge_3Si	0.0191
r-C_4	0.0160
r-Si_4	0.0192
r-Ge_4	0.0193

Table A.6: CASSCF CI coefficients greater than 0.05 for each Ge_xZ_y structure optimized at the CCSD(T)-F12a/cc-pVTZ level of theory (cc-pVDZ basis set used for d-Ge_2C_2) in the MOLPRO 2023 convention, grouped by symmetry block and indicated by occupancy (α and β spins solely indicated by 1, and thus all permutations have the same coefficient). The Configuration column indicates the occupancies of each orbital in each irreducible representation in the active space. Energies in atomic units, followed by relative energies (kJ mol^{-1}).

Configuration	Coefficient	Configuration	Coefficient
d-GeC_3		r-GeC_3	
2222200 200 22000 0	0.91500778	2222000 200 22200 0	0.91049691
2222200 000 22000 2	-0.08600287	2222000 000 22200 2	-0.07851504
2222000 200 22200 0	-0.07156186	2222000 200 22020 0	-0.07427818
2220200 220 22000 0	-0.06760371	2222100 100 22100 1	-0.05855324
2222100 100 22100 1	0.05278737	2222200 200 22000 0	-0.05675071
2220200 202 22000 0	-0.05211771	2222000 020 22200 0	-0.05588636
2222200 200 20200 0	-0.05007854	2022000 220 22200 0	-0.05171822
		2202000 200 22200 2	-0.05167740
Energy:	-2189.04826474	Energy:	-2189.04584629
ΔE	0.000	ΔE	6.350
t-Ge_2C_2		r-Ge_2C_2	
222222200000 2000	0.91294305	2220 20 200 0 220 0 20	0.91611257
222222200000 0020	-0.06725634	2220 00 200 2 220 0 20	-0.09341382
222220220000 2000	-0.06139206	2220 20 220 0 220 0 00	-0.06830261
222222020000 2000	-0.05873929	2220 20 200 0 200 2 20	-0.06641096
222222200000 0200	-0.05858123	2220 20 200 0 220 0 02	-0.05458133
222222000000 2200	-0.05194887		
Energy:	-4226.65657065	Energy:	-4226.64698149
ΔE	0.000	ΔE	25.176
d-Ge_2C_2		r-Ge_3C	
222200 2200 2000 20	0.85737357	2222000 200 22200 0	0.90877243

Continued on next page

Continued from previous page

Configuration	**Coefficient**	**Configuration**	**Coefficient**
222000 2220 2000 20	-0.19148152	2222000 020 22200 0	-0.09272950
220200 2200 2200 20	-0.10693784	2220200 200 22200 0	-0.06993924
222200 2200 2200 00	-0.09535573	2222000 200 22020 0	-0.06414992
222220 2000 2000 20	-0.08468368	2222200 200 22000 0	-0.06382005
222100 2210 2100 10	-0.08209603	2221100 110 22200 0	-0.05266874
222110 2110 2000 20	-0.07053707		
222210 2100 2100 10	0.06040019		
Energy:	-4226.51328711	Energy:	-6264.23589608
ΔE	800.914	ΔE	0.000
d-Ge_3C		d-$GeSi_3$	
2222220000 220000	0.88155276	2222200 200 22000 0	0.89566325
2222202000 220000	-0.12419861	2222200 000 22000 2	-0.08335207
2222220000 202000	-0.08815945	2222200 020 22000 0	-0.08009242
2222211000 211000	0.07182832	2222200 200 20200 0	-0.07195616
2222020000 222000	-0.07110762	2222000 200 22200 0	-0.05917903
2222200000 220200	-0.06157629	2222200 110 21100 0	0.05772836
		2222000 220 22000 0	-0.05410323
Energy:	-6264.16035470	Energy:	-2942.33038920
ΔE	198.331	ΔE	0.000
r-$GeSi_3$		r-Ge_2Si_2	
222222200000 2000	0.89271848	2220 20 200 0 220 0 20	0.89612580
222222200000 0020	-0.08625258	2220 00 200 0 220 2 20	-0.08490783
222220220000 2000	-0.08192842	2200 20 220 0 220 0 20	-0.08474831
222222000000 2200	-0.08038026	2220 00 200 2 220 0 20	-0.08375746
222222200000 0200	-0.07440030	2220 20 220 0 220 0 00	-0.07477118
222202220000 2000	-0.07206337	2220 10 210 0 220 1 10	0.06117203

Continued on next page

Continued from previous page

Configuration	Coefficient	Configuration	Coefficient
222212210000 1100	-0.05822749	2210 10 210 1 220 0 20	0.05610422
222221210000 1010	-0.05545335	2220 20 200 0 200 2 20	-0.05243168
Energy:	-2942.325855	Energy:	-4728.82164806
ΔE	11.904	ΔE	0.000
t-Ge_2Si_2		d-Ge_2Si_2	
222222200000 2000	0.89461682	2220 200 220 20 20 0 0	0.89205310
222222200000 0020	-0.08574146	2220 200 220 20 00 2 0	-0.08849824
222222200000 0200	-0.08142141	2220 200 200 20 20 0 2	-0.08146640
222220220000 2000	-0.07381378	2200 220 220 20 20 0 0	-0.07636940
222221210000 1100	0.05923798	2220 200 220 20 00 0 2	-0.07607603
222222020000 2000	-0.05493710	2220 220 220 00 20 0 0	-0.07549850
222222000000 2200	-0.05322976	2220 210 220 10 10 0 1	-0.05986750
		2210 210 220 20 10 1 0	-0.05533228
		2120 200 210 20 21 0 1	0.05125905
Energy:	-4728.81856409	Energy:	-4728.81324328
ΔE	8.097	ΔE	22.066
r-Ge_3Si		d-Ge_3Si	
222222200000 2000	0.89538416	2222200 200 22000 0	0.89366454
222222200000 0200	-0.08704254	2222200 000 22000 2	-0.08794183
222222200000 0020	-0.08587740	2222200 020 22000 0	-0.08253562
222220220000 2000	-0.08095914	2222200 200 20200 0	-0.07712312
222222020000 2000	-0.07602758	2222200 110 21100 0	0.06120445
222222110000 1100	0.06218950	2222000 220 22000 0	-0.05778279
222221210000 1010	0.05550163	2220200 200 22200 0	-0.05194697
222202200000 2200	-0.05251638		
Energy:	-6515.31097852	Energy:	-6515.30695672

Continued on next page

Continued from previous page

Configuration	**Coefficient**	**Configuration**	**Coefficient**
ΔE	0.000	ΔE	10.559

Table A.7: Equilibrium rotational constants of r- and t-Ge_2C_2 isomers (in MHz) at the F12a/TZ level of theory. Dipole moments (μ, in Debye) of optimized structures are also included. Lastly, relative energies of optimized structures (in kJ mol^{-1}) with and without harmonic zero-point vibrational energy corrections are included. Results are shown for computations with the d-orbitals included in the core and for those where d-orbitals are correlated as part of the valence space.

Mode	r-Ge_2C_2		t-Ge_2C_2	
	d-core	d-val	d-core	d-val
A	41397.3	41234.8	7739.8	7852.1
B	1058.8	1081.3	1855.5	1901.3
C	1032.4	1053.6	1496.7	1530.6
μ	0.00	0.00	3.52	3.45
ΔE_0	20.018	18.762	0.000	0.000
ΔE_0^{ZPVE}	20.414	19.128	0.000	0.000

Table A.8: Harmonic fundamental vibrational frequencies (in cm^{-1}) of r- and t-Ge_2C_2 isomers at the F12a/TZ level of theory. Results are shown for computations with the d-orbitals included in the core and for those where d-orbitals are correlated as part of the valence space.

Mode	r-Ge_2C_2		t-Ge_2C_2	
	d-core	d-val	d-core	d-val
6	147.2	147.3	178.1	180.8
5	276.5	279.7	182.7	185.7
4	281.9	284.7	392.5	393.7
3	816.1	821.8	515.5	521.6
2	868.2	875.1	575.8	585.8
1	1102.1	1093.5	1581.2	1573.3

Table A.9: Harmonic and anharmonic fundamental vibrational frequencies (in cm^{-1}) of Ge_2Si_2 isomers at the F12a/TZ level of theory. Intensities in km mol^{-1}.

Mode	Symmetry	Harmonic	Anharmonic	Intensity
r-Ge_2Si_2				
6	A_g	424.4	418.9	0.0
5	B_{1u}	406.6	402.0	119.8
4	B_{2g}	381.5	376.7	0.0
3	A_g	216.5	215.5	0.0
2	B_{3u}	191.3	190.0	4.4
1	B_{2u}	61.1	62.9	0.3
t-Ge_2Si_2				
6	A'	481.2	479.7	48.9
5	A'	369.7	367.1	8.3
4	A'	309.7	303.9	3.9
3	A'	242.1	240.3	9.4
2	A'	172.8	171.5	0.9
1	A''	65.9	66.3	1.0
d-Ge_2Si_2				
6	B_{2u}	395.7	391.2	86.9
5	A_g	385.2	384.2	0.0
4	B_{1g}	304.8	301.5	0.0
3	A_g	234.7	233.4	0.0
2	B_{3u}	192.0	190.1	0.3
1	B_{1u}	68.4	68.6	1.6

Table A.10: Equilibrium (e) and vibrationally-averaged (0) rotational constants of Ge_2Si_2 isomers in MHz at the F12a/TZ level of theory. Vibrationally-averaged constants for most intense vibration for each isomer are also included.

Constant	r-Ge_2Si_2	Constant	t-Ge_2Si_2	Constant	d-Ge_2Si_2
A_e	6121.1	A_e	3448.8	A_e	2219.9
B_e	804.3	B_e	1295.6	B_e	2051.3
C_e	709.5	C_e	941.7	C_e	1066.2
A_0	6096.8	A_0	3438.7	A_0	2215.1
B_0	803.0	B_0	1293.6	B_0	2046.9
C_0	709.5	C_0	939.7	C_0	1063.5
A_5	6147.0	A_6	3418.2	A_6	2217.1
B_5	801.5	B_6	1295.8	B_6	2039.6
C_5	708.0	C_6	941.7	C_6	1065.0

Table A.11: Harmonic and anharmonic fundamental vibrational frequencies in cm^{-1} of Ge_3Si isomers using F12a/TZ. Intensities in km mol^{-1}.

Mode	Symmetry	Harmonic	Anharmonic	Intensity
d-Ge_3Si				
6	A_1	392.3	387.2	49.1
5	B_2	281.9	279.0	0.0
4	A_1	271.9	269.8	18.5
3	A_1	212.5	211.2	3.6
2	B_2	154.2	153.2	0.1
1	B_1	59.7	59.4	0.9
r-Ge_3Si				
6	B_2	411.6	407.3	81.1
5	A_1	352.1	348.5	2.3
4	B_2	248.1	246.0	15.6
3	A_1	205.6	204.7	0.2
2	A_1	150.3	149.5	0.5
1	B_1	57.2	57.6	0.3

Table A.12: Probability of finding a d- or r- isomer of GeZ_3 with each isotope of germanium.

Combination	**Probability**
Ge-74	0.365
Ge-72	0.274
Ge-70	0.205
Ge-73	0.0776
Ge-76	0.0775
Total arrangements:	5

Table A.13: All possible unique combinations of isotopes and their respective probabilities for d-, r-, and t- isomers of Ge_2Z_2. The t- isomers have ten extra combinations due to the lack of symmetry, but the probabilities are equivalent.

Combination	**Probability**
Ge-74 - Ge-74	0.13322
Ge-72 - Ge-74	0.10001
Ge-72 - Ge-72	0.07508
Ge-70 - Ge-74	0.07482
Ge-70 - Ge-72	0.05617
Ge-70 - Ge-70	0.04202
Ge-73 - Ge-74	0.02832
Ge-74 - Ge-76	0.02829
Ge-72 - Ge-73	0.02126
Ge-72 - Ge-76	0.02124
Ge-70 - Ge-73	0.01591
Ge-70 - Ge-76	0.01589
Ge-73 - Ge-73	0.00602
Ge-73 - Ge-76	0.00601
Ge-76 - Ge-76	0.00601
Total arrangements:	15

Table A.14: All possible unique combinations of isotopes for d- and r- Ge_3Z isomers and their probabilities.

Combination	**Probability**
Ge-74 - Ge-74 - Ge-74	0.04863
Ge-74 - Ge-74 - Ge-72	0.03650
Ge-72 - Ge-74 - Ge-74	0.03650
Ge-72 - Ge-72 - Ge-74	0.02740
Ge-72 - Ge-74 - Ge-72	0.02740
Ge-74 - Ge-74 - Ge-70	0.02731
Ge-70 - Ge-74 - Ge-74	0.02731
Ge-72 - Ge-72 - Ge-72	0.02057
Ge-72 - Ge-74 - Ge-70	0.02050
Ge-70 - Ge-74 - Ge-72	0.02050
Ge-70 - Ge-72 - Ge-74	0.02050
Ge-72 - Ge-72 - Ge-70	0.01539
Ge-70 - Ge-72 - Ge-72	0.01539
Ge-70 - Ge-70 - Ge-74	0.01534
Ge-70 - Ge-74 - Ge-70	0.01534
Ge-70 - Ge-72 - Ge-70	0.01151
Ge-70 - Ge-70 - Ge-72	0.01151
Ge-74 - Ge-74 - Ge-73	0.01034
Ge-73 - Ge-74 - Ge-74	0.01034
Ge-74 - Ge-74 - Ge-76	0.01032
Ge-74 - Ge-76 - Ge-74	0.01032
Ge-70 - Ge-70 - Ge-70	0.00862
Ge-73 - Ge-74 - Ge-72	0.00776
Ge-72 - Ge-74 - Ge-73	0.00776
Ge-72 - Ge-73 - Ge-74	0.00776

Continued on next page

Continued from previous page

Combination	Probability
Ge-74 - Ge-76 - Ge-72	0.00775
Ge-72 - Ge-76 - Ge-74	0.00775
Ge-72 - Ge-74 - Ge-76	0.00775
Ge-72 - Ge-72 - Ge-73	0.00583
Ge-72 - Ge-73 - Ge-72	0.00583
Ge-72 - Ge-72 - Ge-76	0.00582
Ge-72 - Ge-76 - Ge-72	0.00582
Ge-70 - Ge-73 - Ge-74	0.00581
Ge-73 - Ge-74 - Ge-70	0.00581
Ge-70 - Ge-74 - Ge-73	0.00581
Ge-70 - Ge-74 - Ge-76	0.00580
Ge-74 - Ge-76 - Ge-70	0.00580
Ge-70 - Ge-76 - Ge-74	0.00580
Ge-70 - Ge-72 - Ge-73	0.00436
Ge-70 - Ge-73 - Ge-72	0.00436
Ge-72 - Ge-73 - Ge-70	0.00436
Ge-72 - Ge-76 - Ge-70	0.00435
Ge-70 - Ge-72 - Ge-76	0.00435
Ge-70 - Ge-76 - Ge-72	0.00435
Ge-70 - Ge-73 - Ge-70	0.00326
Ge-70 - Ge-70 - Ge-73	0.00326
Ge-70 - Ge-76 - Ge-70	0.00326
Ge-70 - Ge-70 - Ge-76	0.00326
Ge-73 - Ge-73 - Ge-74	0.00220
Ge-73 - Ge-74 - Ge-73	0.00220
Ge-73 - Ge-76 - Ge-74	0.00220

Continued on next page

Continued from previous page

Combination	Probability
Ge-74 - Ge-76 - Ge-73	0.00220
Ge-73 - Ge-74 - Ge-76	0.00220
Ge-76 - Ge-76 - Ge-74	0.00219
Ge-74 - Ge-76 - Ge-76	0.00219
Ge-72 - Ge-73 - Ge-73	0.00165
Ge-73 - Ge-73 - Ge-72	0.00165
Ge-72 - Ge-76 - Ge-73	0.00165
Ge-73 - Ge-76 - Ge-72	0.00165
Ge-72 - Ge-73 - Ge-76	0.00165
Ge-76 - Ge-76 - Ge-72	0.00165
Ge-72 - Ge-76 - Ge-76	0.00165
Ge-73 - Ge-73 - Ge-70	0.00123
Ge-70 - Ge-73 - Ge-73	0.00123
Ge-73 - Ge-76 - Ge-70	0.00123
Ge-70 - Ge-76 - Ge-73	0.00123
Ge-70 - Ge-73 - Ge-76	0.00123
Ge-70 - Ge-76 - Ge-76	0.00123
Ge-76 - Ge-76 - Ge-70	0.00123
Ge-73 - Ge-73 - Ge-73	0.00047
Ge-73 - Ge-76 - Ge-73	0.00047
Ge-73 - Ge-73 - Ge-76	0.00047
Ge-76 - Ge-76 - Ge-73	0.00047
Ge-73 - Ge-76 - Ge-76	0.00047
Ge-76 - Ge-76 - Ge-76	0.00047
Total arrangements:	75

Table A.15: All possible unique combinations of isotopes for Ge_4 and their probabilities.

Combination	**Probability**
Ge-74-Ge-74-Ge-74-Ge-74	0.017749
Ge-72-Ge-74-Ge-74-Ge-74	0.013324
Ge-74-Ge-74-Ge-72-Ge-74	0.013324
Ge-72-Ge-72-Ge-74-Ge-74	0.010002
Ge-72-Ge-74-Ge-72-Ge-74	0.010002
Ge-74-Ge-74-Ge-72-Ge-72	0.010002
Ge-70-Ge-74-Ge-74-Ge-74	0.009969
Ge-74-Ge-74-Ge-70-Ge-74	0.009969
Ge-72-Ge-72-Ge-72-Ge-74	0.007508
Ge-72-Ge-74-Ge-72-Ge-72	0.007508
Ge-72-Ge-74-Ge-70-Ge-74	0.007483
Ge-74-Ge-74-Ge-70-Ge-72	0.007483
Ge-70-Ge-72-Ge-74-Ge-74	0.007483
Ge-70-Ge-74-Ge-72-Ge-74	0.007483
Ge-72-Ge-72-Ge-72-Ge-72	0.005636
Ge-72-Ge-72-Ge-70-Ge-74	0.005618
Ge-72-Ge-74-Ge-70-Ge-72	0.005618
Ge-70-Ge-72-Ge-72-Ge-74	0.005618
Ge-70-Ge-74-Ge-72-Ge-72	0.005618
Ge-70-Ge-70-Ge-74-Ge-74	0.005599
Ge-70-Ge-74-Ge-70-Ge-74	0.005599
Ge-74-Ge-74-Ge-70-Ge-70	0.005599
Ge-70-Ge-72-Ge-72-Ge-72	0.004217
Ge-72-Ge-72-Ge-70-Ge-72	0.004217
Ge-70-Ge-70-Ge-72-Ge-74	0.004203

Continued on next page

Continued from previous page

Combination	Probability
Ge-70-Ge-72-Ge-70-Ge-74	0.004203
Ge-70-Ge-74-Ge-70-Ge-72	0.004203
Ge-72-Ge-74-Ge-70-Ge-70	0.004203
Ge-73-Ge-74-Ge-74-Ge-74	0.003773
Ge-74-Ge-74-Ge-73-Ge-74	0.003773
Ge-74-Ge-76-Ge-74-Ge-74	0.003769
Ge-74-Ge-74-Ge-74-Ge-76	0.003769
Ge-72-Ge-72-Ge-70-Ge-70	0.003155
Ge-70-Ge-70-Ge-72-Ge-72	0.003155
Ge-70-Ge-72-Ge-70-Ge-72	0.003155
Ge-70-Ge-70-Ge-70-Ge-74	0.003145
Ge-70-Ge-74-Ge-70-Ge-70	0.003145
Ge-72-Ge-73-Ge-74-Ge-74	0.002833
Ge-72-Ge-74-Ge-73-Ge-74	0.002833
Ge-73-Ge-74-Ge-72-Ge-74	0.002833
Ge-74-Ge-74-Ge-72-Ge-73	0.002833
Ge-72-Ge-74-Ge-74-Ge-76	0.002829
Ge-72-Ge-76-Ge-74-Ge-74	0.002829
Ge-74-Ge-74-Ge-72-Ge-76	0.002829
Ge-74-Ge-76-Ge-72-Ge-74	0.002829
Ge-70-Ge-70-Ge-70-Ge-72	0.002361
Ge-70-Ge-72-Ge-70-Ge-70	0.002361
Ge-72-Ge-72-Ge-73-Ge-74	0.002126
Ge-72-Ge-73-Ge-72-Ge-74	0.002126
Ge-72-Ge-74-Ge-72-Ge-73	0.002126
Ge-73-Ge-74-Ge-72-Ge-72	0.002126

Continued on next page

Continued from previous page

Combination	Probability
Ge-72-Ge-72-Ge-74-Ge-76	0.002124
Ge-72-Ge-74-Ge-72-Ge-76	0.002124
Ge-72-Ge-76-Ge-72-Ge-74	0.002124
Ge-74-Ge-76-Ge-72-Ge-72	0.002124
Ge-70-Ge-73-Ge-74-Ge-74	0.002119
Ge-70-Ge-74-Ge-73-Ge-74	0.002119
Ge-73-Ge-74-Ge-70-Ge-74	0.002119
Ge-74-Ge-74-Ge-70-Ge-73	0.002119
Ge-70-Ge-74-Ge-74-Ge-76	0.002117
Ge-70-Ge-76-Ge-74-Ge-74	0.002117
Ge-74-Ge-74-Ge-70-Ge-76	0.002117
Ge-74-Ge-76-Ge-70-Ge-74	0.002117
Ge-70-Ge-70-Ge-70-Ge-70	0.001766
Ge-72-Ge-72-Ge-72-Ge-73	0.001596
Ge-72-Ge-73-Ge-72-Ge-72	0.001596
Ge-72-Ge-72-Ge-72-Ge-76	0.001594
Ge-72-Ge-76-Ge-72-Ge-72	0.001594
Ge-72-Ge-74-Ge-70-Ge-73	0.001591
Ge-70-Ge-72-Ge-73-Ge-74	0.001591
Ge-70-Ge-73-Ge-72-Ge-74	0.001591
Ge-72-Ge-73-Ge-70-Ge-74	0.001591
Ge-73-Ge-74-Ge-70-Ge-72	0.001591
Ge-70-Ge-74-Ge-72-Ge-73	0.001591
Ge-70-Ge-76-Ge-72-Ge-74	0.001589
Ge-72-Ge-74-Ge-70-Ge-76	0.001589
Ge-72-Ge-76-Ge-70-Ge-74	0.001589

Continued on next page

Continued from previous page

Combination	Probability
Ge-74-Ge-76-Ge-70-Ge-72	0.001589
Ge-70-Ge-72-Ge-74-Ge-76	0.001589
Ge-70-Ge-74-Ge-72-Ge-76	0.001589
Ge-70-Ge-72-Ge-72-Ge-73	0.001194
Ge-70-Ge-73-Ge-72-Ge-72	0.001194
Ge-72-Ge-72-Ge-70-Ge-73	0.001194
Ge-72-Ge-73-Ge-70-Ge-72	0.001194
Ge-70-Ge-72-Ge-72-Ge-76	0.001193
Ge-70-Ge-76-Ge-72-Ge-72	0.001193
Ge-72-Ge-72-Ge-70-Ge-76	0.001193
Ge-72-Ge-76-Ge-70-Ge-72	0.001193
Ge-70-Ge-70-Ge-73-Ge-74	0.001190
Ge-70-Ge-73-Ge-70-Ge-74	0.001190
Ge-70-Ge-74-Ge-70-Ge-73	0.001190
Ge-73-Ge-74-Ge-70-Ge-70	0.001190
Ge-74-Ge-76-Ge-70-Ge-70	0.001189
Ge-70-Ge-70-Ge-74-Ge-76	0.001189
Ge-70-Ge-74-Ge-70-Ge-76	0.001189
Ge-70-Ge-76-Ge-70-Ge-74	0.001189
Ge-70-Ge-73-Ge-70-Ge-72	0.000894
Ge-72-Ge-73-Ge-70-Ge-70	0.000894
Ge-70-Ge-70-Ge-72-Ge-73	0.000894
Ge-70-Ge-72-Ge-70-Ge-73	0.000894
Ge-72-Ge-76-Ge-70-Ge-70	0.000892
Ge-70-Ge-70-Ge-72-Ge-76	0.000892
Ge-70-Ge-72-Ge-70-Ge-76	0.000892

Continued on next page

Continued from previous page

Combination	Probability
Ge-70-Ge-76-Ge-70-Ge-72	0.000892
Ge-73-Ge-73-Ge-74-Ge-74	0.000802
Ge-73-Ge-74-Ge-73-Ge-74	0.000802
Ge-74-Ge-74-Ge-73-Ge-73	0.000802
Ge-73-Ge-76-Ge-74-Ge-74	0.000801
Ge-74-Ge-76-Ge-73-Ge-74	0.000801
Ge-73-Ge-74-Ge-74-Ge-76	0.000801
Ge-74-Ge-74-Ge-73-Ge-76	0.000801
Ge-76-Ge-76-Ge-74-Ge-74	0.000800
Ge-74-Ge-74-Ge-76-Ge-76	0.000800
Ge-74-Ge-76-Ge-74-Ge-76	0.000800
Ge-70-Ge-73-Ge-70-Ge-70	0.000669
Ge-70-Ge-70-Ge-70-Ge-73	0.000669
Ge-70-Ge-70-Ge-70-Ge-76	0.000668
Ge-70-Ge-76-Ge-70-Ge-70	0.000668
Ge-72-Ge-73-Ge-73-Ge-74	0.000602
Ge-72-Ge-74-Ge-73-Ge-73	0.000602
Ge-73-Ge-73-Ge-72-Ge-74	0.000602
Ge-73-Ge-74-Ge-72-Ge-73	0.000602
Ge-72-Ge-73-Ge-74-Ge-76	0.000601
Ge-72-Ge-74-Ge-73-Ge-76	0.000601
Ge-72-Ge-76-Ge-73-Ge-74	0.000601
Ge-73-Ge-74-Ge-72-Ge-76	0.000601
Ge-73-Ge-76-Ge-72-Ge-74	0.000601
Ge-74-Ge-76-Ge-72-Ge-73	0.000601
Ge-74-Ge-76-Ge-72-Ge-76	0.000601

Continued on next page

Continued from previous page

Combination	Probability
Ge-76-Ge-76-Ge-72-Ge-74	0.000601
Ge-72-Ge-74-Ge-76-Ge-76	0.000601
Ge-72-Ge-76-Ge-74-Ge-76	0.000601
Ge-72-Ge-72-Ge-73-Ge-73	0.000452
Ge-73-Ge-73-Ge-72-Ge-72	0.000452
Ge-72-Ge-73-Ge-72-Ge-73	0.000452
Ge-72-Ge-72-Ge-73-Ge-76	0.000452
Ge-73-Ge-76-Ge-72-Ge-72	0.000452
Ge-72-Ge-73-Ge-72-Ge-76	0.000452
Ge-72-Ge-76-Ge-72-Ge-73	0.000452
Ge-72-Ge-72-Ge-76-Ge-76	0.000451
Ge-76-Ge-76-Ge-72-Ge-72	0.000451
Ge-72-Ge-76-Ge-72-Ge-76	0.000451
Ge-70-Ge-73-Ge-73-Ge-74	0.000451
Ge-70-Ge-74-Ge-73-Ge-73	0.000451
Ge-73-Ge-73-Ge-70-Ge-74	0.000451
Ge-73-Ge-74-Ge-70-Ge-73	0.000451
Ge-73-Ge-76-Ge-70-Ge-74	0.000450
Ge-70-Ge-73-Ge-74-Ge-76	0.000450
Ge-70-Ge-74-Ge-73-Ge-76	0.000450
Ge-73-Ge-74-Ge-70-Ge-76	0.000450
Ge-74-Ge-76-Ge-70-Ge-73	0.000450
Ge-70-Ge-76-Ge-73-Ge-74	0.000450
Ge-70-Ge-74-Ge-76-Ge-76	0.000449
Ge-70-Ge-76-Ge-74-Ge-76	0.000449
Ge-74-Ge-76-Ge-70-Ge-76	0.000449

Continued on next page

Continued from previous page

Combination	Probability
Ge-76-Ge-76-Ge-70-Ge-74	0.000449
Ge-70-Ge-72-Ge-73-Ge-73	0.000338
Ge-70-Ge-73-Ge-72-Ge-73	0.000338
Ge-72-Ge-73-Ge-70-Ge-73	0.000338
Ge-73-Ge-73-Ge-70-Ge-72	0.000338
Ge-73-Ge-76-Ge-70-Ge-72	0.000338
Ge-70-Ge-72-Ge-73-Ge-76	0.000338
Ge-70-Ge-73-Ge-72-Ge-76	0.000338
Ge-70-Ge-76-Ge-72-Ge-73	0.000338
Ge-72-Ge-73-Ge-70-Ge-76	0.000338
Ge-72-Ge-76-Ge-70-Ge-73	0.000338
Ge-70-Ge-72-Ge-76-Ge-76	0.000337
Ge-70-Ge-76-Ge-72-Ge-76	0.000337
Ge-72-Ge-76-Ge-70-Ge-76	0.000337
Ge-76-Ge-76-Ge-70-Ge-72	0.000337
Ge-70-Ge-70-Ge-73-Ge-73	0.000253
Ge-70-Ge-73-Ge-70-Ge-73	0.000253
Ge-73-Ge-73-Ge-70-Ge-70	0.000253
Ge-70-Ge-70-Ge-73-Ge-76	0.000253
Ge-70-Ge-73-Ge-70-Ge-76	0.000253
Ge-70-Ge-76-Ge-70-Ge-73	0.000253
Ge-73-Ge-76-Ge-70-Ge-70	0.000253
Ge-70-Ge-70-Ge-76-Ge-76	0.000252
Ge-70-Ge-76-Ge-70-Ge-76	0.000252
Ge-76-Ge-76-Ge-70-Ge-70	0.000252
Ge-73-Ge-73-Ge-73-Ge-74	0.000171

Continued on next page

Continued from previous page

Combination	Probability
Ge-73-Ge-74-Ge-73-Ge-73	0.000171
Ge-73-Ge-73-Ge-74-Ge-76	0.000170
Ge-74-Ge-76-Ge-73-Ge-73	0.000170
Ge-73-Ge-76-Ge-73-Ge-74	0.000170
Ge-73-Ge-74-Ge-73-Ge-76	0.000170
Ge-73-Ge-76-Ge-74-Ge-76	0.000170
Ge-74-Ge-76-Ge-73-Ge-76	0.000170
Ge-76-Ge-76-Ge-73-Ge-74	0.000170
Ge-73-Ge-74-Ge-76-Ge-76	0.000170
Ge-76-Ge-76-Ge-74-Ge-76	0.000170
Ge-74-Ge-76-Ge-76-Ge-76	0.000170
Ge-72-Ge-73-Ge-73-Ge-73	0.000128
Ge-73-Ge-73-Ge-72-Ge-73	0.000128
Ge-72-Ge-73-Ge-73-Ge-76	0.000128
Ge-72-Ge-76-Ge-73-Ge-73	0.000128
Ge-73-Ge-73-Ge-72-Ge-76	0.000128
Ge-73-Ge-76-Ge-72-Ge-73	0.000128
Ge-72-Ge-76-Ge-73-Ge-76	0.000128
Ge-73-Ge-76-Ge-72-Ge-76	0.000128
Ge-76-Ge-76-Ge-72-Ge-73	0.000128
Ge-72-Ge-73-Ge-76-Ge-76	0.000128
Ge-76-Ge-76-Ge-72-Ge-76	0.000128
Ge-72-Ge-76-Ge-76-Ge-76	0.000128
Ge-70-Ge-73-Ge-73-Ge-73	0.000096
Ge-73-Ge-73-Ge-70-Ge-73	0.000096
Ge-73-Ge-76-Ge-70-Ge-73	0.000096

Continued on next page

Continued from previous page

Combination	**Probability**
Ge-70-Ge-73-Ge-73-Ge-76	0.000096
Ge-73-Ge-73-Ge-70-Ge-76	0.000096
Ge-70-Ge-76-Ge-73-Ge-73	0.000096
Ge-73-Ge-76-Ge-70-Ge-76	0.000096
Ge-76-Ge-76-Ge-70-Ge-73	0.000096
Ge-70-Ge-73-Ge-76-Ge-76	0.000096
Ge-70-Ge-76-Ge-73-Ge-76	0.000096
Ge-70-Ge-76-Ge-76-Ge-76	0.000095
Ge-76-Ge-76-Ge-70-Ge-76	0.000095
Ge-73-Ge-73-Ge-73-Ge-73	0.000036
Ge-73-Ge-73-Ge-73-Ge-76	0.000036
Ge-73-Ge-76-Ge-73-Ge-73	0.000036
Ge-76-Ge-76-Ge-73-Ge-73	0.000036
Ge-73-Ge-73-Ge-76-Ge-76	0.000036
Ge-73-Ge-76-Ge-73-Ge-76	0.000036
Ge-73-Ge-76-Ge-76-Ge-76	0.000036
Ge-76-Ge-76-Ge-73-Ge-76	0.000036
Ge-76-Ge-76-Ge-76-Ge-76	0.000036
Total arrangements:	225

A.2 XYZ Coordinates

XYZ Coordinates (in Å) of all optimized geometries with energies (in atomic units).

r-C_4

4

CCSD(T)-F12A/CC-PVTZ-F12 ENERGY=-151.85227732

C 0.0000000000 0.0000000000 1.2352821139

C 0.0000000000 -0.7556784571 0.0000000000

C 0.0000000000 0.7556784571 0.0000000000

C 0.0000000000 0.0000000000 -1.2352821139

r-Si_4

4

CCSD(T)-F12A/CC-PVTZ-F12 ENERGY=-1156.20564048

Si 0.0000000000 0.0000000000 1.9758338538

Si 0.0000000000 -1.2039195887 0.0000000000

Si 0.0000000000 1.2039195887 0.0000000000

Si 0.0000000000 0.0000000000 -1.9758338538

r-Ge_4

4

CCSD(T)-F12A/CC-PVTZ-F12,GE=CC-PVTZ-PP-F12 ENERGY=-1174.08116329

Ge 0.0000000000 0.0000000000 -2.0984484658

Ge 0.0000000000 -1.3029462592 0.0000000000

Ge 0.0000000000 1.3029462592 0.0000000000

Ge 0.0000000000 0.0000000000 2.0984484658

d-GeC_3

4

CCSD(T)-F12A/CC-PVTZ-F12,GE=CC-PVTZ-PP-F12 ENERGY=-407.42723870

Ge 0.0000000000 0.0000000000 -1.6551152235

C 0.0000000000 -0.7478165238 0.1438703604

C 0.0000000000 0.7478165238 0.1438703604

C 0.0000000000 0.0000000000 1.3673745027

r-GeC_3

4

CCSD(T)-F12A/CC-PVTZ-F12,GE=CC-PVTZ-PP-F12 ENERGY=-407.42306306

Ge 0.0000000000 0.0000000000 -1.3612293390

C 0.0000000000 -1.3140459057 0.3594953033

C 0.0000000000 0.0000000000 0.6422387323

C 0.0000000000 1.3140459057 0.3594953033

d-$GeSi_3$

4

CCSD(T)-F12A/CC-PVTZ-F12,GE=CC-PVTZ-PP-F12 ENERGY=-1160.67655045

Ge 0.0000000000 0.0000000000 -2.0442757414

Si 0.0000000000 -1.2094073788 0.0257136117

Si 0.0000000000 1.2094073788 0.0257136117

Si 0.0000000000 0.0000000000 1.9928485180

r-$GeSi_3$

4

CCSD(T)-F12A/CC-PVTZ-F12,GE=CC-PVTZ-PP-F12 ENERGY=-1160.66997800

Ge 0.0000000000 1.3061320910 -0.0000072714

Si 0.0000000000 -0.0577347643 1.9970225191

Si 0.0000000000 -1.1906403269 0.0000066285

Si 0.0000000000 -0.0577569998 -1.9970218761

d-Ge_2C_2

4

RCCSD(T)-F12A/CC-PVDZ-F12,GE=CC-PVDZ-PP-F12 ENERGY=-662.84609899

Ge 0.0000000000 1.2596628824 -0.1821373901

Ge 0.0000000000 -1.2596628824 -0.1821373901

C -1.4551974193 0.0000000000 0.1821373901

C 1.4551974193 0.0000000000 0.1821373901

r-Ge_2C_2

4

CCSD(T)-F12A/CC-PVTZ-F12,GE=CC-PVTZ-PP-F12 ENERGY=-662.99192599

Ge 0.0000000000 0.0000000000 -1.8132322714

C 0.0000000000 -0.7128822973 0.0000000000

C 0.0000000000 0.7128822973 0.0000000000

Ge 0.0000000000 0.0000000000 1.8132322714

t-Ge_2C_2

4

CCSD(T)-F12A/CC-PVTZ-F12,GE=CC-PVTZ-PP-F12 ENERGY=-662.99955059

Ge 0.0000000000 -0.5438889817 1.3089888862

Ge 0.0000000000 1.7966112640 0.0339148273

C 0.0000000000 -1.2818403219 -0.6633871410

C 0.0000000000 0.0291180395 -0.6795165724

d-Ge_2Si_2

4

CCSD(T)-F12A/CC-PVTZ-F12,GE=CC-PVTZ-PP-F12 ENERGY=-1165.13449683

Si 0.0000000000 2.0170927373 0.0000000000

Ge -1.2908917737 0.0000000000 0.0000000000

Ge 1.2908917737 0.0000000000 0.0000000000

Si 0.0000000000 -2.0170927373 0.0000000000

r-Ge_2Si_2

4

CCSD(T)-F12A/CC-PVTZ-F12,GE=CC-PVTZ-PP-F12 ENERGY=-1165.14715830

Si 0.0000000000 -1.2147317315 0.0000000000

Si 0.0000000000 1.2147317315 0.0000000000

Ge 0.0000000000 0.0000000000 2.0616145832

Ge 0.0000000000 0.0000000000 -2.0616145832

t-Ge_2Si_2

4

CCSD(T)-F12A/CC-PVTZ-F12,GE=CC-PVTZ-PP-F12 ENERGY=-1165.14216572

Ge 0.0000000000 1.2988349460 0.1869438610

Ge 0.0000000000 0.1954449131 -2.0552978221

Si 0.0000000000 -0.3036949951 1.9909830894

Si 0.0000000000 -1.1905848641 -0.1226291283

d-Ge_3C

4

CCSD(T)-F12A/CC-PVTZ-F12,GE=CC-PVTZ-PP-F12 ENERGY=-918.47301424

Ge 1.9952363379 0.0000000000 -0.0769221634

Ge -0.1877773554 1.2699499757 -0.0948089935

Ge -0.1877773554 -1.2699499757 -0.0948089935

C -1.6196816272 0.0000000000 0.2665401504

r-Ge_3C

4

CCSD(T)-F12A/CC-PVTZ-F12,GE=CC-PVTZ-PP-F12 ENERGY=-918.54630557

Ge 0.0000000000 0.3912531062 1.8465538068

Ge 0.0000000000 -1.4271260806 0.0000000000

C 0.0000000000 0.6446198681 0.0000000000

Ge 0.0000000000 0.3912531062 -1.8465538068

d-Ge_3Si

4

CCSD(T)-F12A/CC-PVTZ-F12,GE=CC-PVTZ-PP-F12 ENERGY=-1169.60796915

Ge 0.0000000000 0.0000000000 2.0823861042

Ge 0.0000000000 1.2970388806 -0.0248003046

Ge 0.0000000000 -1.2970388806 -0.0248003046

Si 0.0000000000 0.0000000000 -2.0327854950

r-Ge_3Si

4

CCSD(T)-F12A/CC-PVTZ-F12,GE=CC-PVTZ-PP-F12 ENERGY=-1169.61405662

Ge 2.0804788391 0.0000000000 0.0585789885

Ge 0.0000000000 0.0000000000 -1.3183013145

Ge -2.0804788391 0.0000000000 0.0585789885

Si 0.0000000000 0.0000000000 1.2011433375

Appendix B: Chapter 3 Supporting Information

Presented in this Appendix to Chapter 3 are results obtained with all functionals for the group of structures studied. This data includes relative electronic energies with zero-point energy corrections, Gibbs free energies, zero-point vibrational energies, and Cartesian coordinates of optimized structures with corresponding electronic energies. Barrier heights on both sides of each transition state for the B2GP-PLYP functional are also found in this Appendix.

B.1 Supporting Data

Table B.1: X_xY_{4-x} ($x \in \{1, 2, 3\}$) family relative energies (in kJ mol^{-1}) of optimized geometries with inclusion of harmonic zero-point vibrational energy (ZPVE). Relative energies are taken with respect to the lowest energy isomer in each group. Results calculated using the B3LYP, M06-2X, and ωB97X-D4 functionals, all using the aug-cc-pVTZ basis set.

Structure	SiC	GeC	GeSi	SiC	GeC	GeSi	SiC	GeC	GeSi
	B3LYP			M06-2X			ωB97X-D4		
XY_3									
d	0.0	0.0	0.0	0.0	0.0	0.0	0.0	0.0	0.0
r	14.9	-0.5	14.1	31.7	22.1	15.8	31.7	20.8	21.5
TS	152.9	148.0	85.2	196.3	179.1	139.4	206.6	186.5	151.5
X_2Y_2									
r	0.0	25.8	0.0	0.0	15.9	0.0	0.0	17.6	0.0
t	19.4	0.0	10.7	32.4	0.0	11.3	30.0	0.0	18.4
d	345.6	395.6	27.5	376.9	435.5	30.1	384.1	425.9	41.7
TS r-t	136.8	176.1	82.2	188.8	163.6	141.9	196.4	170.7	143.9
TS d-r	336.2	420.3	89.7	405.4	460.7	146.7	424.9	468.4	158.1
X_3Y									
r	0.0	0.0	0.0	0.0	0.0	0.0	0.0	0.0	0.0
d	216.1	199.2	13.5	232.0	225.0	13.5	232.2	217.6	20.3
TS	219.2	238.1	107.6	272.2	265.8	135.5	283.1	266.6	138.3

Table B.2: X_xY_{4-x} ($x \in \{1, 2, 3\}$) family barrier heights (in kJ mol^{-1}) of optimized geometries with inclusion of harmonic zero-point vibrational energy (ZPVE). Each barrier height is shown as going from either structure to its respective transition state. All results at the B2GP-PLYP/AVTZ level of theory.

Structure	SiC	GeC	GeSi
XY_3			
r-d	164.1	155.2	127.6
d-r	187.9	166.2	138.8
X_2Y_2			
t-r	155.4	158.3	138.7
r-t	181.3	142.4	147.5
d-r	15.2	21.4	118.3
r-d	351.9	371.4	139.5
X_3Y			
d-r	48.6	47.9	120.3
r-d	258.7	241.2	130.5

Table B.3: X_xY_{4-x} ($x \in \{1, 2, 3\}$) family zero-point energy contributions in kJ mol^{-1}. Results calculated using the B3LYP and M06-2X functionals, all using the aug-cc-pVTZ basis set.

Structure	SiC	GeC	GeSi	SiC	GeC	GeSi
	B3LYP			M06-2X		
XY_3						
d	28.5	26.2	11.0	30.3	28.2	11.8
r	27.6	26.3	10.7	28.5	27.1	11.4
TS	23.5	22.6	9.5	24.8	23.4	9.7
X_2Y_2						
r	24.6	20.9	9.7	25.8	22.1	10.5
t	23.4	20.5	9.5	24.2	21.5	10.2
d	18.4	14.9	9.2	19.0	15.5	9.8
TS r-t	19.9	17.4	9.1	21.0	17.8	9.4
TS d-r	18.1	14.0	8.1	18.4	14.6	8.5
X_3Y						
r	18.4	13.5	8.3	19.1	14.3	9.7
d	15.6	11.0	8.0	16.2	11.7	8.6
TS	15.1	10.4	7.0	15.3	11.0	7.3

Table B.4: X_xY_{4-x} ($x \in \{1, 2, 3\}$) family zero-point energy contributions in kJ mol^{-1}. Results calculated using the ωB97X-D4 and B2GP-PLYP functionals, all using the aug-cc-pVTZ basis set.

Structure	SiC	GeC	GeSi	SiC	GeC	GeSi
	ωB97X-D4			B2GP-PLYP		
XY_3						
d	30.3	28.3	12.3	28.9	26.8	11.4
r	29.0	27.5	12.0	28.3	26.9	11.1
TS	24.9	23.4	9.7	24.0	22.5	9.9
X_2Y_2						
r	26.2	22.4	11.0	24.8	21.3	10.2
t	24.7	21.6	10.7	23.7	20.9	9.8
d	19.3	16.0	10.4	18.8	15.5	9.6
TS r-t	21.7	18.9	10.2	20.1	17.7	9.0
TS d-r	18.5	14.7	8.9	23.9	18.4	8.6
X_3Y						
r	19.7	14.7	9.4	18.7	14.0	8.7
d	16.7	12.3	9.1	15.8	11.4	8.5
TS	15.6	11.0	7.8	15.2	10.5	7.5

Table B.5: X_xY_{4-x} ($x \in \{1, 2, 3\}$) family Gibbs energy contributions (at T = 298.15K) in kJ mol^{-1}. Results calculated using the B3LYP and M06-2X functionals, all using the aug-cc-pVTZ basis set.

Structure	SiC	GeC	GeSi	SiC	GeC	GeSi
	B3LYP			M06-2X		
XY_3						
d	-38.0	-43.9	-68.6	-36.0	-41.5	-69.1
r	-39.9	-44.8	-70.5	-38.6	-43.5	-69.5
TS	-44.9	-51.3	-72.8	-43.1	-48.1	-70.0
X_2Y_2						
r	-44.7	-55.1	-72.7	-43.4	-53.7	-71.5
t	-48.9	-58.6	-74.6	-47.8	-57.0	-73.5
d	-50.2	-61.6	-73.0	-49.5	-60.9	-72.0
TS r-t	-51.9	-60.9	-74.6	-50.8	-61.1	-73.1
TS d-r	-50.8	-60.8	-72.6	-50.4	-60.2	-72.1
X_3Y						
r	-55.0	-69.4	-76.8	-54.1	-68.2	-77.4
d	-60.1	-73.7	-78.7	-59.4	-72.6	-77.6
TS	-59.7	-73.0	-78.3	-58.8	-71.1	-77.7

Table B.6: X_xY_{4-x} ($x \in \{1, 2, 3\}$) family Gibbs energy contributions (at T = 298.15K) in kJ mol^{-1}. Results calculated using the ωB97X-D4, and B2GP-PLYP functionals, all using the aug-cc-pVTZ basis set.

Structure	SiC	GeC	GeSi	SiC	GeC	GeSi
	ωB97X-D4			B2GP-PLYP		
XY_3						
d	-35.8	-41.3	-66.5	-37.5	-42.9	-69.6
r	-38.0	-42.9	-66.8	-38.9	-43.7	-69.7
TS	-43.0	-48.0	-71.3	-44.3	-49.5	-73.0
X_2Y_2						
r	-42.9	-53.1	-70.6	-44.4	-54.5	-71.8
t	-47.2	-56.7	-72.5	-48.5	-57.7	-74.0
d	-49.1	-60.2	-71.0	-49.7	-60.8	-72.2
TS r-t	-49.8	-58.7	-71.5	-51.8	-60.4	-74.1
TS d-r	-50.3	-60.1	-71.3	-44.7	-55.9	-72.0
X_3Y						
r	-53.2	-67.3	-76.5	-54.6	-68.5	-77.7
d	-58.6	-71.6	-74.9	-60.0	-73.0	-77.7
TS	-58.4	-71.9	-76.9	-59.0	-71.8	-77.2

Table B.7: Harmonic fundamental vibrational frequencies (in cm^{-1}) of SiC isomers at the B3LYP/AVTZ level of theory. Intensities in km mol^{-1}.

Mode	Frequency	Intensity	Frequency	Intensity	Frequency	Intensity
	d-SiC_3		r-SiC_3		TS-SiC_3	
6	1406.2	203.2	1592.4	52.6	-813.4	n/a
5	1037.4	1.6	1155.9	3.5	1464.1	34.2
4	1007.2	54.7	784.8	20.1	1053.6	33.6
3	674.1	49.5	499.2	50.6	726.8	60.1
2	398.9	40.6	384.9	3.5	427.5	5.3
1	236.8	10.6	198.4	52.6	263.8	11.8
	r-Si_2C_2		t-Si_2C_2		d-Si_2C_2	
6	1126.6	0.0	1588.8	14.3	-214.4	n/a
5	973.5	310.6	710.0	26.4	757.1	0.0
4	957.9	0.0	628.9	70.4	662.3	17.1
3	503.1	0.0	494.3	5.2	600.7	0.0
2	357.7	58.8	283.8	1.2	547.0	0.0
1	196.4	3.7	204.0	11.4	506.1	0.0
	TS-r-t-Si_2C_2		TS-d-rSi_2C_2		r-Si_3C	
6	-479.7	n/a	-607.9	n/a	1107.3	74.8
5	1171.1	13.1	771.9	1.7	648.7	52.7
4	902.9	113.6	720.4	8.4	507.2	23.0
3	609.7	15.3	620.0	10.6	336.1	10.7
2	474.6	54.8	599.8	12.5	296.1	5.5
1	171.9	2.5	308.9	13.3	179.1	0.1
	d-Si_3C		TS-Si_3C			
6	745.1	4.7	-543.5	n/a		
5	658.4	0.2	851.5	13.7		
4	454.4	1.8	267.3	33.3		
3	397.9	29.1	394.6	5.7		
2	262.7	0.2	731.5	5.4		
1	91.3	47.0	851.5	1.0		

Table B.8: Harmonic fundamental vibrational frequencies (in cm^{-1}) of GeC isomers at the B3LYP/AVTZ level of theory. Intensities in km mol^{-1}.

Mode	Frequency	Intensity	Frequency	Intensity	Frequency	Intensity
	d-GeC_3		r-GeC_3		TS-SiC_3	
6	1403.6	169.0	1612.6	87.4	-714.3	n/a
5	1009.8	1.3	1141.7	4.4	1449.5	37.1
4	933.6	28.6	704.3	29.2	1141.8	51.2
3	510.2	43.2	397.1	22.3	590.8	40.5
2	325.3	33.2	311.3	4.5	381.9	10.4
1	199.7	11.8	210.9	44.4	132.7	8.8
	r-Ge_2C_2		t-Ge_2C_2		d-Ge_2C_2	
6	1165.4	0.0	1622.4	25.7	643.6	6.4
5	856.0	0.0	561.2	32.7	550.8	6.0
4	796.0	212.6	505.7	48.4	457.1	0.0
3	279.3	0.0	374.8	13.1	396.5	3.2
2	258.7	58.3	184.1	7.7	313.3	0.2
1	145.3	8.0	170.9	1.0	123.6	56.1
	TS-r-t-Ge_2C_2		TS-d-rGe_2C_2		r-Ge_3C	
6	-467.8	n/a	-496.8	n/a	959.2	94.5
5	1258.0	35.4	586.4	17.7	506.5	71.5
4	720.4	86.4	551.0	13.3	295.8	6.0
3	456.2	25.9	488.4	3.4	185.9	3.3
2	363.3	43.6	467.2	14.4	169.2	1.1
1	112.7	0.6	250.7	7.0	148.3	0.8
	d-Ge_3C		TS-Ge_3C			
6	637.3	0.5	-420.4	n/a		
5	499.3	4.4	674.2	28.3		
4	270.1	1.3	533.7	39.6		
3	224.4	10.8	213.3	2.5		
2	142.8	0.4	191.1	2.0		
1	65.9	36.2	123.9	0.2		

Table B.9: Harmonic fundamental vibrational frequencies (in cm^{-1}) of GeSi isomers at the B3LYP/AVTZ level of theory. Intensities in km mol^{-1}.

Mode	Frequency	Intensity	Frequency	Intensity	Frequency	Intensity
	d-$GeSi_3$		r-$GeSi_3$		TS-SiC_3	
6	475.9	47.2	483.3	54.6	-410.7	n/a
5	410.4	15.0	416.1	0.5	449.1	0.1
4	400.2	0.0	315.0	6.7	396.4	1.2
3	268.7	3.6	300.7	0.7	297.0	2.3
2	202.9	1.3	194.7	0.1	269.0	1.5
1	74.9	1.2	80.0	2.8	152.1	0.0
	r-Ge_2Si_2		t-Ge_2Si_2		d-Ge_2Si_2	
6	407.6	0.0	463.8	42.6	381.8	43.1
5	392.7	59.8	358.4	3.5	375.7	0.0
4	368.4	0.0	298.7	3.5	294.6	0.0
3	214.5	0.0	238.6	4.5	231.8	0.0
2	178.4	1.2	162.2	0.1	177.3	0.0
1	66.7	0.8	72.2	1.7	75.5	2.3
	TS-r-t-Ge_2Si_2		TS-d-rGe_2Si_2		r-Ge_3Si	
6	-129.5	n/a	-365.8	n/a	398.5	39.2
5	456.1	31.0	357.8	5.6	340.6	1.0
4	404.6	5.2	323.1	0.1	242.0	7.4
3	272.2	0.3	282.3	0.2	204.6	0.1
2	261.6	2.4	265.4	3.2	141.0	0.1
1	91.7	0.6	134.6	0.0	63.0	0.7
	d-Ge_3Si		TS-Ge_3Si			
6	379.9	24.3	-335.0	n/a		
5	272.2	0.1	343.5	4.9		
4	267.0	8.9	299.9	2.0		
3	211.0	1.5	221.0	1.7		
2	144.1	0.0	191.1	0.7		
1	65.8	1.4	114.5	0.0		

Table B.10: Harmonic fundamental vibrational frequencies (in cm^{-1}) of SiC isomers at the M06-2X/AVTZ level of theory. Intensities in km mol^{-1}.

Mode	Frequency	Intensity	Frequency	Intensity	Frequency	Intensity
	d-SiC_3		r-SiC_3		TS-SiC_3	
6	1455.4	221.9	1582.6	81.2	-834.0	n/a
5	1110.4	1.6	1180.0	0.5	1534.1	31.8
4	1099.2	69.8	826.0	48.4	1061.4	39.6
3	709.3	61.8	534.3	26.6	752.0	77.6
2	425.6	43.5	424.2	1.8	437.8	2.7
1	257.9	7.1	224.1	47.5	468.3	11.4
	r-Si_2C_2		t-Si_2C_2		d-Si_2C_2	
6	1182.9	0.0	1623.3	14.9	-139.9	n/a
5	1011.1	356.6	729.8	28.2	784.9	0.0
4	1008.9	0.0	657.5	67.0	675.7	33.9
3	534.2	0.0	514.7	8.5	636.0	0.0
2	380.9	59.9	313.1	0.7	561.6	0.0
1	198.8	4.6	215.7	9.9	512.1	1.1
	TS-r-t-Si_2C_2		TS-d-rSi_2C_2		r-Si_3C	
6	-507.2	n/a	-664.2	n/a	1128.6	85.8
5	1209.7	18.2	800.9	1.8	679.0	57.5
4	943.2	115.0	726.4	6.1	526.3	23.1
3	650.9	17.3	642.7	9.6	362.2	15.3
2	531.9	58.7	610.2	15.9	311.9	5.5
1	167.6	5.6	300.6	15.8	178.5	0.3
	d-Si_3C		TS-Si_3C			
6	773.5	5.2	-561.4	n/a		
5	674.9	0.5	874.0	17.3		
4	477.9	0.7	755.0	35.7		
3	419.4	38.3	417.3	10.1		
2	275.8	0.7	279.6	6.5		
1	81.6	48.2	235.5	1.6		

Table B.11: Harmonic fundamental vibrational frequencies (in cm^{-1}) of GeC isomers at the M06-2X/AVTZ level of theory. Intensities in km mol^{-1}.

Mode	Frequency	Intensity	Frequency	Intensity	Frequency	Intensity
	d-GeC_3		r-GeC_3		TS-SiC_3	
6	1457.9	188.3	1597.3	111.6	-785.9	n/a
5	1082.7	0.8	1168.0	3.5	1537.9	29.6
4	1028.0	48.3	754.7	28.5	1080.9	51.8
3	541.6	49.3	432.4	25.7	599.4	53.4
2	360.7	36.9	350.3	3.7	408.5	4.5
1	242.4	7.7	227.3	41.4	283.8	11.0
	r-Ge_2C_2		t-Ge_2C_2		d-Ge_2C_2	
6	1202.2	0.0	1676.0	24.2	674.5	7.7
5	911.8	0.0	593.4	34.1	571.6	14.3
4	841.2	223.9	534.2	41.0	481.8	0.0
3	297.7	0.0	400.4	16.8	411.3	0.0
2	280.9	60.1	202.0	8.0	323.5	0.2
1	153.2	8.0	193.3	1.0	120.6	62.7
	TS-r-t-Ge_2C_2		TS-d-rGe_2C_2		r-Ge_3C	
6	-471.6	n/a	-492.2	n/a	996.5	85.8
5	1290.5	65.9	634.7	13.7	542.1	72.7
4	763.7	51.4	554.7	7.7	311.0	6.2
3	502.5	19.6	512.6	6.0	202.8	5.9
2	404.5	62.2	493.5	18.3	184.9	1.2
1	111.0	4.2	245.6	9.2	152.9	0.9
	d-Ge_3C		TS-Ge_3C			
6	672.3	0.1	-378.2	n/a		
5	516.1	1.4	719.3	34.4		
4	284.0	1.2	559.3	42.2		
3	236.7	14.9	228.7	4.7		
2	150.0	0.1	192.4	2.7		
1	96.5	39.4	136.3	0.5		

Table B.12: Harmonic fundamental vibrational frequencies (in cm^{-1}) of GeSi isomers at the M06-2X/AVTZ level of theory. Intensities in km mol^{-1}.

Mode	Frequency	Intensity	Frequency	Intensity	Frequency	Intensity
	d-$GeSi_3$		r-$GeSi_3$		TS-SiC_3	
6	511.8	58.1	508.6	75.5	-450.9	n/a
5	439.6	20.6	441.0	0.7	473.5	0.0
4	435.2	0.0	341.8	9.5	414.4	1.7
3	286.2	4.5	324.2	1.1	309.7	3.3
2	214.6	2.2	207.3	0.4	273.5	1.4
1	80.3	1.6	77.0	2.6	150.6	0.2
	r-Ge_2Si_2		t-Ge_2Si_2		d-Ge_2Si_2	
6	436.1	0.0	495.6	56.0	407.1	64.0
5	423.4	77.3	382.6	5.4	400.9	0.0
4	401.6	0.0	323.8	5.5	316.1	0.0
3	229.7	0.0	254.5	6.0	250.4	0.0
2	187.6	2.0	173.0	0.4	187.0	0.2
1	70.6	0.7	74.2	1.6	75.7	2.2
	TS-r-t-Ge_2Si_2		TS-d-rGe_2Si_2		r-Ge_3Si	
6	-150.5	n/a	-381.0	n/a	425.6	53.6
5	473.5	36.6	379.2	6.2	364.0	1.5
4	433.4	8.6	337.2	0.1	262.6	10.8
3	289.8	1.0	294.2	1.0	219.7	0.2
2	276.4	3.3	273.1	2.0	150.8	0.3
1	106.2	1.6	132.7	0.0	66.7	0.7
	d-Ge_3Si		TS-Ge_3Si			
6	408.4	34.8	-336.1	n/a		
5	292.2	0.0	365.5	5.4		
4	284.7	13.3	308.7	3.2		
3	226.1	2.2	231.1	1.9		
2	151.4	0.1	202.2	0.4		
1	68.5	1.4	112.4	0.1		

Table B.13: Harmonic fundamental vibrational frequencies (in cm^{-1}) of SiC isomers at the ωB97X-D4/AVTZ level of theory. Intensities in km mol^{-1}.

Mode	Frequency	Intensity	Frequency	Intensity	Frequency	Intensity
	d-SiC_3		r-SiC_3		TS-SiC_3	
6	1461.8	231.1	1594.9	69.4	-908.0	n/a
5	1099.0	1.4	1193.3	0.4	1561.1	33.1
4	1087.3	74.6	831.1	47.9	1026.3	42.5
3	719.5	62.2	553.7	27.9	749.2	89.5
2	432.1	46.0	436.9	1.9	444.3	0.9
1	272.0	7.4	245.6	46.1	380.7	12.8
	r-Si_2C_2		t-Si_2C_2		d-Si_2C_2	
6	1170.7	0.0	1627.1	17.1	-45.6	n/a
5	1036.0	378.3	746.2	26.8	811.7	0.0
4	1024.8	0.0	662.6	64.6	693.2	39.7
3	548.6	0.0	524.4	9.1	641.4	0.0
2	393.0	59.9	343.8	0.4	570.5	0.0
1	203.0	3.3	218.3	10.7	512.0	9.6
	TS-r-t-Si_2C_2		TS-d-rSi_2C_2		r-Si_3C	
6	-487.4	n/a	-747.1	n/a	1150.3	86.0
5	1201.2	25.3	826.3	2.1	702.7	51.5
4	981.6	118.0	716.2	5.3	539.7	26.1
3	673.1	16.6	644.8	8.2	391.6	20.9
2	565.3	58.6	613.2	34.1	334.6	6.6
1	198.8	8.6	299.8	14.4	177.2	0.1
	d-Si_3C		TS-Si_3C			
6	798.7	5.9	-600.9	n/a		
5	673.0	4.0	907.0	34.8		
4	502.3	0.5	745.5	36.3		
3	441.5	49.3	436.3	17.0		
2	288.2	3.3	293.8	6.8		
1	91.6	58.9	233.2	2.6		

Table B.14: Harmonic fundamental vibrational frequencies (in cm^{-1}) of GeC isomers at the ωB97X-D4/AVTZ level of theory. Intensities in km mol^{-1}.

Mode	Frequency	Intensity	Frequency	Intensity	Frequency	Intensity
	d-GeC_3		r-GeC_3		TS-SiC_3	
6	1462.5	202.7	1609.4	93.5	-853.8	n/a
5	1070.1	1.1	1180.1	3.4	1544.9	32.2
4	1025.6	48.6	755.8	28.5	1050.7	49.0
3	552.3	57.2	441.3	32.2	603.3	63.2
2	368.4	38.8	357.6	3.4	410.8	3.7
1	249.4	7.1	247.0	40.4	303.1	10.5
	r-Ge_2C_2		t-Ge_2C_2		d-Ge_2C_2	
6	1179.8	0.0	1671.7	26.8	741.0	0.0
5	932.6	0.0	604.3	36.1	582.5	35.1
4	873.0	295.0	536.7	44.4	495.0	0.0
3	312.5	0.0	399.6	19.4	399.1	0.0
2	297.5	61.7	208.0	0.6	341.6	0.0
1	155.4	7.5	197.7	7.8	116.7	85.9
	TS-r-t-Ge_2C_2		TS-d-rGe_2C_2		r-Ge_3C	
6	-472.7	n/a	-601.4	n/a	1015.4	112.5
5	1254.7	37.7	648.0	19.7	564.4	80.9
4	800.6	78.5	559.6	8.3	320.3	8.3
3	539.7	23.7	514.7	2.4	221.0	6.9
2	432.1	58.9	494.8	16.1	195.4	1.1
1	138.4	4.3	236.5	8.0	149.0	0.8
	d-Ge_3C		TS-Ge_3C			
6	700.2	0.4	-469.4	n/a		
5	528.5	0.9	727.5	51.6		
4	296.6	0.3	558.1	47.7		
3	253.9	19.9	236.7	5.8		
2	162.7	0.0	185.6	2.2		
1	107.8	37.6	138.3	0.4		

Table B.15: Harmonic fundamental vibrational frequencies (in cm^{-1}) of GeSi isomers at the ωB97X-D4/AVTZ level of theory. Intensities in km mol^{-1}.

Mode	Frequency	Intensity	Frequency	Intensity	Frequency	Intensity
	d-$GeSi_3$		r-$GeSi_3$		TS-SiC_3	
6	533.0	71.6	535.7	88.9	-501.7	n/a
5	464.0	30.0	469.6	1.2	525.3	0.2
4	451.4	0.1	361.3	11.7	433.2	2.8
3	299.3	6.1	334.3	1.5	324.3	3.4
2	224.8	4.7	214.0	1.3	271.9	1.2
1	82.3	1.9	88.3	2.8	149.0	0.9
	r-Ge_2Si_2		t-Ge_2Si_2		d-Ge_2Si_2	
6	465.8	0.0	517.0	68.6	431.1	73.7
5	440.8	99.9	406.6	6.7	428.5	0.0
4	418.3	0.0	340.3	7.3	336.8	0.0
3	240.1	0.0	267.6	7.6	256.7	0.0
2	200.4	4.0	181.4	1.0	196.4	0.5
1	72.1	0.8	78.9	1.7	83.8	2.4
	TS-r-t-Ge_2Si_2		TS-d-rGe_2Si_2		r-Ge_3Si	
6	-161.1	n/a	-446.3	n/a	445.7	65.0
5	496.0	34.9	420.9	7.5	388.5	2.2
4	464.8	16.3	350.4	0.1	279.5	13.7
3	313.7	1.6	308.2	0.1	230.1	0.2
2	289.1	3.9	261.3	1.3	159.3	0.8
1	148.3	2.3	150.8	0.5	68.1	0.7
	d-Ge_3Si		TS-Ge_3Si			
6	432.2	40.1	-400.1	n/a		
5	311.1	0.0	405.1	6.7		
4	304.5	17.3	320.8	3.0		
3	235.2	2.5	248.7	3.1		
2	162.4	0.3	199.5	0.4		
1	72.6	1.5	121.8	0.1		

Table B.16: Harmonic fundamental vibrational frequencies (in cm^{-1}) of SiC isomers at the B2GP-PLYP/AVTZ level of theory. Intensities in km mol^{-1}.

Mode	Frequency	Intensity	Frequency	Intensity	Frequency	Intensity
	d-SiC_3		r-SiC_3		TS-SiC_3	
6	1409.2	205.8	1614.9	59.8	-888.4	n/a
5	1052.2	1.9	1146.9	0.2	1462.8	49.4
4	989.2	44.1	800.3	51.6	1078.8	39.8
3	683.4	49.8	516.8	19.2	734.6	71.0
2	428.4	40.0	411.5	3.9	422.2	6.1
1	261.1	8.5	233.9	53.8	309.0	12.6
	r-Si_2C_2		t-Si_2C_2		d-Si_2C_2	
6	1091.3	0.0	1572.8	18.9	-165.9	n/a
5	993.9	316.0	724.5	27.3	747.8	0.0
4	969.2	0.0	639.9	66.8	688.5	6.3
3	512.6	0.0	511.9	6.3	622.9	0.0
2	373.3	61.4	299.5	1.2	553.0	0.0
1	206.1	3.7	208.3	10.6	534.3	1.5
	TS-r-t-Si_2C_2		TS-d-rSi_2C_2		r-Si_3C	
6	-509.0	n/a	-744.7	n/a	1118.5	79.4
5	1163.0	12.3	1503.3	1225.5	654.4	48.9
4	913.5	99.5	761.6	29.1	507.1	20.6
3	628.2	14.4	742.2	24.8	358.8	11.3
2	489.8	65.9	649.3	28.7	307.1	5.8
1	163.6	3.1	333.8	6.8	175.0	0.1
	d-Si_3C		TS-Si_3C			
6	755.0	1.3	-591.5	n/a		
5	668.1	0.1	847.9	23.7		
4	473.5	1.1	754.5	52.0		
3	403.4	24.3	413.9	6.0		
2	282.3	0.1	286.9	5.9		
1	54.3	59.8	238.5	3.0		

Table B.17: Harmonic fundamental vibrational frequencies (in cm^{-1}) of GeC isomers at the B2GP-PLYP/AVTZ level of theory. Intensities in km mol^{-1}.

Mode	Frequency	Intensity	Frequency	Intensity	Frequency	Intensity
	d-GeC_3		r-GeC_3		TS-SiC_3	
6	1404.6	177.2	1633.3	81.5	-791.5	n/a
5	1031.2	1.7	1135.0	2.9	1453.0	41.5
4	919.0	21.0	725.9	31.6	1123.9	59.9
3	524.7	43.4	420.0	21.9	603.3	48.8
2	366.6	33.2	339.7	4.7	387.9	10.4
1	242.1	9.9	236.2	47.0	200.6	10.0
	r-Ge_2C_2		t-Ge_2C_2		d-Ge_2C_2	
6	1118.3	0.0	1593.4	25.5	630.8	6.2
5	880.6	0.0	587.9	31.4	589.3	0.3
4	830.1	218.2	530.7	48.9	500.7	0.0
3	288.5	0.0	402.1	16.1	447.5	7.0
2	277.1	58.7	200.2	8.8	315.2	0.4
1	163.6	7.3	183.7	0.9	113.1	50.8
	TS-r-t-Ge_2C_2		TS-d-rGe_2C_2		r-Ge_3C	
6	-498.1	n/a	-896.5	n/a	982.6	97.7
5	1232.7	40.5	1121.1	58.0	529.4	64.8
4	748.0	80.2	607.0	24.4	297.6	5.8
3	486.3	24.0	536.7	24.0	203.2	3.5
2	384.4	51.5	525.5	61.4	180.3	1.1
1	111.9	0.8	283.1	4.6	149.2	0.4
	d-Ge_3C		TS-Ge_3C			
6	649.7	0.4	-419.3	n/a		
5	523.2	5.6	682.6	20.3		
4	281.8	0.9	578.3	66.0		
3	231.2	8.2	235.8	2.7		
2	158.5	0.3	200.8	2.3		
1	66.7	40.7	149.7	0.2		

Table B.18: Harmonic fundamental vibrational frequencies (in cm^{-1}) of GeSi isomers at the B2GP-PLYP/AVTZ level of theory. Intensities in km mol^{-1}.

Mode	Frequency	Intensity	Frequency	Intensity	Frequency	Intensity
	d-$GeSi_3$		r-$GeSi_3$		TS-SiC_3	
6	486.7	42.6	490.3	47.4	-359.9	n/a
5	421.1	1.6	421.4	0.5	448.7	0.2
4	412.0	0.0	332.4	5.6	406.2	0.7
3	272.5	2.7	308.2	0.4	327.8	4.5
2	225.0	1.1	212.9	0.1	309.1	0.5
1	88.6	2.3	94.6	3.4	156.3	0.0
	r-Ge_2Si_2		t-Ge_2Si_2		d-Ge_2Si_2	
6	418.3	0.0	470.1	36.9	396.7	37.2
5	406.2	53.5	367.9	2.7	381.8	0.0
4	381.2	0.0	314.1	3.4	303.2	0.0
3	218.0	0.0	242.7	3.3	237.2	0.0
2	200.9	1.2	177.6	0.1	196.5	0.3
1	83.2	1.6	65.7	2.4	96.2	3.0
	TS-r-t-Ge_2Si_2		TS-d-rGe_2Si_2		r-Ge_3Si	
6	-140.0	n/a	-315.3	n/a	405.6	34.9
5	462.3	22.2	367.1	2.9	352.0	0.7
4	416.7	4.4	345.3	0.2	259.1	7.2
3	291.7	0.1	310.7	5.6	208.9	0.1
2	271.0	2.3	295.9	1.4	156.3	0.1
1	86.6	0.6	149.0	0.1	75.2	1.0
	d-Ge_3Si		TS-Ge_3Si			
6	390.8	22.1	-277.1	n/a		
5	283.4	0.0	350.9	3.1		
4	276.9	7.0	313.3	2.0		
3	217.2	1.2	247.3	2.3		
2	162.2	0.0	219.7	0.7		
1	86.1	1.4	127.2	0.0		

B.2 XYZ Coordinates

XYZ Coordinates (in Å) of all optimized geometries, with the B3LYP-D3BJ, M06-2X, ωB97X-D4, and B2GP-PLYP functionals.

B3LYP-D3BJ XYZ coordinate files in the following format: XY_3 (d, r, ts), X_2Y_2 (r, t, d, r-t, d-r), X_3Y (r, d, ts), for SiC, GeC, and GeSi structures.

4

d_sic3_b3lyp FINAL SINGLE POINT ENERGY -403.505339200356

Si 0.00000001453629 0.00000000308306 -1.57671945802498

C -0.00000001723124 -0.73465591912625 0.11658244781703

C -0.00000001723124 0.73465591293438 0.11658244587831

C 0.00000001992618 0.00000000310881 1.34355456432964

4

r_sic3_b3lyp FINAL SINGLE POINT ENERGY -403.499325581585

Si -0.00000005724499 0.00000101070517 -1.27150762421545

C 0.00000016102604 -1.29631015674896 0.31808821465440

C -0.00000026480680 0.00000025697875 0.63533237323063

C 0.00000016102576 1.29630888906503 0.31808703643042

4

sic3_ts_b3lyp FINAL SINGLE POINT ENERGY -403.445238191192

Si 1.08359687764284 0.07603954601411 0.06936709152425

C -1.30140424798975 -0.22143659657816 0.33059052545319

C -0.38398984303973 -0.93603625649665 -0.28279849631073

C -0.84196478661335 0.98612230706070 -0.20088512066671

4

r_si2c2_b3lyp FINAL SINGLE POINT ENERGY -654.967468767826

Si -0.00000005833392 -0.00000000801073 -1.69537987859669

Si -0.00000005833392 -0.00000001094985 1.69537988187010

C 0.00000005833392 -0.71503533072260 0.00000000181720

C 0.00000005833392 0.71503534968319 -0.00000000509061

4

t_si2c2_b3lyp FINAL SINGLE POINT ENERGY -654.959610572625

Si -0.00000005002328 -0.01586280418521 1.71622182574307

Si 0.00000001956838 1.24255810013324 -0.48320741946948

C 0.00000010195739 -0.63977168199845 0.03694109084863

C -0.00000007150249 -0.58692361404958 -1.26995549712222

4

d_si2c2_b3lyp FINAL SINGLE POINT ENERGY -654.833445668458

Si -0.00048037630075 -0.00000044720575 -1.14987144252081

Si -0.00048037626788 -0.00000046089499 1.14987159712109

C 0.00048037663901 -1.48584657802215 -0.00000007195592

C 0.00048037592962 1.48584748612289 -0.00000008264436

4

ts_r_t_si2c2_b3lyp FINAL SINGLE POINT ENERGY -654.913593193358

Si -1.59623142146324 -0.35255754557393 0.06622278273798

Si 1.74203347257605 -0.19178683078949 0.09169540485890

C -0.46065687842490 1.18037706893556 0.12483641398386

C 0.12046926731209 0.08703554742786 -0.49997996158074

4

ts_d_r_si2c2_b3lyp FINAL SINGLE POINT ENERGY -654.836924442939

Si -0.20713319041983 0.00226804458272 -1.27631143689550

Si -0.20713296481381 -0.00226929921279 1.27631106900643

C 0.20713304228770 -1.24820381879020 0.00189583856436

C 0.20713311294594 1.24820507342027 -0.00189547067530

4

r_si3c_b3lyp FINAL SINGLE POINT ENERGY -906.396894528034

C 0.00000011797323 0.60304376647115 0.00000000519471

Si -0.00000006786246 0.36959247372887 1.74794025066727

Si 0.00000001775168 -1.34222869614143 -0.00000001717961

Si -0.00000006786246 0.36959245604142 -1.74794023868237

4

d_si3c_b3lyp FINAL SINGLE POINT ENERGY -906.313531631194

Si -0.20266795219439 -1.18772665173361 0.04603289837409

Si -0.12244242264153 0.36369175627489 1.84415405258660

Si 0.03136498176572 1.13804268102914 -0.39702876289327

C 0.29374539307020 -0.31400778567042 -1.49315818806742

4

si3c_ts_b3lyp FINAL SINGLE POINT ENERGY -906.312661516924

C 0.95275774449833 -0.97718894727322 0.58860575330330

Si -0.60400217298343 -1.20974065302660 -0.19378312047026

Si 1.31839196853470 0.61312529102448 -0.17338946964433

Si -1.12322646004959 1.01608418927534 0.11440083681128

4

d_gec3_b3lyp FINAL SINGLE POINT ENERGY -2191.020659549245

Ge -0.00000038736500 0.00000002884175 -1.66037704696016

C 0.00000047835462 -0.73649841733774 0.14583446149723

C 0.00000047835451 0.73649837451454 0.14583441516537

C -0.00000056934413 0.00000001398145 1.36870817029757

4

r_gec3_b3lyp FINAL SINGLE POINT ENERGY -2191.020839860046

Ge -0.00000034220607 0.00000010432238 -1.37703333750229

C 0.00000122779787 -1.30672461057227 0.37140294722348

C -0.00000211339023 -0.00000006752834 0.63422759457285

C 0.00000122779843 1.30672457377822 0.37140279560596

4

gec3_ts_b3lyp FINAL SINGLE POINT ENERGY -2190.963178088134

Ge 0.75781900772062 0.00682440660172 0.02017951058779

C -1.77787210935538 -0.22288576020374 0.33996992003759

C -0.86159611363241 -0.93116989290608 -0.28816598894390

C -1.38658078473283 0.98439924650810 -0.17830844168149

4

r_ge2c2_b3lyp FINAL SINGLE POINT ENERGY -4229.993538367041

Ge -0.00000143967048 0.00000008230732 -1.82222093992856

C 0.00000143967082 -0.70066419388063 -0.00000005272679

C 0.00000143967017 0.70066400066834 0.00000002181115

Ge -0.00000143967051 0.00000011090497 1.82222097084420

4

t_ge2c2_b3lyp FINAL SINGLE POINT ENERGY -4230.003171589439

Ge -0.00000018786107 -0.55673475443103 1.32179308449845

Ge 0.00000048789671 1.79934539600687 0.01801403163007

C 0.00000074276093 -1.27114424730801 -0.67252422917979

C -0.00000104279658 0.02853360563217 -0.66728288684873

4

d_ge2c2_b3lyp FINAL SINGLE POINT ENERGY -4229.850372586073

Ge 0.00000018657684 1.23598539761772 -0.11211945658082

Ge 0.00000009329897 -1.23598636645594 -0.11211962561258

C -1.52609649509689 0.00000043924234 0.11211953370286

C 1.52609621522108 0.00000052959589 0.11211954849054

4

ts_r_t_ge2c2_b3lyp FINAL SINGLE POINT ENERGY -4229.934976337649

Ge 1.73949445105408 -0.17987074447197 -0.03021004279128

Ge -1.79478438273176 -0.12500124532066 -0.04051554128098

C 0.38068131348445 1.33452384463975 -0.17135693384490

C -0.08822038180678 0.29872714515288 0.56354051791716

4

ts_d_r_ge2c2_b3lyp FINAL SINGLE POINT ENERGY -4229.840642529244

Ge 0.00111134895872 -1.34854426451400 0.21126609553063

Ge -0.00112778971454 1.34854134819346 0.21125554235722

C -1.32983104162220 0.00036956265408 -0.21129451413564

C 1.32984748237803 -0.00036664633354 -0.21122712375220

4

r_ge3c_b3lyp FINAL SINGLE POINT ENERGY -6268.954526322353

Ge 0.00000041272994 0.41197420935494 1.84290140055666

Ge -0.00000014105003 -1.44644382084107 0.00000009223279

C -0.00000068440983 0.62249529568287 -0.00000010410769

Ge 0.00000041272992 0.41197431570325 -1.84290138868176

4

d_ge3c_b3lyp FINAL SINGLE POINT ENERGY -6268.877684434413

Ge 2.00124049017147 -0.00000022168210 -0.19264004211940

Ge -0.17715658800717 1.26970517973085 0.04724351897170

Ge -0.17715609351286 -1.26970505483287 0.04724354947777

C -1.64692780875143 0.00000009678412 0.09815297366992

4

ge3c_ts_b3lyp FINAL SINGLE POINT ENERGY -6268.862630389071

Ge -0.47474134112075 0.87797288333384 1.52854402330212

Ge 0.00313572714665 -1.31266107110536 0.51623182283920

Ge -0.37459476294525 0.94545134954938 -1.11781975310261

C 0.84620037691936 -0.51076316177786 -0.92695609303870

4

d_gesi3_b3lyp FINAL SINGLE POINT ENERGY -2945.310961818176

Ge 0.00000658933133 0.00000000658849 -2.04810741312057

Si -0.00004976835671 -1.21965397296907 0.02312194759832

Si -0.00004976898917 1.21965395890653 0.02312194839782

Si 0.00009294801454 0.00000000747405 2.00186351702442

4

r_gesi3_b3lyp FINAL SINGLE POINT ENERGY -2945.305580696788

Ge 0.00050308978040 1.31004631401980 -0.00000633501416

Si -0.00055234672225 -0.05589305880905 2.00699978793932

Si 0.00060160319824 -1.19823917684388 0.00000669209035

Si -0.00055234625639 -0.05591407846688 -2.00700014501552

4

gesi3_ts_b3lyp FINAL SINGLE POINT ENERGY -2945.279397679951

Ge -1.15229447142437 -0.01573435843558 0.16569482740310

Si 1.93649278854813 0.04699351852240 0.48417837897837

Si 0.51200239264790 1.55093945817234 -0.46630611053538

Si 0.59468229022834 -1.55614913825916 -0.45422325584609

4

r_ge2si2_b3lyp FINAL SINGLE POINT ENERGY -4732.835830424353

Si -0.00002848339172 -1.22574540875594 -0.00000000543189

Si -0.00002848339571 1.22574530392047 0.00000000362457

Ge 0.00002848339371 0.00000005509261 2.06336262661813

Ge 0.00002848339372 0.00000004974286 -2.06336262481080

4

t_ge2si2_b3lyp FINAL SINGLE POINT ENERGY -4732.831740095640

Ge -0.00003921394571 1.30489723533370 0.18540250646545

Ge 0.00004216819070 0.19632081946334 -2.05897199871258

Si 0.00004410951048 -0.30448836287309 1.99936405994825

Si -0.00004706375546 -1.19672969192394 -0.12579456770112

4

d_ge2si2_b3lyp FINAL SINGLE POINT ENERGY -4732.825357185267

Si 0.00000003227143 2.02575096475062 -0.00185146790448

Ge -1.29333691232074 -0.00000007324609 0.00185146796029

Ge 1.29333685516875 -0.00000006159035 0.00185146813208

Si 0.00000002488055 -2.02575082991418 -0.00185146818789

4

ts_r_t_ge2si2_b3lyp FINAL SINGLE POINT ENERGY -4732.804713699195

Ge -0.31548647211724 1.72528035355410 1.13182373464969

Ge -1.03240952262361 -0.80402888647426 -1.21260589813288

Si -0.03688230463417 -0.48287487326422 0.97258976482821

Si 1.38477729937503 -0.43837559381561 -0.89180660134502

4

ts_d_r_ge2si2_b3lyp FINAL SINGLE POINT ENERGY -4732.801653334569

Si 0.39160091972067 -1.58646541931234 -0.01191885210188

Ge -0.39160147736940 -0.02022600520897 1.57845259791815

Ge -0.39160111733165 0.02022638792897 -1.57845263927120

Si 0.39160167498037 1.58646503659234 0.01191889345493

4

r_ge3si_b3lyp FINAL SINGLE POINT ENERGY -6520.357741816435

Ge 2.08270330158506 0.00001103267208 0.05782098065258

Ge 0.00000003718426 -0.00001003067449 -1.32427168923840

Ge -2.08270336263043 0.00001103267158 0.05782099213746

Si 0.00000002386110 -0.00001203466917 1.20862971634836

4

d_ge3si_b3lyp FINAL SINGLE POINT ENERGY -6520.352609969302

Ge 0.00115448786363 -0.00000000093368 2.08514435825973

Ge -0.00118023848054 1.29985984476753 -0.02253896802948

Ge -0.00118023847290 -1.29985984713394 -0.02253896136064

Si 0.00120598908981 0.00000000330010 -2.04006642876961

4

ge3si_ts_b3lyp FINAL SINGLE POINT ENERGY -6520.327442438876

Ge 1.30151197968207 -0.39626896664886 1.01203608553485

Ge 0.94059214209434 0.40810125565096 -1.30671606394577

Ge -0.99534449602035 0.40315071162039 1.24144267007782

Si -1.24675962575606 -0.41498300062249 -0.94676269166690

M06-2X XYZ coordinate files in the following format: XY_3 (d, r, ts), X_2Y_2 (r, t, d, r-t, d-r), X_3Y (r, d, ts), for SiC, GeC, and GeSi structures.

4

d_sic3_m062x FINAL SINGLE POINT ENERGY -403.559944122043

Si 0.00000004709044 -0.00000000670829 -1.57309986218375

C -0.00000005570557 -0.72587603914010 0.11510572292803

C -0.00000005570558 0.72587605641179 0.11510572025845

C 0.00000006432071 -0.00000001056339 1.34288841899728

4

r_sic3_m062x FINAL SINGLE POINT ENERGY -403.547224491504

Si -0.00000013132895 -0.00000002096993 -1.25902726654968

C 0.00000036907564 -1.29378936202895 0.31196842121129

C -0.00000060682233 -0.00000000084912 0.63509039894781

C 0.00000036907564 1.29378938384800 0.31196844649058

4

ts_sic3_m062x FINAL SINGLE POINT ENERGY -403.483119989638

Si 1.05647388484155 0.08166287642542 0.07965048368985

C -1.27643954505942 -0.22263469378551 0.36654952807263

C -0.40522246711450 -0.92198821549369 -0.30684165891939

C -0.81857387266763 0.96764903285378 -0.22308435284308

4

r_si2c2_m062x FINAL SINGLE POINT ENERGY -655.032431000822

Si 0.00000007170968 0.00000000627880 -1.68660870240172

Si 0.00000007170968 0.00000000917363 1.68660870020683

C -0.00000007170968 -0.71238501917854 -0.00000000231381

C -0.00000007170968 0.71238500372611 0.00000000450869

4

t_si2c2_m062x FINAL SINGLE POINT ENERGY -655.019480931129

Si -0.00000014620233 -0.00579422249203 1.70666196907837

Si 0.00000005703216 1.23249228583253 -0.46910790900353

C 0.00000029877304 -0.64096245156371 0.03256342211272

C -0.00000020960287 -0.58573561187679 -1.27011748218756

4

d_si2c2_m062x FINAL SINGLE POINT ENERGY -654.886272318852

Si -0.00001545803545 0.00000086538055 -1.14372945820544

Si -0.00001545803552 0.00000085468499 1.14372945609998

C 0.00001545801359 -1.48071439450019 0.00000000515680

C 0.00001545805739 1.48071267443465 -0.00000000305134

4

ts_r_t_si2c2_m062x FINAL SINGLE POINT ENERGY -654.958685217819

Si -1.53148815232948 -0.37821281075841 0.10940745327387

Si 1.65903030193913 -0.21207418072266 0.13665332852905

C -0.44237227227670 1.17668701232360 0.12405527055762

C 0.12044456266705 0.13666821915747 -0.58734141236054

4

ts_d_r_si2c2_m062x FINAL SINGLE POINT ENERGY -654.875193095936

Si -0.22139033970505 -0.00128218217081 -1.27418515247187

Si -0.22139027319305 0.00128227949895 1.27418539793458

C 0.22139052299920 -1.23267549558971 -0.00169129943957

C 0.22139008989891 1.23267539826158 0.00169105397686

4

r_si3c_m062x FINAL SINGLE POINT ENERGY -906.467809812020

C -0.00000005476292 0.60548620326262 0.00000000491595

Si 0.00000003103605 0.35983953599428 1.74110754989232

Si -0.00000000730919 -1.32516525502857 -0.00000002000982

Si 0.00000003103606 0.35983951587168 -1.74110753479845

4

d_si3c_m062x FINAL SINGLE POINT ENERGY -906.378351915341 Si -0.18593767717303

-1.17540101267984 0.05255766790447

Si -0.13575023830026 0.36291987217241 1.83279044990116

Si 0.04564000873077 1.12570654422092 -0.38594534190917

C 0.27604790674252 -0.31322540381349 -1.49940277589645

4

ts_si3c_m062x FINAL SINGLE POINT ENERGY -906.362722612059

C 0.93359999684762 -0.96211462954377 0.61759789863696

Si -0.58473725892510 -1.19467657995151 -0.21856161809195

Si 1.30475358416915 0.59743143303977 -0.19732013505727

Si -1.10969524209166 1.00163965645552 0.13411785451226

4

d_gec3_m062x FINAL SINGLE POINT ENERGY -2191.133949513945

Ge 0.00000004220495 0.00000001214957 -1.65447497097084

C -0.00000005192069 -0.72915382166042 0.14408228723023

C -0.00000005192069 0.72915379085052 0.14408228812346

C 0.00000006163644 0.00000001866032 1.36631039561715

4

r_gec3_m062x FINAL SINGLE POINT ENERGY -2191.125114472279

Ge 0.00000002181090 0.00000005254599 -1.35996793079166

C -0.00000007897674 -1.30318473629153 0.36206351306320

C 0.00000013614258 -0.00000000991123 0.63584097614756

C -0.00000007897674 1.30318469365677 0.36206344148090

4

ts_gec3_m062x FINAL SINGLE POINT ENERGY -2191.063900893763

Ge 0.69702902041528 0.07624696268030 0.04317888381322

C -1.74364402746849 -0.25021971967036 0.38102471210862

C -0.88346891834881 -0.93649145477579 -0.31677214313424

C -1.33814607459798 0.94763221176585 -0.21375645278760

4

r_ge2c2_m062x FINAL SINGLE POINT ENERGY -4230.178376240896

Ge -0.00000052853002 0.00000000151477 -1.80879872976023

C 0.00000052853003 -0.70032137668444 0.00000000165490

C 0.00000052853000 0.70032137765841 -0.00000000857175

Ge -0.00000052853001 -0.00000000248874 1.80879873667708

4

t_ge2c2_m062x FINAL SINGLE POINT ENERGY -4230.184215333130

Ge -0.00000008768229 -0.54212352306052 1.31104851093472

Ge 0.00000023721737 1.78926867660281 0.02988952256637

C 0.00000036200606 -1.27010576083063 -0.66859543104053

C -0.00000051154113 0.02296060718834 -0.67234260236056

4

d_ge2c2_m062x FINAL SINGLE POINT ENERGY -4230.016012346624

Ge 0.00000007788737 1.23130048547108 -0.11035216778103

Ge 0.00000014396289 -1.23130006593275 -0.11035211365375

C -1.51978562847848 -0.00000018607549 0.11035211184395

C 1.51978540662823 -0.00000023346284 0.11035216959082

4

ts_r_t_ge2c2_m062x FINAL SINGLE POINT ENERGY -4230.121007843345

Ge 1.67549179253763 -0.21151294598710 -0.06601218938620

Ge -1.71220282856873 -0.14643333363560 -0.07955722684133

C 0.36366935150710 1.33219392349056 -0.17221212048184

C -0.08978731547600 0.35413135613214 0.63923953670937

4

ts_d_r_ge2c2_m062x FINAL SINGLE POINT ENERGY -4230.006124559039

Ge 0.01095153004269 -1.34348541245551 0.21723625295663

Ge -0.01095685353886 1.34348466305577 0.21724207442597

C -1.32480782084543 0.01214035376100 -0.21723630230986

C 1.32481314434158 -0.01213960436126 -0.21724202507273

4

r_ge3c_m062x FINAL SINGLE POINT ENERGY -6269.119298753042

Ge -0.00000015222865 0.40459065215644 1.83387144754625

Ge 0.00000002992953 -1.43151087925270 0.00000005063636

C 0.00000027452776 0.62232951897331 -0.00000004264809

Ge -0.00000015222864 0.40459070802296 -1.83387145553451

4

d_ge3c_m062x FINAL SINGLE POINT ENERGY -6269.205971087075

Ge 1.99887566753798 0.00000040679379 -0.16066326627714

Ge -0.18012404004649 1.26123581779163 0.00822551902083

Ge -0.18012378364692 -1.26123705380916 0.00822549264903

C -1.63862784394457 0.00000082922374 0.14421225460728

4

ts_ge3c_m062x FINAL SINGLE POINT ENERGY -6269.103488175148

Ge -0.42626158180953 0.85410489635511 1.55440357448698

Ge 0.00668888827142 -1.30573781864122 0.46734322938956

Ge -0.42779802570467 0.93727885046035 -1.07516904911880

C 0.84737071924278 -0.48564592817423 -0.94657775475773

4

d_gesi3_m062x FINAL SINGLE POINT ENERGY -2945.454047981951

Ge 0.00091972502334 0.00000000583494 -2.03812852397352

Si -0.00094430491632 -1.20142331871748 0.02626667669930

Si -0.00094430493362 1.20142330892276 0.02626667312656

Si 0.00096888482659 0.00000000395978 1.98559517404766

4

r_gesi3_m062x FINAL SINGLE POINT ENERGY -2945.447862211628

Ge -0.00076013657849 1.29162133841858 -0.00000676120427

Si 0.00083806053328 -0.05687588557520 1.99788184441432

Si -0.00091598451392 -1.17784860658138 0.00000591330061

Si 0.00083806055914 -0.05689684636199 -1.99788099651066

4

ts_gesi3_m062x FINAL SINGLE POINT ENERGY -2945.400160702461

Ge -1.12929503778675 -0.01605151200421 0.21456408129374

Si 1.89624792857083 0.04979056886204 0.52734348772214

Si 0.52385689829513 1.50933791480472 -0.51184246806403

Si 0.60007321092079 -1.51702749166254 -0.50072126095185

4

r_ge2si2_m062x FINAL SINGLE POINT ENERGY -4733.042420707833

Si 0.00094139320076 -1.20957369444571 0.00000000016606

Si 0.00094139318507 1.20957370725984 0.00000000093620

Ge -0.00094139319431 -0.00000000617868 2.04678518899647

Ge -0.00094139319152 -0.00000000663545 -2.04678519009873

4

t_ge2si2_m062x FINAL SINGLE POINT ENERGY -4733.038002203122

Ge -0.00027024191359 1.28808843496060 0.18756328151772

Ge 0.00029096803600 0.19300521411541 -2.05224285196522

Si 0.00030661305385 -0.30420854187277 1.98482806968623

Si -0.00032733917626 -1.17688510720324 -0.12014849923872

4

d_ge2si2_m062x FINAL SINGLE POINT ENERGY -4733.030716587840

Si 0.00000000314587 2.02069426860055 0.00000776984200

Ge -1.27239827049619 0.00000300781065 -0.00000777229292

Ge 1.27239825448937 0.00000299247983 -0.00000777228945

Si 0.00000001286094 -2.02070026889103 0.00000777474037

4

r_t_ts_ge2si2_m062x FINAL SINGLE POINT ENERGY -4732.987998277499

Ge -0.32238728100382 1.68109066186911 1.01728510864287

Ge -0.91612328888995 -0.66474676697647 -1.32543973684281

Si -0.20073538349261 -0.53415977794670 0.98131919484073

Si 1.43924495338638 -0.48218311694594 -0.67316356664079

4

d_r_ts_ge2si2_m062x FINAL SINGLE POINT ENERGY -4732.985800049411

Si 0.43172406600169 -1.55210450655765 -0.02028316255368

Ge -0.43172444101918 -0.01188191969403 1.55502489104745

Ge -0.43172417144919 0.01188256798987 -1.55502466154080

Si 0.43172454646668 1.55210385826181 0.02028293304703

4

r_ge3si_m062x FINAL SINGLE POINT ENERGY -6520.627282259057

Ge 2.06926874328728 -0.00054931240082 0.05918882428532

Ge 0.00000001719465 0.00049761661971 -1.30908976358647

Ge -2.06926872193560 -0.00054931241946 0.05918885680406

Si -0.00000003854633 0.00060100820057 1.19071208239708

4

d_ge3si_m062x FINAL SINGLE POINT ENERGY -6520.621712800930

Ge 0.00017315898918 -0.00000000350009 2.08236926680777

Ge -0.00017714220778 1.28097729150105 -0.02659449486238

Ge -0.00017714217895 -1.28097728965361 -0.02659448647219

Si 0.00018112539755 0.00000000165265 -2.02918028537321

4

ts_gesi3_m062x FINAL SINGLE POINT ENERGY -6520.574749461143

Ge 1.28601212122739 -0.43738273813869 0.98595518724213

Ge 0.93151508313957 0.45058693298652 -1.27997829777600

Ge -0.98895640802557 0.44555063050591 1.21074670132793

Si -1.22857079634139 -0.45875482535374 -0.91672359079406

ωB97X-D4 XYZ coordinate files in the following format: XY_3 (d, r, ts), X_2Y_2 (r, t, d, r-t, d-r), X_3Y (r, d, ts), for SiC, GeC, and GeSi structures.

4

d_sic3_wb97xd4 FINAL SINGLE POINT ENERGY -403.668559544015

Si 0.00000003512378 0.00000000372936 -1.56664927678898

C -0.00000004166147 -0.72981887441370 0.11337556346727

C -0.00000004166148 0.72981887643152 0.11337554539048

C 0.00000004819918 -0.00000000574718 1.33989816793123

4

r_sic3_wb97xd4 FINAL SINGLE POINT ENERGY -403.656005966265

Si -0.00000016814785 -0.00000002762932 -1.25284598789256

C 0.00000047327352 -1.29289306693553 0.30781782325714

C -0.00000077839919 0.00000001808771 0.63721030346263

C 0.00000047327352 1.29289307647714 0.30781786127279

4

ts_sic3_wb97xd4 FINAL SINGLE POINT ENERGY -403.587798992723

Si 1.04653798527252 0.08995124659772 0.07757934751248

C -1.27547638000533 -0.22872135216299 0.37201641548285

C -0.41122193871312 -0.92489607183821 -0.30698734382944

C -0.80360166655406 0.96835517740348 -0.22633441916589

4

r_si2c2_wb97xd4 FINAL SINGLE POINT ENERGY -655.143913254213

Si -0.00000134055174 -0.00000000155943 -1.67399223633391

Si -0.00000134055174 -0.00000000320555 1.67399223306675

C 0.00000134055176 -0.71786397291459 0.00000000354309

C 0.00000134055172 0.71786397767957 -0.00000000027593

4

t_si2c2_wb97xd4 FINAL SINGLE POINT ENERGY -655.131915148770

Si -0.00000015171327 0.00920058441582 1.68971534172449

Si 0.00000006092835 1.22514979742466 -0.44972212528311

C 0.00000030666105 -0.65125316864002 0.03159540702647

C -0.00000021587613 -0.58309721330047 -1.27158862346785

4

d_si2c2_wb97xd4 FINAL SINGLE POINT ENERGY -654.995016335516

Si 0.00183269499148 0.00000228613055 -1.13795236629863

Si 0.00183269516470 0.00000226479250 1.13795234432062

C -0.00183269922426 -1.47620868293510 0.00000001917103

C -0.00183269093192 1.47620413201205 0.00000000280698

4

ts_r_t_si2c2_wb97xd4 FINAL SINGLE POINT ENERGY -655.067392363517

Si -1.50629140864306 -0.38140064432904 0.11309676668471

Si 1.63694215757844 -0.21958286948942 0.14014539957464

C -0.44717466948675 1.18506242623426 0.12640998753110

C 0.12213836055138 0.13898932758419 -0.59687751379045

4

ts_d_r_si2c2_wb97xd4 FINAL SINGLE POINT ENERGY -654.979190064290

Si -0.22217614433515 0.00723987067200 -1.26620586108650

Si -0.22217606434371 -0.00723932852885 1.26620605663251

C 0.22217640132321 -1.23467562929819 0.00732186856342

C 0.22217580735565 1.23467508715504 -0.00732206410944

4

r_si3c_wb97xd4 FINAL SINGLE POINT ENERGY -906.587081855736

C -0.00000011533563 0.62041890875755 0.00000001308990

Si 0.00000006745917 0.34456669203393 1.72813200604479

Si -0.00000001958270 -1.30955226955730 -0.00000002199882

Si 0.00000006745917 0.34456666886582 -1.72813199713587

4

d_si3c_wb97xd4 FINAL SINGLE POINT ENERGY -906.497517708302

Si -0.09815817742519 -1.17133004094053 0.06841270724106

Si -0.20722683609341 0.36768043995154 1.82065966399236

Si 0.13152610968328 1.11129924948695 -0.36643854918308

C 0.17385890383532 -0.30764964859796 -1.52263382205033

4

ts_si3c_wb97xd4 FINAL SINGLE POINT ENERGY -906.477689927165

C 0.92741140580377 -0.96898097235391 0.62784935502662

Si -0.56898909820162 -1.18000048350787 -0.22427381179542

Si 1.28885771654186 0.59365763112122 -0.20557221896624

Si -1.10335894414401 0.99760370474056 0.13783067573505

4

d_gec3_wb97xd4 FINAL SINGLE POINT ENERGY -2191.154009029142

Ge -0.00000003758683 -0.00000002622406 -1.64177186892734

C 0.00000004311850 -0.73179802073996 0.13992825952605

C 0.00000004311838 0.73179807613253 0.13992827463627

C -0.00000004865004 -0.00000002916851 1.36191533476502

4

r_gec3_wb97xd4 FINAL SINGLE POINT ENERGY -2191.145761652725

Ge -0.00000012695495 0.00000000544839 -1.34573561974944

C 0.00000044958301 -1.30159157712526 0.35329843625910

C -0.00000077221108 -0.00000000138819 0.63913875474784

C 0.00000044958302 1.30159157306505 0.35329842864251

4

ts_gec3_wb97xd4 FINAL SINGLE POINT ENERGY -2191.081100927340

Ge 0.68175794857558 0.08247336641895 0.04366121667441

C -1.74530786734808 -0.25559944377220 0.38084900807684

C -0.88244284436327 -0.93821612529617 -0.31773609197300

C -1.32223723686423 0.94851020264941 -0.21309913277825

4

r_ge2c2_wb97xd4 FINAL SINGLE POINT ENERGY -4230.112275477486

Ge 0.00000014494304 -0.00000001684568 -1.78237226833920

C -0.00000014494314 -0.70786136812082 0.00000000669147

C -0.00000014494293 0.70786140797657 -0.00000000930378

Ge 0.00000014494304 -0.00000002301008 1.78237227095151

4

t_ge2c2_wb97xd4 FINAL SINGLE POINT ENERGY -4230.118690133898

Ge -0.00000010728297 -0.51781238844121 1.29576316368246

Ge 0.00000029260412 1.76337862038813 0.04615531999704

C 0.00000044375017 -1.27050505240579 -0.66286820703524

C -0.00000062907131 0.02493882035887 -0.67905027654425

4

d_ge2c2_wb97xd4 FINAL SINGLE POINT ENERGY -4229.954345920915

Ge 0.00000030666624 1.21057902051453 0.00012565691836

Ge 0.00000035376161 -1.21057863626132 0.00012564163889

C -1.53655237622516 -0.00000016921170 -0.00012558753242

C 1.53655171579730 -0.00000021504150 -0.00012571102483

4

ts_r_t_ge2c2_wb97xd4 FINAL SINGLE POINT ENERGY -4230.052634708729

Ge 1.70052597414976 -0.40443391854054 -0.03004667882507

Ge -1.57240565883945 0.02226446732519 -0.09606685489617

C -0.08871407501607 1.35656016452425 -0.21759269991390

C 0.19776475970575 0.35398828669110 0.66516423363514

4

ts_d_r_ge2c2_wb97xd4 FINAL SINGLE POINT ENERGY -4229.937631740379

Ge 0.01490378465299 -1.33898886793726 0.21452374429794

Ge -0.01490269779392 1.33898793247670 0.21452950428612

C -1.30964802351609 0.01619696951392 -0.21452483015931

C 1.30964693665701 -0.01619603405336 -0.21452841842475

4

r_ge3c_wb97xd4 FINAL SINGLE POINT ENERGY -6269.060323956971

Ge -0.00000006686937 0.38034896987851 1.81122566147283

Ge 0.00000001706725 -1.39983029569459 0.00000000596931

C 0.00000011667150 0.63913235171859 0.00000001246934

Ge -0.00000006686938 0.38034897399750 -1.81122567991149

4

d_ge3c_wb97xd4 FINAL SINGLE POINT ENERGY -6268.976502863228

Ge 1.95598288901650 0.00000000386862 -0.16040848841730

Ge -0.16887213519442 1.24384710592350 0.01147726321042

Ge -0.16887216924956 -1.24384708725405 0.01147725545008

C -1.61823858467252 -0.00000002253807 0.13745396975679

4

ts_ge3c_wb97xd4 FINAL SINGLE POINT ENERGY -6268.957382257867

Ge -0.44607652278271 0.82420711435032 1.52364804503111

Ge -0.00948730519886 -1.29621910121725 0.45036681685955

Ge -0.40613909360215 0.94501870782599 -1.05627893798169

C 0.86170292158372 -0.47300672095904 -0.91773592390896

4

d_gesi3_wb97xd4 FINAL SINGLE POINT ENERGY -2945.497374772174

Ge -0.00000079070022 -0.00000000714000 -2.00785396228264

Si 0.00000086703425 -1.19166202700934 0.02096860489945

Si 0.00000086702226 1.19166204788298 0.02096859508832

Si -0.00000094335629 -0.00000001373364 1.96591676219487

4

r_gesi3_wb97xd4 FINAL SINGLE POINT ENERGY -2945.489079928742

Ge -0.00000941863271 1.27209877732692 -0.00000664950622

Si 0.00000333707422 -0.04818837601904 1.96831233142272

Si 0.00000274442780 -1.17570150995118 0.00000613119852

Si 0.00000333713068 -0.04820889145670 -1.96831181311501

4

ts_gesi3_wb97xd4 FINAL SINGLE POINT ENERGY -2945.439451146525

Ge -1.10840636124921 -0.01862188329575 0.22443756126371

Si 1.86890394305519 0.06183241954818 0.53012510932934

Si 0.53485916304879 1.48686120331079 -0.51463792239130

Si 0.59552625514523 -1.50402225956323 -0.51058090820175

4

r_ge2si2_wb97xd4 FINAL SINGLE POINT ENERGY -4732.999133599685

Si -0.00121713210290 -1.19629470056084 -0.00000000469591

Si -0.00121713215666 1.19629468749187 0.00000001221426

Ge 0.00121713213403 0.00000001152636 2.01993298645378

Ge 0.00121713212553 0.00000000154261 -2.01993299397213

4

t_ge2si2_wb97xd4 FINAL SINGLE POINT ENERGY -4732.992021420863

Ge -0.00003816618107 1.26594923271408 0.17820493961821

Ge 0.00003309286041 0.19876131767068 -2.01271457478941

Si 0.00003326931366 -0.29162606692824 1.95912316224254

Si -0.00002819599300 -1.17308448345653 -0.12461352707133

4

d_ge2si2_wb97xd4 FINAL SINGLE POINT ENERGY -4732.983025364732

Si 0.00000003972752 1.98145735671598 -0.00002178480554

Ge -1.25968970462430 0.00000000781948 0.00002178493713

Ge 1.25968964001584 0.00000003083285 0.00002178472166

Si 0.00000002488094 -1.98145739536831 -0.00002178485324

4

r_t_ts_ge2si2_wb97xd4 FINAL SINGLE POINT ENERGY -4732.944019689444

Ge -0.30869170504963 1.62515108202095 0.94415031244488

Ge -0.90728480178407 -0.61666168469451 -1.28876715984597

Si -0.20078200876865 -0.55988669877941 0.99658992241483

Si 1.41675751560236 -0.44860169854703 -0.65197207501374

4

d_r_ts_ge2si2_wb97xd4 FINAL SINGLE POINT ENERGY -4732.938135946766

Si 0.42851821061112 -1.53900584513841 -0.00509256516969

Ge -0.42851876516817 -0.02580959942899 1.52995742164420

Ge -0.42851843218833 0.02580997701778 -1.52995757638790

Si 0.42851898674536 1.53900546754962 0.00509271991339

4

r_ge3si_wb97xd4 FINAL SINGLE POINT ENERGY -6520.494686528539

Ge 2.03380374111897 -0.00021965681407 0.04937034182201

Ge -0.00000001064597 0.00019885690747 -1.28304074989628

Ge -2.03380373340112 -0.00021965681521 0.04937033353871

Si 0.00000000292812 0.00024045672181 1.18430007443556

4

d_ge3si_wb97xd4 FINAL SINGLE POINT ENERGY -6520.486844952709

Ge -0.00001242245487 0.00000000065217 2.03446556979531

Ge 0.00000640281516 1.26513742056817 -0.02078852410559

Ge 0.00000640281855 -1.26513741703872 -0.02078853168627

Si -0.00000038317884 -0.00000000418162 -1.99288851390345

4

ts_gesi3_wb97xd4 FINAL SINGLE POINT ENERGY -6520.441388124490

Ge 1.26680828544568 -0.43459216316544 0.97216278191283

Ge 0.91981496494214 0.44949486288748 -1.25714747513954

Ge -0.97069528169816 0.44155428676438 1.18589565060314

Si -1.21592796868965 -0.45645698648642 -0.90091095737642

B2GP-PLYP XYZ coordinate files in the following format: XY_3 (d, r, ts), X_2Y_2 (r, t, d, r-t, d-r), X_3Y (r, d, ts), for SiC, GeC, and GeSi structures.

4

d_sic3_b2gpplyp FINAL SINGLE POINT ENERGY -403.330444075067

Si -0.00000005048201 -0.00000000383245 -1.57134510040620

C 0.00000006030487 -0.74186359901960 0.11587686232705

C 0.00000006030487 0.74186359566238 0.11587688270835

C -0.00000007012773 0.00000000718967 1.33959135537079

4

r_sic3_b2gpplyp FINAL SINGLE POINT ENERGY -403.321127869227

Si -0.00000019946332 -0.00000001785550 -1.26091884882843

C 0.00000055946853 -1.29786061070511 0.31026708188371

C -0.00000091947374 -0.00000001451631 0.64038466722666

C 0.00000055946854 1.29786064307691 0.31026709981806

4

ts_sic3_b2gpplyp FINAL SINGLE POINT ENERGY -403.257007981411

Si 1.05967918616493 0.08476200730706 0.06523168338160

C -1.28971811301625 -0.21884741226222 0.34322919546798

C -0.39414755858037 -0.94905453177646 -0.28707400867336

C -0.81957551456831 0.98782893673161 -0.20511287017621

4

r_si2c2_b2gpplyp FINAL SINGLE POINT ENERGY -654.686691646399

Si -0.00000026020797 0.00000000454666 -1.68808926044532

Si -0.00000026020797 -0.00000000509712 1.68808926627540

C 0.00000026020797 -0.72213983835662 0.00000000824638

C 0.00000026020797 0.72213983890708 -0.00000001407646

4

d_si2c2_b2gpplyp FINAL SINGLE POINT ENERGY -654.676426050503

Si -0.00395870811990 -0.00000112301781 -1.14904660960308

Si -0.00395870809297 -0.00000096133503 1.14904653473442

C 0.00395870791470 -1.49282146293351 -0.00000002474313

C 0.00395870829818 1.49282354728635 0.00000009961179

4

t_si2c2_b2gpplyp FINAL SINGLE POINT ENERGY -654.556169394022

Si -0.00000009390145 -0.00644649324445 1.71124689659996

Si 0.00000003716042 1.23251771311316 -0.47481870992189

C 0.00000019054015 -0.64568996534402 0.03879341889739

C -0.00000013379912 -0.58038125462468 -1.27522160557546

4

ts_r_t_si2c2_b2gpplyp FINAL SINGLE POINT ENERGY -654.615859774580

Si -1.57129968742112 -0.36182618046827 0.08681439838380

Si 1.71333048114021 -0.20182226085709 0.11096550610874

C -0.45942059968807 1.18261092215317 0.12202069343313

C 0.12300424596898 0.10410575917218 -0.53702595792566

4

ts_d_r_si2c2_b2gpplyp FINAL SINGLE POINT ENERGY -654.552291959416

Si -0.22116209258282 0.00816145668903 -1.25301979830840

Si -0.22116194464406 -0.00816180266696 1.25301986493542

C 0.22116189324792 -1.26221275445800 -0.00178331383467

C 0.22116214397896 1.26221310043593 0.00178324720764

4

r_si3c_b2gpplyp FINAL SINGLE POINT ENERGY -906.010216711249

C 0.00000037501479 0.61720969456170 0.00000001419506

Si -0.00000021775661 0.35641001386294 1.74806923940027

Si 0.00000006049843 -1.33002968607597 -0.00000003569098

Si -0.00000021775661 0.35640997775133 -1.74806921790434

4

d_si3c_b2gpplyp FINAL SINGLE POINT ENERGY -905.929101689268

Si -0.15284566688739 -1.18645122146829 0.05631580467823

Si -0.16557444560513 0.37012760106179 1.85402775225107

Si 0.08034442503493 1.13063999941761 -0.38498863877622

C 0.23807568745758 -0.31431637911110 -1.52535491815308

4

ts_si3c_b2gpplyp FINAL SINGLE POINT ENERGY -905.910368975070

C 0.95184831845076 -0.98789612863946 0.52693017280903

Si -0.63881798893070 -1.20700652248390 -0.21496872422202

Si 1.31242114833619 0.63101956993814 -0.16927426832146

Si -1.08153039785625 1.00616296118522 0.19314681973445

4

d_gec3_b2gpplyp FINAL SINGLE POINT ENERGY -2190.520257712043

Ge 0.00000023646312 -0.00000001292451 -1.64653400185160

C -0.00000029180382 -0.74475042094468 0.14238763124591

C -0.00000029180382 0.74475043607034 0.14238765865541

C 0.00000034714452 -0.00000000220115 1.36175871195028

4

r_gec3_b2gpplyp FINAL SINGLE POINT ENERGY -2190.516069668950

Ge -0.00000004263228 0.00000000064418 -1.35390238017510

C 0.00000015170263 -1.30746927955334 0.35723979167584

C -0.00000026077298 0.00000000545800 0.63942279648200

C 0.00000015170263 1.30746927345116 0.35723979191725

4

ts_gec3_b2gpplyp FINAL SINGLE POINT ENERGY -2190.455328558584

Ge 0.70995851535297 0.03517745503513 0.02489746016044

C -1.76167874701363 -0.22692060961059 0.34964758935257

C -0.87398969797096 -0.95367050566082 -0.29982983269274

C -1.34252007036838 0.98258166023628 -0.18104021682028

4

r_ge2c2_b2gpplyp FINAL SINGLE POINT ENERGY -4229.065854985803

Ge -0.00000010890614 -0.00000014678881 -1.80302228824051

C 0.00000010890189 -0.70918326626390 0.00000001762929

C 0.00000010891044 0.70918356978737 -0.00000000786382

Ge -0.00000010890619 -0.00000015673466 1.80302227847504

4

t_ge2c2_b2gpplyp FINAL SINGLE POINT ENERGY -4229.071759819572

Ge 0.00000002905279 -0.54508850774120 1.29995399502866

Ge -0.00000008270498 1.78613393108166 0.02875855195271

C -0.00000012222746 -1.27480884433214 -0.65893811457696

C 0.00000017587965 0.03376342089169 -0.66977443230441

4

d_ge2c2_b2gpplyp FINAL SINGLE POINT ENERGY -4228.930374917354

Ge -0.00000000858724 1.23102501404743 -0.15057934009650

Ge 0.00000012159976 -1.23102509471914 -0.15057937282429

C -1.50598912500572 0.00000009086501 0.15057948053332

C 1.50598901199320 -0.00000001019330 0.15057923238747

4

ts_r_t_ge2c2_b2gpplyp FINAL SINGLE POINT ENERGY -4229.010252134877

Ge 1.70848284843918 -0.16193297748309 -0.04557697893662

Ge -1.74809429551997 -0.16018010938675 -0.07528312115721

C 0.37033666559884 1.34608329275414 -0.15255586789437

C -0.09355421851805 0.30440879411570 0.59487396798819

4

ts_d_r_ge2c2_b2gpplyp FINAL SINGLE POINT ENERGY -4228.923295144365

Ge 0.00348049455537 -1.32209264284239 0.23375044887848

Ge -0.00348009332436 1.32209186899517 0.23375617441630

C -1.33182428595216 0.00446720811274 -0.23375142029027

C 1.33182388472114 -0.00446643426553 -0.23375520300451

4

r_ge3c_b2gpplyp FINAL SINGLE POINT ENERGY -6267.598999747858

Ge 0.00000026368578 0.39000971481747 1.83730652688113

Ge -0.00000006407906 -1.41831546547330 0.00000000475931

C -0.00000046329250 0.63829602816958 -0.00000002103675

Ge 0.00000026368578 0.39000972238625 -1.83730651060368

4

d_ge3c_b2gpplyp FINAL SINGLE POINT ENERGY -6267.524398462359

Ge 2.00001992439322 0.00000008000825 -0.15554958804844

Ge -0.17599655834234 1.25795635867113 0.00108418751163

Ge -0.17599634045784 -1.25795674873263 0.00108413995996

C -1.64802702569304 0.00000031005326 0.15338126057685

4

ts_ge3c_b2gpplyp FINAL SINGLE POINT ENERGY -6267.506254193121

Ge -0.45638041207094 0.81901931492304 1.50225757616713

Ge 0.01309170643849 -1.33819687971007 0.49288993608152

Ge -0.38573197404991 0.98017734236914 -1.06485884293005

C 0.82902067968235 -0.46099977758210 -0.93028866931859

4

d_gesi3_b2gpplyp FINAL SINGLE POINT ENERGY -2944.499890015158

Ge 0.00092016601239 0.00000006951821 -2.03874875727608

Si -0.00093872368390 -1.21752108020520 0.02015827134978

Si -0.00093872396912 1.21752093148392 0.02015828235966

Si 0.00095728164063 0.00000007920307 1.99843220346665

4

r_gesi3_b2gpplyp FINAL SINGLE POINT ENERGY -2944.495520314865

Ge 0.00004920964830 1.28926960122364 -0.00000691600105

Si -0.00005109532440 -0.04179772574312 2.00319283213271

Si 0.00005298125236 -1.20565340528964 0.00000633891390

Si -0.00005109557627 -0.04181847029088 -2.00319225504555

4

ts_gesi3_b2gpplyp FINAL SINGLE POINT ENERGY -2944.447744945959

Ge -1.13442178005024 -0.00856201096813 0.16054212073695

Si 1.93879528722614 0.03066191520012 0.48907369689940

Si 0.49084427178681 1.55111461055309 -0.47015235744454

Si 0.59566522103729 -1.54716503478508 -0.45011962019182

4

r_ge2si2_b2gpplyp FINAL SINGLE POINT ENERGY -4731.704812673272

Si -0.00017776286599 -1.22293219126535 0.00000000917775

Si -0.00017776286536 1.22293218714276 -0.00000001137392

Ge 0.00017776286525 -0.00000000400014 2.05219298434464

Ge 0.00017776286611 0.00000000812273 -2.05219298214847

4

t_ge2si2_b2gpplyp FINAL SINGLE POINT ENERGY -4731.701330959535

Ge -0.00006122880684 1.28472306796114 0.17930842407454

Ge 0.00006459777683 0.20883359633353 -2.04618135071130

Si 0.00006742384945 -0.29060875162714 1.99545841335434

Si -0.00007079281943 -1.20294791266753 -0.12858548671758

4

d_ge2si2_b2gpplyp FINAL SINGLE POINT ENERGY -4731.696521653847

Si 0.00000000217907 2.02176403352213 0.00005019413856

Ge -1.28113009198930 -0.00000009974016 -0.00005019423495

Ge 1.28113007917326 -0.00000011288431 -0.00005019424657

Si 0.00000001063697 -2.02176382089766 0.00005019434296

4

r_t_ts_ge2si2_b2gpplyp FINAL SINGLE POINT ENERGY -4731.648330662371

Ge -0.34444508997589 1.72620828605497 1.09295649543717

Ge -0.89738096062266 -0.70505330366978 -1.34078379201219

Si -0.20481512351996 -0.49353942907683 0.95488610609714

Si 1.44664017411851 -0.52761455330836 -0.70705780952213

4

d_r_ts_ge2si2_b2gpplyp FINAL SINGLE POINT ENERGY -4731.651248440664

Si 0.39459928947972 -1.57983779713308 -0.00017796893055

Ge -0.39460050466926 -0.03182529039119 1.56718744059873

Ge -0.39459992943182 0.03182381499339 -1.56718731300174

Si 0.39460114462134 1.57983927253088 0.00017784133356

4

r_ge3si_b2gpplyp FINAL SINGLE POINT ENERGY -6518.907085885699

Ge 2.06990226346479 -0.00011184338505 0.04245069202935

Ge 0.00000002322488 0.00010289496936 -1.30083709473659

Ge -2.06990227858724 -0.00011184337771 0.04245071269615

Si -0.00000000810242 0.00012079179340 1.21593568991109

4

d_ge3si_b2gpplyp FINAL SINGLE POINT ENERGY -6518.903126804251

Ge -0.00126770558256 0.00000001259876 2.07416263280639

Ge 0.00129298722857 1.28733379462047 -0.01982849220781

Ge 0.00129298716845 -1.28733382692794 -0.01982848209177

Si -0.00131826881446 0.00000001970871 -2.03450565840681

4

ts_gesi3_b2gpplyp FINAL SINGLE POINT ENERGY -6518.856945852242

Ge 1.30165293025494 -0.39410221119412 0.97091352395768

Ge 0.95041240297905 0.40541685377775 -1.26746439192568

Ge -1.00291296859530 0.41068371994162 1.23390139629068

Si -1.24915236463868 -0.42199836252525 -0.93735052832269